

University of Alberta

Dosimetric verification of radiation treatment fields using radiographic film

by

Alana Dawn Hudson



A thesis submitted to the Faculty of Graduate Studies and Research in partial fulfillment of the requirements for the degree of Master of Science

in

Medical Physics

Department of Physics

Edmonton, Alberta

Fall 2004



Library and
Archives Canada

Bibliothèque et
Archives Canada

Published Heritage
Branch

Direction du
Patrimoine de l'édition

395 Wellington Street
Ottawa ON K1A 0N4
Canada

395, rue Wellington
Ottawa ON K1A 0N4
Canada

Your file *Votre référence*
ISBN: 0-612-95769-1
Our file *Notre référence*
ISBN: 0-612-95769-1

The author has granted a non-exclusive license allowing the Library and Archives Canada to reproduce, loan, distribute or sell copies of this thesis in microform, paper or electronic formats.

L'auteur a accordé une licence non exclusive permettant à la Bibliothèque et Archives Canada de reproduire, prêter, distribuer ou vendre des copies de cette thèse sous la forme de microfiche/film, de reproduction sur papier ou sur format électronique.

The author retains ownership of the copyright in this thesis. Neither the thesis nor substantial extracts from it may be printed or otherwise reproduced without the author's permission.

L'auteur conserve la propriété du droit d'auteur qui protège cette thèse. Ni la thèse ni des extraits substantiels de celle-ci ne doivent être imprimés ou autrement reproduits sans son autorisation.

In compliance with the Canadian Privacy Act some supporting forms may have been removed from this thesis.

Conformément à la loi canadienne sur la protection de la vie privée, quelques formulaires secondaires ont été enlevés de cette thèse.

While these forms may be included in the document page count, their removal does not represent any loss of content from the thesis.

Bien que ces formulaires aient inclus dans la pagination, il n'y aura aucun contenu manquant.

Canada

For Erin, Tara and Steven
Thank you, Merci, Gracias!

Acknowledgements

I would like to thank Colin Field for taking time out of his busy schedule to help in this whole masters operation. Without his direction and support this project would not have been possible. I would also like to thank Dr. Gino Fallone and the rest of the Medical Physics department for their support of the graduate program and of me.

Appreciation also goes out to my magnificent friends in the program who have been with me throughout my Masters. Steven, Erin, and Tara you rock and I love you! I literally would not of stuck this out if it had not been for you. Thank you all for your help during the last few years. Thank you also to Keith and Anna who brightened up our downstairs office for the last year or so (even if it was with sarcasm). Thanks Pavel and Nadia for your inspiration, history lessons, and laughs.

To my crew of reference letter writers, a big thanks for the kind words that helped me get into and move beyond my masters: Karen McDonald, Walter Jones, Maya Wheelock, Sherry Connors, Pavel Stavrev, and Colin Field.

Special thanks goes out to my parents who just happen to be the best parents on the planet. Thanks for the “scholarships”, meal deliveries and everything else that makes you so great to have in my life. I would also like to thank my siblings (Chad, Krista, and Kelsey) for their friendship and for giving me a family that I am so happy and proud to be a part of. Thank you Kelsey for doing the lawn so that I could study in undergrad. Thank you dad for making Kelsey do the lawn instead of me. And to my favourite nomad, Nathan, thanks for all of the remarkable adventures we’ve had together and those to come. You mean everything to me.

To my best friend Katherine, who is currently working on her 2nd degree, hang in there. You are an amazing person and I know that you will always be successful in anything you try. It will all be worth it in the end....

Table of Contents

| | |
|------------------------------------------------------------------------------------------|-----------|
| Chapter 1 Thesis Overview | 1 |
| 1.1 THESIS OVERVIEW | 1 |
| 1.2 CHAPTER 2 – INTRODUCTION..... | 2 |
| 1.3 CHAPTER 3 – THEORY OF FILM DOSIMETRY AND COMPARISON OF DOSE DISTRIBUTIONS | 2 |
| 1.4 CHAPTER 4 – MATERIALS AND METHODS | 3 |
| 1.5 CHAPTER 5 – RESULTS AND DISCUSSION..... | 4 |
| 1.6 CHAPTER 6 – CONCLUSIONS | 5 |
| 1.7 REFERENCES | 5 |
| Chapter 2 Introduction..... | 6 |
| 2.1 CANCER | 6 |
| 2.2 TREATMENT OF CANCER..... | 7 |
| 2.2.1 <i>Biological Response to Radiation Therapy</i> | 8 |
| 2.2.2 <i>Definitions Relating to Tumour Dose Prescription</i> | 11 |
| 2.2.3 <i>External Beam Radiation Therapy</i> | 13 |
| 2.2.3.1 Conventional External Beam Radiation Therapy..... | 13 |
| 2.2.3.2 Three-dimensional Conformal Radiation Therapy..... | 14 |
| 2.2.3.3 Inverse-Planned Intensity Modulated Radiation Therapy | 15 |
| 2.2.3.4 Treatment Plan Verification..... | 16 |
| 2.3 REFERENCES | 17 |
| Chapter 3 Theory of Film Dosimetry and Comparison of Dose Distributions | 20 |
| 3.1 DOSIMETRY | 20 |
| 3.1.1 <i>Measuring Dose to a Point Using an Ionization Chamber</i> | 20 |
| 3.1.1.1 TG-51 Protocol..... | 21 |
| 3.1.1.2 Day-to-day Linac Output Variation | 23 |
| 3.1.2 <i>Measuring a 2-D Dose Distribution</i> | 24 |
| 3.1.3 <i>General Properties of Film</i> | 25 |
| 3.2 COMPARISON OF DOSE DISTRIBUTIONS | 29 |
| 3.2.1 <i>Qualitatively Comparing Dose Distributions</i> | 30 |
| 3.2.2 <i>Quantitatively Comparing Dose Distributions</i> | 30 |
| 3.2.2.1 Dose Distribution Comparison Guidelines | 30 |
| 3.2.2.2 Two Metric Software Tool | 33 |
| 3.2.2.3 The Gamma Evaluation | 33 |
| 3.2.3 <i>Beam’s Eye View Software</i> | 36 |
| 3.2.4 <i>Image Registration</i> | 36 |
| 3.2.4.1 Use of Fiducial Markers and Pinpricks for Image Registration ... | 37 |
| 3.2.4.2 Image Registration using Cross Correlation | 37 |
| 3.3 REFERENCES | 39 |

Chapter 4 Materials and Methods.....42

| | |
|-----------------------------------------------------------------------------|----|
| 4.1 DOSIMETRY | 42 |
| 4.1.1 <i>Selection of Film</i> | 42 |
| 4.1.2 <i>Generation of Sensitometric Curves</i> | 42 |
| 4.1.2.1 Ion Chamber Measurements | 45 |
| 4.1.2.2 Film Irradiation for Sensitometric Curves | 46 |
| 4.1.2.3 Creation of Sensitometric Curves | 46 |
| 4.1.3 <i>Generation of Calculated Dose Distribution</i> | 47 |
| 4.1.4 <i>Generation of Measured Dose Distribution</i> | 47 |
| 4.1.5 <i>Film Processing</i> | 47 |
| 4.1.6 <i>Film Scanning</i> | 48 |
| 4.1.7 <i>Examination of Film Spectral Response</i> | 49 |
| 4.1.8 <i>Determination of Error in Film Dosimetry Technique</i> | 51 |
| 4.2 COMPARISON OF DOSE DISTRIBUTIONS..... | 52 |
| 4.2.1 <i>Quantitative Comparison of Dose Distributions using DDComp</i> ... | 52 |
| 4.2.2 <i>Image Resampling and Registration</i> | 54 |
| 4.2.3 <i>Test Cases to Validate DDComp</i> | 57 |
| 4.2.4 <i>Dependence of DDComp on Various Parameters</i> | 59 |
| 4.2.4.1 Selection of Region of Interest | 60 |
| 4.2.4.2 Dose Distribution Uncertainties..... | 60 |
| 4.2.4.3 Dose Distribution Normalization..... | 61 |
| 4.2.4.4 Definition of the Reference Dose Distribution | 62 |
| 4.2.4.5 Impact of Changing Metric Thresholds for the Metrics..... | 62 |
| 4.3 CLINICAL APPLICATION | 63 |
| 4.4 REFERENCES | 64 |

Chapter 5 Results and Discussions.....66

| | |
|------------------------------------------------------------------------------|-----|
| 5.1 DOSIMETRY | 66 |
| 5.1.1 <i>Generation of Sensitometric Curves</i> | 66 |
| 5.1.1.1 Sensitometric Curves for XV and EDR Films | 66 |
| 5.1.1.2 Film Scanning - Linearity of Pixel Value with Optical Density | 70 |
| 5.1.2 <i>Examination of Film Spectral Response</i> | 71 |
| 5.1.2.1 Results of Perpendicular Film Irradiation..... | 71 |
| 5.1.2.2 Results of Parallel Film Irradiation..... | 73 |
| 5.1.3 <i>Error in Film Dosimetry Technique</i> | 76 |
| 5.2 COMPARISON OF DOSE DISTRIBUTIONS..... | 79 |
| 5.2.1 <i>Quantitative Comparison of Dose Distribution Using DDComp</i> | 79 |
| 5.2.1.1 DDComp User-Interface..... | 79 |
| 5.2.1.2 Example of Output Generated by DDComp | 80 |
| 5.2.2 <i>Image Registration</i> | 89 |
| 5.2.3 <i>Results of Test Cases to Validate DDComp</i> | 91 |
| 5.2.4 <i>Dependence of DDComp on Various Parameters</i> | 94 |
| 5.2.4.1 Dose Distribution Uncertainties..... | 94 |
| 5.2.4.2 Dose Distribution Normalization..... | 95 |
| 5.2.4.3 Definition of the Reference Dose Distribution | 97 |
| 5.2.4.4 Impact of Changing Metric Thresholds for the Metrics..... | 98 |
| 5.3 CLINICAL APPLICATION | 100 |
| 5.3.1 <i>Conventional 10x10 and 5x5 fields</i> | 100 |

| | | |
|------------------------------------|---------------------------------------------------------|------------|
| 5.3.2 | <i>IMRT Treatment Verification for 5 Patients</i> | 102 |
| 5.3.3 | <i>Reproducibility</i> | 103 |
| 5.4 | REFERENCES | 104 |
| Chapter 6 Conclusions | | 105 |
| 6.1 | DOSIMETRY | 105 |
| 6.2 | COMPARISON OF DOSE DISTRIBUTIONS | 106 |
| 6.3 | CLINICAL APPLICATION | 108 |
| 6.4 | FUTURE WORK..... | 109 |
| 6.5 | FINAL CONCLUSIONS | 110 |
| Bibliography | | 111 |

List of Figures

| | |
|------------------------------------------------------------------------------------------------------------------------------------------------------------------------------|----|
| Figure 2.1 Schematic of two possible theoretical radiation cellular response curve scenarios for tumour control probability and normal tissue complication probability | 9 |
| Figure 2.2 Simple conception of GTV, CTV, PTV, treated volume and irradiated volume | 12 |
| Figure 3.1 Simplified schematic of the film dosimetry process. | 25 |
| Figure 3.2 Structure of a double-sided radiographic film..... | 26 |
| Figure 3.3 Example of an H&D curve. | 27 |
| Figure 3.4 Sample sensitometric curves for XV2 and EDR2 film. | 29 |
| Figure 3.5 Illustration of how distance to agreement is determined..... | 31 |
| Figure 3.6 Beam's eye view of different regions of a treatment field for a conventional square treatment field..... | 32 |
| Figure 3.7 Example of systematic offset between two dose distributions..... | 39 |
| Figure 4.1 Experimental setup for generating sensitometric curve. | 43 |
| Figure 4.2 Film calibration step window. | 44 |
| Figure 4.3 Experimental setup for perpendicular and parallel film irradiation | 50 |
| Figure 4.4 Schematic of pinprick positioning tray..... | 55 |
| Figure 5.1 Sample sensitometric curve for XV film irradiated with a 6 MV photon beam..... | 67 |
| Figure 5.2 Sample sensitometric curve for EDR film irradiated with a 6 MV photon beam..... | 67 |
| Figure 5.3 Sample sensitometric curve for XV film irradiated with a 15 MV photon beam..... | 68 |

| | |
|----------------------------------------------------------------------------------------------------------------------------------------------|----|
| Figure 5.4 Sample sensitometric curve for EDR film irradiated with a 15 MV photon beam..... | 68 |
| Figure 5.5 Pixel value versus optical density for XV and EDR films irradiated with 6 MV photons in the step window pattern..... | 70 |
| Figure 5.6 Doses at 5 cm depth in solid water for XV and EDR films irradiated with a 6 MV beam..... | 71 |
| Figure 5.7 Doses at 20 cm depth in solid water for XV and EDR films irradiated with a 6 MV beam. | 72 |
| Figure 5.8 XV film measured and Helax TMS calculated vertical and horizontal dose distributions..... | 74 |
| Figure 5.9 EDR film measured and Helax TMS calculated vertical and horizontal dose distributions..... | 75 |
| Figure 5.10 Screen shot of user-interface to input thresholds in DDComp..... | 79 |
| Figure 5.11 Measured dose distribution..... | 83 |
| Figure 5.12 Calculated dose distribution. | 83 |
| Figure 5.13 Absorbed dose difference..... | 84 |
| Figure 5.14 Histogram of dose difference.. | 84 |
| Figure 5.15 Percent dose difference..... | 85 |
| Figure 5.16 Histogram of percent dose difference..... | 85 |
| Figure 5.17 Distance to agreement | 86 |
| Figure 5.18 Histogram of distance to agreement. | 86 |
| Figure 5.19 Combined metric results..... | 87 |
| Figure 5.20 Dose-pixels passing at least one test. | 87 |
| Figure 5.21 Distance to agreement polar plot..... | 88 |
| Figure 5.22 Polar plot created by comparing two dose distributions where the calculated dose distribution was identical to the measured dose | |

distribution but it was shifted by 10 pixels (15 mm) in the right and down directions..... 94

List of Tables

| | |
|---------------------------------------------------------------------------------------------------------------------------------------------------------------------------------|----|
| Table 4.1 Number of monitor units delivered to each subfield for irradiation of calibration step window for XV and EDR films..... | 45 |
| Table 4.2 Metric pass/fail for software test cases.. | 57 |
| Table 4.3 Simple hypothetical measured and calculated dose distributions..... | 58 |
| Table 4.4 Absorbed dose difference, percent dose difference and DTA matrices calculated for the above measured and calculated dose distributions..... | 58 |
| Table 4.5 Test case criteria to achieve metric pass/fail combinations shown in Table 4.2. | 59 |
| Table 5.1 Summary of curve fits for XV and EDR films irradiated with 6 and 15 MV photons. | 69 |
| Table 5.2 Average and % standard deviation for doses measured using an ion chamber at the centre of each subfield for 6 and 15 MV photons. | 77 |
| Table 5.3 Average pixel value for 5 XV and 5 EDR films at the centre of each subfield and the error in the average pixel..... | 78 |
| Table 5.4 Standard deviation in dose in the linear dose range due to differences in pixel value measurements and sensitometric fits between 5 films. | 78 |
| Table 5.5 Goodness of fit parameters for 6 simple test cases..... | 89 |
| Table 5.6 Peak offset and correlation coefficients for 8 beams from an IMRT patient treatment..... | 90 |
| Table 5.7 Absorbed dose difference, percent dose difference and DTA matrices calculated using DDComp for the measured and calculated dose distributions shown in Table 4.3..... | 91 |
| Table 5.8 Binary pass/fail matrices for each metric as well as the combined metric.. | 92 |
| Table 5.9 Metric % failure results for dose distributions compared with the same distribution plus noise..... | 95 |

| | |
|-------------------------------------------------------------------------------------------------------------------------------------------------------------------------------------------------------------------------------------------------------------------------------------------------------------------------------------------------------------|-----|
| Table 5.10 Percent failure statistics for the dose distribution software for an unnormalized comparison dose distribution; a comparison dose distribution normalized to the maximum dose-pixel value in the reference dose distribution; and a comparison dose distribution normalized to the mean dose-pixel value in the reference dose distribution..... | 96 |
| Table 5.11 Percent failure statistics for a calculated/measured dose distribution pair when the reference dose distribution was defined to be the first the measured dose distribution and second the calculated dose distribution..... | 98 |
| Table 5.12 Percent failure statistics for a absorbed dose difference, percent dose difference and distance to agreement when the threshold values are changed. | 99 |
| Table 5.13 Percent of dose-pixels in an IMRT field that are passed by each of the metrics..... | 100 |
| Table 5.14 Calculated and measured doses for conventional square fields irradiated with 6 and 15 MV photons.. | 101 |
| Table 5.15 Percent failure of metrics for conventional square fields analysed using DDComp. | 101 |
| Table 5.16 Percent failure of metrics for 5 clinical IMRT treatment verifications done with film and analysed using the dose distribution software tool..... | 103 |
| Table 5.17 Percent failure of metrics for a single IMRT clinical treatment beam verified using film on three separate days..... | 104 |

List of Abbreviations

| | |
|---------|--------------------------------------------------------------|
| 3-D CRT | Three-dimensional Conformal Radiotherapy |
| BEV | Beam's Eye View |
| CTV | Clinical Target Volume |
| DTA | Distance to Agreement |
| EDR | Extended Dose Range |
| GTV | Gross Tumour Volume |
| ICRU | International Commission on Radiation Units and Measurements |
| IMRT | Intensity Modulated Radiation Therapy |
| MLC | Multileaf Collimator |
| MU | Monitor Units |
| NRCC | National Research Council of Canada |
| NSL | National Standards Lab |
| NTCP | Normal Tissue Complication Probability |
| PRV | Planning Organ at Risk Volume |
| PTV | Planning Target Volume |
| ROI | Region of Interest |
| TCP | Tumour Control Probability |
| TMS | Treatment Management System |
| XV | X-ray Verification |

Chapter 1 Thesis Overview

1.1 Thesis Overview

Verification of radiation treatments is clinically necessary. In the dose verification process, the dose or energy deposited in a small volume is measured in a phantom that is used to simulate the patient. The measured dose distribution is then compared to the planned dose distribution determined using a radiotherapy treatment planning system. The hypothesis of this thesis is that film dosimetry together with a quantitative method of comparing calculated and measured dose distributions can be used to quantitatively verify treatment fields.

Film dosimetry is often used to measure relative dose distributions in phantom for external beam radiotherapy. This work expands on previous film dosimetry techniques that were used at the Cross Cancer Institute for verification of inverse-planned intensity modulated radiation therapy (IMRT) (Gagne, Warkentin et al. 2002; MacKenzie, Lachaine et al. 2002).

Once calculated and measured dose distributions have been obtained, the measured dose distributions must be quantitatively compared with the calculated ones to determine whether the treatment is clinically acceptable. A software tool has been developed that uses various parameters to quantify the differences between two dose distributions.

The film dosimetry and dose distribution comparison techniques were applied to conventional square fields and to a number of clinically delivered inverse-planned IMRT head and neck treatment fields.

1.2 Chapter 2 – Introduction

Chapter 2 introduces the reader to basic concepts of cancer and its treatment. It then focuses on different types of external beam radiation therapy since the dosimetric verification techniques presented in these works are most applicable to this treatment modality. Included are discussions on conventional and conformal external beam radiotherapy, and intensity modulated radiation therapy. The importance of having a sound method of comparing measured and calculated dose distributions is then discussed.

1.3 Chapter 3 – Theory of Film Dosimetry and Comparison of Dose Distributions

Theories behind dosimetry and comparison of dose distributions are discussed in Chapter 3. First, the determination of absorbed dose is discussed, as it is directly applicable to the generation of the sensitometric curve. The basic concepts of film dosimetry are then introduced with emphasis on properties of film, sensitometric curves, film dosimetry techniques, and problems with film dosimetry.

The section on the comparison of dose distributions discusses two common types of image registration and different qualitative and quantitative comparison techniques. Dose distribution comparison guidelines, a two-metric software tool, and the gamma evaluation are introduced as quantitative comparison techniques. These are discussed as precursors to the software we have developed to compare dose distributions.

1.4 Chapter 4 – Materials and Methods

Chapter 4 outlines the materials and methods used in the three sections of the chapter: dosimetry, comparison of dose distributions and clinical application of the techniques. Because the film dosimetry process involves selection of an appropriate measurement film, a comparison of two potentially useful films, Kodak XV and EDR2, was made. The step window technique used to generate the calibration dose – pixel value pairs is described in terms of ion chamber measurements, film measurements, film processing and scanning, and the creation of sensitometric curves. Methods examining the validity of using a sensitometric curve created at 10 cm depth and perpendicular to the beam at other depths and orientations are then described. Steps in determining error and how to limit errors in film dosimetry are discussed.

The software tool to quantitatively compare distributions (DDComp) is also discussed in Chapter 4. Three metrics to quantitatively compare dose distributions (absorbed dose difference, percent dose difference and distance to agreement), and the test cases used to validate the software are examined. Several parameters that affect the comparison of dose distributions are investigated including the addition of noise/uncertainty, whether the reference dose distribution is defined as the measured or the calculated dose distribution, the effect of normalizing the dose distributions, and the impact of changing the metric thresholds.

Finally, the application of film dosimetry and the dose-distribution comparison techniques to conventional and IMRT fields are discussed in Chapter 4.

1.5 Chapter 5 – Results and Discussion

As in Chapter 4, experimental results are broken into 3 sections in Chapter 5: dosimetry results, the comparison of dose distributions, and the clinical application of these techniques. The dosimetry results include examination of the sensitometric curves for XV and EDR films. Discussion of scanner non-linearity between pixel value and optical density is presented. The spectral dependence of film is studied through the irradiation of film oriented perpendicular and parallel to the central axis of the beam. Reproducibility and error estimates in the film dosimetry techniques are also given.

Typical output from our software tool is shown for an IMRT treatment field. Results are also given for the dependence of DDComp on uncertainty in the dose distributions, the definition of the reference dose distribution (measured or calculated), normalizing the dose distributions, and the metric thresholds.

The percentage of pixels failing the three metrics (absorbed dose difference, percent dose difference, and distance to agreement) for conventional $10 \times 10 \text{ cm}^2$ and $5 \times 5 \text{ cm}^2$ fields are given. The agreement between the measured dose distribution and the Helax Treatment Management System (Helax-TMS) calculated dose distribution is then discussed. Statistics obtained for the 3 quantitative metrics are given for five IMRT verifications to provide an idea of measured and Helax-TMS calculated dose distribution agreement. Results are also given for a single IMRT beam analysis that was repeated on three separate days to examine reproducibility of these techniques for a clinical case.

1.6 Chapter 6 – Conclusions

Chapter 6 summarizes the techniques presented in this thesis, the results obtained, and the conclusions that were consequently made for each of the 3 sections: dosimetry, comparison of dose distributions, and clinical application of the techniques. Recommendations for future work are also provided.

1.7 References

Gagne, I., B. Warkentin, H. Thompson, M. A. MacKenzie and G. C. Field (2002). "A procedure to improve the reliability of IMRT film verification." Med Phys **29**(8): 1943.

MacKenzie, M. A., M. Lachaine, B. Murray, B. G. Fallone, D. Robinson and G. C. Field (2002). "Dosimetric verification of inverse planned step and shoot multileaf collimator fields from a commercial treatment planning system." J. Appl. Clin. Med. Phys. **3**(2): 97-109.

Chapter 2 Introduction

2.1 Cancer

Cancer is defined by the Canadian Cancer Society as “a general term for more than 200 diseases. It is the uncontrolled, abnormal growth of cells that can invade and destroy healthy tissues” (Canadian Cancer Society 2003). Cancer is responsible for much mortality and morbidity throughout the world, and impacts the lives of virtually all Canadians: either directly, or indirectly, through family and friends. In the most recent publicly available Statistics Canada data on the cause of death, it was found that 29% of deaths in Canada were attributed to cancer while cardiovascular disease was responsible for 36%. Furthermore, cancer is the leading cause of person-years of life lost in Canada (Statistics Canada 1997). Person-years of life lost is defined as the “the sum of the difference between the actual age at death and the expected remaining lifetime for each person who died of cancer” (Horm and Sondik 1989).

It is estimated that 145,500 new cancer cases will be diagnosed in Canada in 2004, and an estimated 68,300 Canadians will die from cancer in the same year. Perhaps most alarming is that about 40% of Canadians will develop cancer at some point in their lives based on current incident rates of cancer. The majority of new cases and deaths will be among men and women who are 60 years of age or older. At any given time about 2% of men and 2.5% of women are afflicted with this type of disease (National Cancer Institute of Canada 2004).

The most commonly diagnosed cancers in Canada are breast for women, and prostate for men, although lung cancer is the leading cause of cancer deaths for both sexes. Incidence of non-Hodgkin’s lymphoma and thyroid cancer, as well as mortality rates due to lung cancer in women are all on the rise in Canada.

A slight decrease has been shown in many other types of cancer. Smoking is to blame for about 1/3 of the potential years life lost (National Cancer Institute of Canada 2004). Not smoking is the single biggest step in preventing cancer. Other preventative measures include eating healthily, having an active lifestyle, limiting alcohol, and reducing sun exposure (Canadian Cancer Society 2003). Advances in cancer treatment and early detection may have decreased cancer mortality and may increase the quality of life for individuals with cancer.

2.2 Treatment of Cancer

There are three main cancer treatment techniques: surgery, chemotherapy, and radiation therapy. The different treatment modalities are often combined to give the best chance of tumour control for the patient. Surgery is used to remove tumour masses plus a margin of tissue surrounding the visible tumour in hopes to remove any micrometastases as well. Chemotherapy involves the administration of cytotoxic drugs that interfere with the cancer cell cycle. Chemotherapy is used to treat cancers that are widespread throughout the body such as leukaemia, to shrink large tumours so they can become operable, and to destroy microscopic residual cancer cells after the patient undergoes another type of treatment (CancerBACUP 2002). Radiation therapy can be divided into brachytherapy and external beam therapy. Brachytherapy is a form of treatment where the radiation source is placed in or near the tumour through temporary or permanent placement of radioactive sources in tissue, or in an adjacent cavity. Brachytherapy is an effective method of treatment in gynaecologic sites as well as breast, prostate, lung, esophagus, head and neck, and eye metastases (Glasgow 1999). External beam therapy uses a radiation source outside of the body directed at the tumour volume to deposit dose in it and cause damage to the cancer cells. Radiation sources for external beam radiotherapy include photons, electrons, protons, neutrons, and heavy ions. For purposes of this thesis, the discussion of external

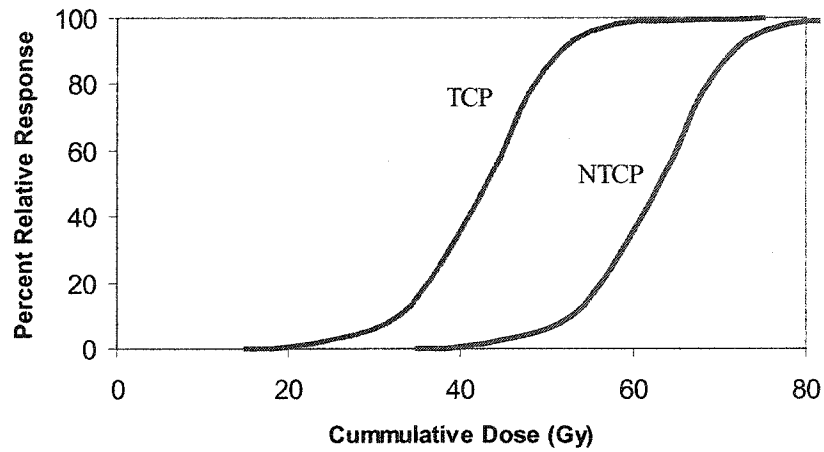
beam radiation therapy will be focused on megavoltage photon treatment beams using a linear accelerator (linac).

About half the cancer patients in North America undergo radical treatment (Van Dyk 1999). These patients are treated aggressively in hopes of a cure. Patients with cancer that is deemed incurable, as determined by the oncologist, undergo palliative treatment. The purpose of this less aggressive type of treatment is to alleviate pain and side effects that are attributed to the cancer in hopes of providing better quality of life for the patient in the short term.

2.2.1 Biological Response to Radiation Therapy

Hypothetical dose response curves for tumour control probability (TCP) and normal tissue complication probability (NTCP) are shown in Figure 2.1. The TCP and NTCP curves show sigmoidal responses to dose for a given population. The percent relative response (the y-axis variable) can be defined by a number of different endpoints. Endpoints for the response of normal tissue may be defined using a measure for the severity of damage to a tissue; loss of tissue function; or inability to proliferate. Likewise, tumour control endpoints can be measured by regrowth failure, lack of clonogenic cell survival or delay in tumour growth (Steel 2003).

a)



b)

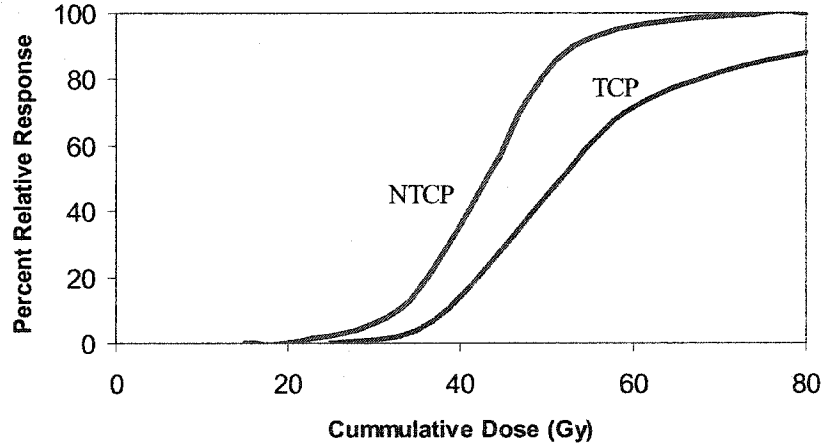


Figure 2.1 Schematic of two possible theoretical radiation cellular response curve scenarios for tumour control probability (TCP) and normal tissue complication probability (NTCP) (Van Dyk 1999).

The goal of radiation therapy is to obtain tumour control without exceeding tolerable damage of surrounding normal tissues. In situations where

the TCP curve is to the left of the NTCP curve (Figure 2.1(a)), radiotherapy is a viable treatment option and doses are chosen such that tumour control is maximized while normal tissue complications are minimized. The therapeutic ratio, which is defined as the ratio of tumour to normal tissue doses at the 50% response level can be used as a tool to determine the best dose to provide adequate tumour control without devastating nearby critical structures (Johns and Cunningham 1983).

Data to generate dose response curves is limited; therefore, precise curves are very difficult to obtain. Normal tissue complication responses are usually generated using clinical data points clustered only around low doses, and tumour control response typically use data points clustered only around higher doses. It has been suggested that because of these uncertainties, a more typical dose response curve may have the TCP curve to the right of the NTCP curve as shown in Figure 2.1(b). In this model, the slope of the TCP curve is shallower than that of the NTCP curve due to tumour heterogeneity, and full tumour control may not be reached due to spread of the disease (Van Dyk 1999). In this situation, radiation therapy is not a good course of treatment unless radiobiological separation between the TCP and NTCP curves is possible or the radiation can be tightly conformed to the tumour cells while avoiding much of the normal tissues. Radiobiological separation of the TCP and NTCP curves may be achieved by fractionation of treatments, the use of radiosensitizers to increase the vulnerability of tumours to radiation, or radioprotectors to reduce the effect of radiation on normal tissues. The chemical modifiers, unfortunately, have had limited clinical success due to, for example, their toxicity or lack of differential effect between tumours and normal tissues (Hall 2000).

In situations where the NTCP curve is not well to the right of the TCP curve and in the absence of an effective radiobiological agent, there must be

highly conformal coverage of the PTV for external beam radiation therapy to be successful. This scenario stresses the importance of accurate dose delivery, and, in turn, of a sound dose verification procedure. Conformal radiation therapy can be achieved by using, for example, field shaping or beam placement to deliver one dose to the target and another much lower dose to nearby organs at risk.

A relatively small change in the delivered dose can cause a much larger change in response. For example, a 5% change in absorbed dose in the steep part of the dose response curve can result in a 5 to 20% change in response. The large variation in response is more pronounced for tumours than normal tissue since tumour doses are selected in the steep dose gradient and normal tissue doses are selected to be in the tail of the dose-response curves. A reasonable clinical goal is to deliver the prescribed absorbed dose to within 5% of the prescription dose after the entire treatment has been completed (ICRU 1976).

2.2.2 Definitions Relating to Tumour Dose Prescription

Several definitions are important to understand the targeting of radiation towards cancerous tissues. Ideally, treatment would deposit dose exclusively in tumours, but as the external beam radiation transverses normal tissues, it deposits dose in them as well. Prior to delivering external beam radiation therapy, radiation oncologists with assistance from radiologists determine spatial characteristics of the tumour and critical structures using an imaging modality such as computed tomography (CT). During the design of the treatment plan, this information is used to select beam characteristics to provide a good balance between tumour control and normal tissue sparing.

The International Commission on Radiation Units and Measurements (ICRU) introduced some standardized terminology to address tumour dose

prescriptions in the ICRU Report 50 (ICRU 1993). The gross tumour volume, or GTV, is the gross visible or palpable extent of the tumour (Figure 2.2). Because individual cancerous cells are too small to be seen, it is necessary to expand the GTV by adding a margin to include micrometastases. This volume is defined as the clinical target volume (CTV) and is the volume that must receive a sufficient dose during each treatment fraction to kill the tumour. The planning target volume (PTV) encompasses the CTV and adds a setup and movement margin to ensure that the clinical target volume is adequately radiated every treatment fraction. The margin accounts for physiologic and geometric uncertainties including variations in organ size, shape and position caused by, for instance, movement due to respiratory function, fullness of the bladder, difficulties in patient repositioning, or mechanical setup uncertainties as discussed in ICRU Report 62 (ICRU 1999). Two other volumes are defined for the radiated regions. The treated volume is the volume receiving a relatively high dose, and the irradiated volume is that which receives a significant dose in terms of normal tissue tolerance (ICRU 1993).

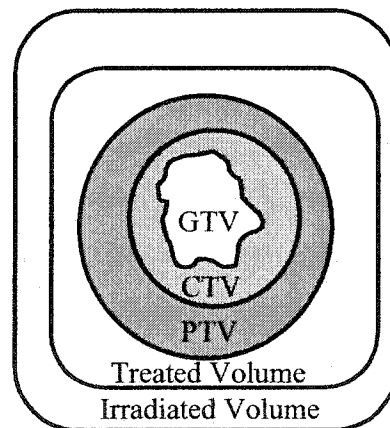


Figure 2.2 Simple conception of GTV, CTV, PTV, treated volume and irradiated volume (ICRU 1993).

ICRU Report 62 also takes the ideas of margins and applies them to organs at risk. Organs at risk are radiosensitive organs near the CTV. A planning organ at risk volume or PRV is defined by adding a margin around the organs at risk to account for physiologic and geometric uncertainties. In situations where there is overlap between the PTV and PRV, a compromise must be made between treating the PTV and sparing the PRV (ICRU 1999).

2.2.3 External Beam Radiation Therapy

2.2.3.1 Conventional External Beam Radiation Therapy

Historically, the PTV was treated using rectangular beams. To achieve uniform dose in the PTV and to adequately spare normal tissues, several strategies were employed. These included choosing an appropriate field size, increasing the number of treatment beams, selecting appropriate beam directions, beam weights, and beam energies. If these methods do not provide a desirable dose distribution, beam modifiers can also be used (Khan 1994).

Alloy blocks have been used historically to shape the radiation beam. These blocks, composed of lead or Cerrobend, were positioned between the patient and the radiation source. They were either custom-made for a patient, or pre-made with a desired shape or size. The blocks created problems because of their heavy weight and because they lengthen treatment times since they have to be manually inserted in the treatment head (Boyer, Xing et al. 1999).

Wedges are used to compensate for oblique beam incidence and curved surfaces, and to alter dose distributions by decreasing the intensity across the beam (Khan 1994). Several types of wedges are used in external beam radiotherapy namely physical wedges, internal wedges, and dynamic wedges.

Conventional physical wedges are composed of brass or lead and are inserted in the linac accessory tray as required during the treatment. Internal wedges are typically 60° wedges permanently mounted on the linac. If these are required during a treatment, the wedge is inserted into the field for the appropriate length of time to generate the desired wedge angle. Dynamic wedges act the same as the physical or internal wedges to produce a graduated dose distribution but they utilize the collimator jaws to do so. Over the course of the treatment, a collimator jaw is slowly closed (Boyer, Xing et al. 1999).

Missing tissue compensating filters selectively attenuate regions of the incident radiation beam in order to achieve a uniform dose at depth in the presence of irregular surface contours (Boyer, Xing et al. 1999).

2.2.3.2 Three-dimensional Conformal Radiation Therapy

For most treatments, a rectangular treatment field is undesirable because a large volume of normal tissue and/or critical structure(s) is likely to receive significant dose. In three-dimensional conformal radiotherapy, or 3-D CRT, a precise delineation of the PTV and PRV is required and then the dose distribution is “sculpted” to match the PTV. Beam conformation is achieved through the use of multileaf collimators (MLCs) or beam shaping blocks. The use of 3-D CRT allows us to deliver an adequate dose to the PTV while at the same time delivering an acceptably low dose to the surrounding normal tissue. In this case, the treatment must be tightly conformed to the PTV in order to prevent significant dose from being deposited in the PRV. The development of sophisticated imaging techniques in, for example, computed tomography, magnetic resonance imaging and positron emission tomography, has allowed for more detailed PTV and PRV spatial and functional information required for 3-D CRT (Van Dyk, Barnett et al. 1999).

2.2.3.3 Inverse-Planned Intensity Modulated Radiation Therapy

Intensity modulated radiation therapy (IMRT) further shapes dose distributions to the PTV compared to 3-D CRT by modulating the intensity of each field. This allows doses to be more tightly conformed to more complex PTV shapes (Ezzell, Galvin et al. 2003).

There are two main approaches to optimising external beam treatment plans. These are forward planning and inverse planning. In forward planning, beam weights, directions, energies, and modulations are first determined by the treatment planner followed by the calculation of the resulting dose distribution. If an undesirable dose distribution is obtained, changes are made to the beam parameters and the process is repeated until a satisfactory treatment plan is obtained. Inverse treatment planning, on the other hand, has the planner defining the treatment constraints rather than the beam parameters, which are subsequently determined through a variety of computer-aided optimisation techniques (Webb 1997). Conventional and 3-D CRT use forward planning whereas IMRT can be planned using either forward planning or inverse planning.

The goal of IMRT is to modulate the beam intensities so that the dose distribution resulting from all of the beams conforms closely to the PTV (Boyer, Xing et al. 1999). The most significant advantage of this type of treatment is better avoidance of the PRV. Inverse-planned IMRT is especially advantageous for treating concave targets surrounded by sensitive structures (Khan 2003). In cases where the PTV and PRV are spatially separated, IMRT may not be necessary. Inverse-planned IMRT generally uses the multileaf collimator (MLC) to shape the beam during treatment.

There are two major delivery techniques for MLC-IMRT: sliding window or dynamic MLC, and step and shoot or segmental MLC. With dynamic MLC-IMRT, a gap is defined by the position of the paired MLC leaves. The leaves are then moved in one direction during irradiation, each leaf with a different velocity that changes as a function of time (Ezzell, Galvin et al. 2003). In step and shoot IMRT, the collimator leaves are moved into position while the beam is off. The treatment field segment is then irradiated and the beam is turned off. The leaves are then moved to another position. Then the beam is turned on again. This pattern of “stepping” the leaves while the beam is off and then “shooting” while the leaves are stationary is repeated until all of the treatment segments have been delivered for the beam. The dose distribution for the entire treatment field is the sum of all of the segments weighted by the number of monitor units (MU) delivered to each subfield (Ezzell, Galvin et al. 2003). Step and shoot IMRT allows for treatment of complicated fields including regions in the field that receive no dose (Webb 1997). Problems with IMRT include the demand for increased monitor units during treatment, leakage, possible errors in field shape (MLC position), and problems with treatment verification (Webb 1997).

2.2.3.4 Treatment Plan Verification

External beam radiation treatment plans are established to give a tumouricidal dose to the PTV while conforming to it as closely as possible to avoid significant normal tissue damage. As described in Section 2.2.1, this is of particular importance if the tumour control probability curve is close to or to the right of the normal tissue complication probability curve. Complex radiation therapies, such as inverse-planned IMRT, require a sound verification technique that can determine whether or not delivered dose distributions agree with the calculated dose distribution. Film verification is currently performed 2-dimensionally in the beam’s eye view one treatment field at a time, or 3-

dimensionally where the entire treatment is verified all at once. In our case, treatment verifications are performed for a single field at a time with the verification film placed perpendicular to the beam, and one film is irradiated for each field. In order to verify the entire treatment all at once, film is irradiated edge-on and all of the fields are delivered at their respective gantry angles. This 3-D verification technique may not be accurate if the film over-responds in the edge-on position as investigated in Section 4.1.7. If there is a large discrepancy between delivered and planned dose distributions, there is a good chance that the goals of the treatment, namely tumour control and normal tissue sparing, will not be achieved. This stresses the importance of being able to accurately measure 2-D dose distributions for treatment fields, having a quantitative way of comparing the measured dose distribution with the calculated dose distribution, and applying these techniques to clinical situations. These topics are the focus of the thesis.

2.3 References

- Boyer, A. L., L. Xing and P. Xia (1999). Beam Shaping and Intensity Modulation. The Modern Technology of Radiation Oncology: A Compendium for Medical Physicists and Radiation Oncologists. J. Van Dyk. Madison, WI, Medical Physics Publishing.
- Canadian Cancer Society (2003). Cancer glossary. <http://www.cancer.ca>
- Canadian Cancer Society (2003). Risk Reduction. <http://www.cancer.ca>
- CancerBACUP (2002). Booklet series. <http://www.cancerbacup.org.uk/>
- Ezzell, G. A., J. M. Galvin, D. Low, J. R. Palta, I. Rosen, M. B. Sharpe, P. Xia, Y. Xiao, L. Xing and C. X. Yu (2003). "Guidance document on delivery, treatment planning, and clinical implementation of IMRT: Report of the IMRT subcommittee of the AAPM radiation therapy committee." Med Phys **30**(8): 2089-2115.

- Glasgow, G. P. (1999). Brachytherapy. The Modern Technology of Radiation Oncology: A Compendium for Medical Physicists and Radiation Oncologists. J. Van Dyk. Madison, WI, Medical Physics Publishing.
- Hall, E. J. (2000). Radiobiology for the Radiologist. Philadelphia, PA, Lippincott Williams & Wilkins.
- Horn, J. W. and E. J. Sondik (1989). "Person-years of life lost due to cancer in the United States, 1970 and 1984." Am J Public Health **79**(11): 1490-3.
- ICRU, International Commission on Radiation Units and Measurements (1976). ICRU Report 24: Determination of Absorbed Dose in a Patient Irradiated by Beams of X or Gamma Rays in Radiotherapy Procedures. Washington, DC.
- ICRU, International Commission on Radiation Units and Measurements (1993). ICRU Report 50: Prescribing, Recording, and Reporting Photon Beam Therapy. Washington, DC.
- ICRU, International Commission on Radiation Units and Measurements (1999). ICRU Report 62: Prescribing, Recording and Reporting Photon Beam Therapy (Supplement to ICRU Report 50). Washington, DC.
- Johns, H. E. and J. R. Cunningham (1983). The Physics of Radiology. Springfield, IL, Charles C Thomas.
- Khan, F. M. (1994). The Physics of Radiation Therapy. Baltimore, MD, Lippincott Williams & Wilkins.
- Khan, F. M. (2003). Intensity-Modulated Radiation Therapy. The Physics of Radiation Therapy. Philadelphia, PA, Lippincott Williams & Wilkins.
- National Cancer Institute of Canada (2004). Canadian Cancer Statistics 2004. Toronto, ON. <http://www.ncic.cancer.ca>
- Statistics Canada (1997). Health Statistics. <http://www.statcan.ca/>
- Steel, G. G. (2003). The radiobiology of tumours. Basic Clinical Radiobiology, 3rd Edition. G. G. Steel. New York, NY, Arnold.
- Van Dyk, J., Ed. (1999). Radiation Oncology Overview. The Modern Technology of Radiation Oncology: A Compendium for Medical Physicists and Radiation Oncologists. Madison, WI, Medical Physics Publishing.

Van Dyk, J., R. B. Barnett and J. J. Battista, Eds. (1999). Computerized Radiation Treatment Planning Systems. The Modern Technology of Radiation Oncology. Madison, WI, Medical Physics Publishing.

Webb, S. (1997). The Physics of Conformal Radiotherapy: Advances in Technology. Philadelphia, PA, Institute of Physics Publishing.

Chapter 3 Theory of Film Dosimetry and Comparison of Dose Distributions

In this chapter, the theory of film dosimetry and some methods of comparing dose distributions are discussed.

3.1 Dosimetry

It is necessary to ensure that the dose distribution delivered to the patient agree with the dose distribution calculated by the treatment planning system. If the delivered and calculated dose distributions differ significantly, the goal of the radiation therapy, for example local tumour control, may not be achieved. In the verification process, a patient treatment field is delivered to a phantom, which approximates the patient radiologically. Planar or point measurements are made in the phantom and these results are compared to the calculated values. The absorbed dose to a point can be measured using an ion chamber. It is often desirable to use a 2-D detector, such as film, to obtain a 2-D dose distribution. However, since film is not an absolute dosimeter, calibration within a known radiation field is required to approximate a measurement of absorbed dose.

3.1.1 Measuring Dose to a Point Using an Ionization Chamber

Absorbed dose measurements can be obtained using an ionization chamber with a calibration factor that is traceable to a national standards laboratory (NSL) (Van Dyk 1999). In Canada, the NSL is the Institute for National Measurement Standards of the National Research Council of Canada (NRCC) (Almond, Biggs et al. 1999). Gas-filled ionization chambers used in conjunction with an electrometer can be used to measure ionization charge (Khan

1994). Several types of ion chambers exist including cylindrical, parallel-plate, linear accelerator monitor chambers, well chambers, and radiation survey meters. Farmer-type chambers have been found to be stable, reliable secondary standards for therapeutic x-rays at all applicable energies and were used to measure absorbed dose to water in this work (Almond, Biggs et al. 1999).

3.1.1.1 TG-51 Protocol

The TG-51 protocol (Almond, Biggs et al. 1999) was developed as a standardized method of determining absorbed dose to water in clinical photon and electron beams, to ensure uniformity of the reference dosimetry. The protocol is applicable to photon beams of energies from ^{60}Co to 50 MV and electron beams ranging in energy from 4 to 50 MeV. TG-51 uses absorbed dose to water calibration factors combined with ion chamber measurements in its determination of absorbed dose. (Almond, Biggs et al. 1999).

Absorbed dose calculations for a photon beam from TG-51 Worksheet A are summarized below (Almond, Biggs et al. 1999). The absorbed dose to water calibration factor for an ion chamber is given by:

$$D_w^Q = k_Q * M * N_{D,w}^{60\text{Co}} \quad (3.1)$$

where D_w^Q is the absorbed dose to water at the reference depth for a beam quality Q , M is the fully corrected electrometer reading, and $N_{D,w}^Q$ is the absorbed dose to water calibration coefficient for an ion chamber located under reference conditions for beam quality Q . k_Q is the chamber-specific quality conversion factor and it accounts for the change in the absorbed dose to water calibration factor between the beam quality of interest, Q , and the ^{60}Co beam quality ($k_Q=1$

for ^{60}Co). For photon beams Section IX B of TG-51 gives values of k_Q for common ion chambers.

NRCC stipulates that the dose to water calibration coefficient for a particular ion chamber and electrometer combination using a ^{60}Co beam is given by the following:

$$N_{D,w}^{60\text{Co}} = \frac{D_w^{60\text{Co}}}{M} \quad (3.2)$$

where $D_w^{60\text{Co}}$ is the dose delivered to the measurement point in the absence of the chamber and M is the corrected electrometer reading.

The corrected electrometer reading is calculated using the following relationship:

$$M = P_{ion} * P_{T,P} * P_{elec} * P_{pol} * M_{raw} \quad (3.3)$$

where P_{ion} is the correction for incomplete ion collection efficiency, $P_{T,P}$ is the correction to standard temperature and pressure, P_{elec} is the electrometer calibration factor, P_{pol} is the correction for chamber polarity effects, and M_{raw} is the raw electrometer reading. In Canada, the electrometer calibration factor is unity because the primary substandard electrometer and ion chamber pair used for absolute dosimetry are calibrated as a single unit at the NRCC.

Beam quality for photon beams is given by, $\%dd(10)_x$, the percent depth dose at 10 cm depth in a water phantom for a source to surface distance of 100 cm and a field size of $10 \times 10 \text{ cm}^2$. The subscript 'x' denotes the dose from photons only without any electron contamination. Quality conversion factors can be

obtained from the Figure 4 in TG-51 for the corresponding $\%dd(10)_x$ values. For photon beams lower in energy than 10 MV, depth dose is measured using an open beam and $\%dd(10)_x = \%dd(10)$. At these lower energies there is no significant electron contamination at 10 cm depth, and therefore, a filter is not required to remove the electrons from the beam. For energies greater than 10 MV, the dose is measured with a 1 mm lead foil positioned about 50 cm from the phantom surface to remove contaminant electrons. The quality factor represented by the percent depth dose at 10 cm for these higher energy beams is given by:

$$\%dd(10)_x = [0.8905 + 0.0015 * \%dd(10)_{pb}] * \%dd(10)_{pb}$$

for $\%dd(10)_{pb} \geq 73\%$

and

$$\%dd(10)_x = \%dd(10)_{pb} \quad \text{for } \%dd(10)_{pb} < 73\% \quad (3.4).$$

3.1.1.2 Day-to-day Linac Output Variation

For each batch of verification films irradiated, linac output checks, or constancy checks, were made to determine relative changes in linac output between measurement days. In this centre, linac output is monitored using a Farmer-type chamber in a constancy device or “jig” that ensures uniform probe position in the linac accessory mount. At the time of absorbed dose measurement using the secondary standard dosimetry system, the clinical practice is to make dosimetry measurements using the Farmer-type chamber in the constancy device. In this manner a factor relating the absorbed dose to water in the reference conditions outlined in TG-51 to the Farmer chamber reading in the constancy device is obtained. The absorbed dose is obtained from the Farmer-type chamber in the “jig” measurements according to Equation 3.5. Initially the dose deposition increases with depth due to the build up of electrons set in motion through photon interactions. At a depth equal to the electron range, a maximum dose is

deposited. This depth is called d_{\max} . At depths deeper than d_{\max} , the dose decreases with depth due to photon attenuation in phantom. For a 6 MV photon beam in water, d_{\max} is 1.5 cm, and for a 15 MV photon beam, d_{\max} is 3.0 cm (Johns and Cunningham 1983). The constancy check dose corresponds to the dose at a reference point, d_{\max} in water at the centre of a 10 x 10 cm² open field for a source-axis distance of 100 cm.

$$D = M_{raw} * \text{linac output factor (cGy/R)} * \frac{760 \text{ (mm Hg)}}{P} * \frac{273.2 \text{ (K)} + T}{295.2 \text{ (K)}} \quad (3.5)$$

where D is the beam output at the reference point in cGy, M_{raw} is the raw electrometer reading, P is the pressure in mm Hg, T is the temperature in °C, and the linac output factor is used to convert the output to dose at the reference point and is specific to the ion chamber, beam energy, and linear accelerator unit.

Doses were corrected for day-to-day output variation by comparing the linac outputs measured by the ion chamber on a reference day to that of a particular day of interest, as follows:

$$Dose_i = Dose_{ref} * \frac{Output_i}{Output_{ref}} \quad (3.6).$$

3.1.2 Measuring a 2-D Dose Distribution

The process of measuring a 2-D dose distribution is shown in Figure 3.1. It involves choosing an appropriate film for the application and then generating a sensitometric curve that relates pixel values to dose for the specific film type, energy, and treatment unit. The treatment field that needs to be verified is then

used to irradiate a film. Once this film has been developed and converted into a pixelated image via the process of film scanning, it is converted into a dose distribution using the calibration sensitometric curve. The resultant dose distribution is then evaluated.

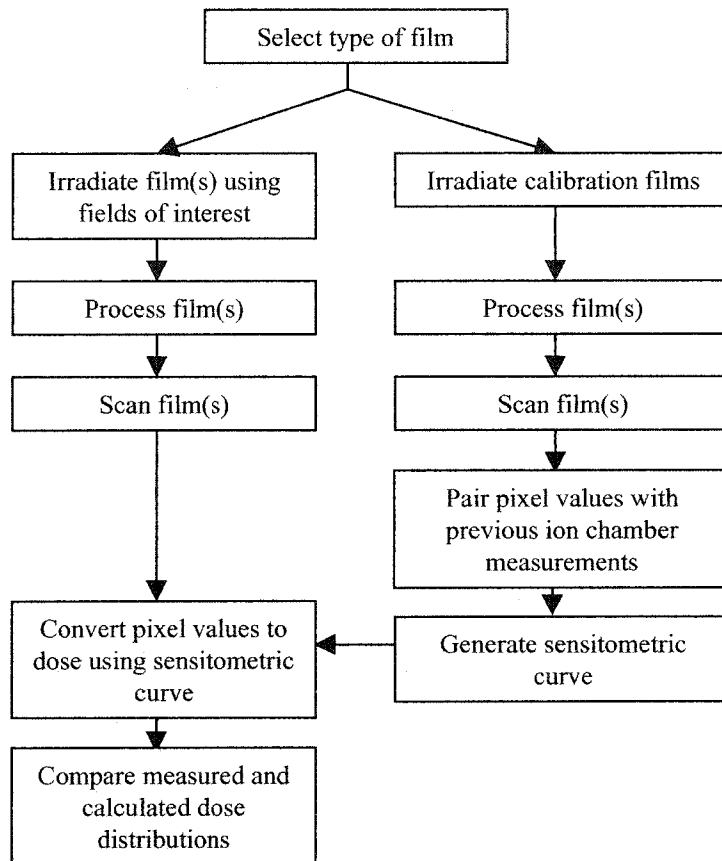


Figure 3.1 Simplified schematic of the film dosimetry process.

3.1.3 General Properties of Film

Radiographic film is composed of silver halide crystals embedded in a gelatin matrix (Figure 3.2). The silver ions in the crystals can be reduced to metallic silver when they are exposed to ionizing radiation or visible light. This chemical change is brought about when electrons in the halide are liberated by the

radiation and then recaptured in the crystal where they convert free silver ions to metallic silver. During film development, only grains with more than about four silver atoms are reduced to metallic silver. While silver halide is transparent, grains that have been reduced to metallic silver become opaque thereby creating a latent image (Barrett and Swindell 1981).

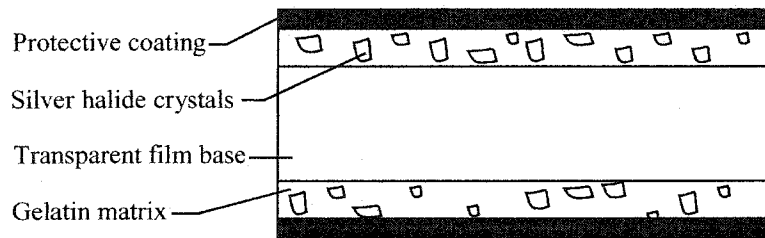


Figure 3.2 Structure of a double-sided radiographic film (Barrett and Swindell 1981).

The opacity of the film is described through the optical density. Optical density is defined as the negative log of the transmittance, T , of the film, which is the ratio of light transmitted through the film, I_t , to light collected without film, I_0 , as shown in Equation (3.7):

$$OD = -\log_{10}(T) = \log_{10} \frac{I_0}{I_t} \quad (3.7).$$

Film is often characterized using a plot of optical density versus the logarithm of radiation exposure or dose, as measured using, for example, an ion chamber. This graph is called the characteristic curve or the H&D curve (named after Hurter and Driffield who first described it in 1890). An example of an H&D curve is shown in Figure 3.3. Sensitometric curves, which are similar to H&D curves, except that the x-axis is dose not log of relative exposure and the y-axis is pixel value not optical density, are used in this work.

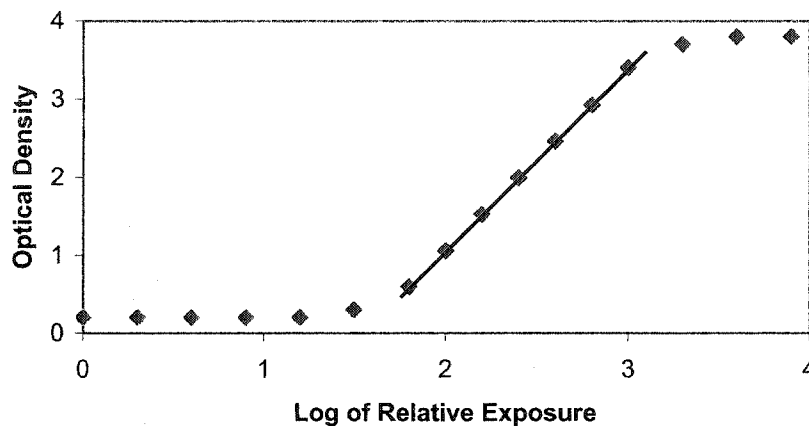


Figure 3.3 Example of an H&D curve.

The latitude of the film is the range of exposures or doses over which the densities will lie in the linear portion of the H&D curve (Johns and Cunningham 1983). The slope of the linear portion of the characteristic curve is often referred to as the film gamma. It is mathematically described as:

$$\gamma = \frac{D_2 - D_1}{\log_{10}(X_2/X_1)} \quad (3.8)$$

where γ is the film gamma, X_1 and X_2 are exposures at two points that lie in the film's latitude, and D_1 and D_2 are their corresponding optical densities from the H&D curve (Johns and Cunningham 1983). In the underexposed region, there is not sufficient radiation to produce enough chemical effect for distinguishing the irradiated area of the film from the film's inherent density plus background fog. Saturation exists in the overexposed regions of the film. In this region, all of the silver halide grains are reduced to metallic silver. Consequently, underexposed and overexposed film regions are not useful for film dosimetry. Typically, a sensitometric curve is sufficient for each batch of film, but in our case, a

sensitometric curve was created for every set of films to limit differences introduced by film processing.

Film has many limitations. Photon energy spectra, film orientation, film emulsion differences, and the processing conditions all affect the film's sensitivity to radiation (Danciu, Proimos et al. 2001). Film irradiated parallel to the beam central axis may exhibit an over-response compared to film irradiated perpendicular to the beam. This over-response may result from an air gap or spectral effects. Because the film response depends on the energy spectrum, its response is also expected to change with depth in a phantom since beam quality changes with depth (Suchowerska, Hoban et al. 2001).

Danciu et al. found the film sensitivity varied insignificantly for films irradiated in perpendicular orientation when the field sizes were equal to or less than $15 \times 15 \text{ cm}^2$ at depths less than 15 cm for photon beams (Danciu, Proimos et al. 2001). The effect of irradiation in the parallel or "edge-on" film orientation is less well known and published results are not consistent. For example, the parallel response was reported to be 4% lower for all beam energies in the maximum dose region only (Danciu, Proimos et al. 2001). Others found a large increase in film response for parallel versus perpendicular film orientation (Suchowerska, Hoban et al. 2001). The last study attributed the over-response to a film air gap that could be eliminated using a 2° gantry offset.

Film is known to over-respond to low-energy photons. For this reason, it is not a very useful tool for doing dosimetry in kilovoltage photon beams but can be used to do fairly accurate dosimetry at megavoltage energies ($\pm 3\%$) (Khan 1994). Film over-response is also a concern for IMRT fields because there is potential for numerous penumbral regions which contain a large proportion of low-energy photons (Ju, Ahn et al. 2002).

Kodak X-Omat V (XV) film, which has a latitude of 5-100 cGy, has been, and continues to be, used extensively for dosimetric applications on linear accelerators. Kodak Extended Dose Range (EDR) film has a higher latitude than XV film (25-400 cGy) (Eastman Kodak Co 2001), and it is also suitable for dosimetric applications. To give a general idea of response for XV and EDR films, measured sensitometric curves are given in Figure 3.4. It can be seen that XV film does not exhibit linearity with dose while the EDR film does.

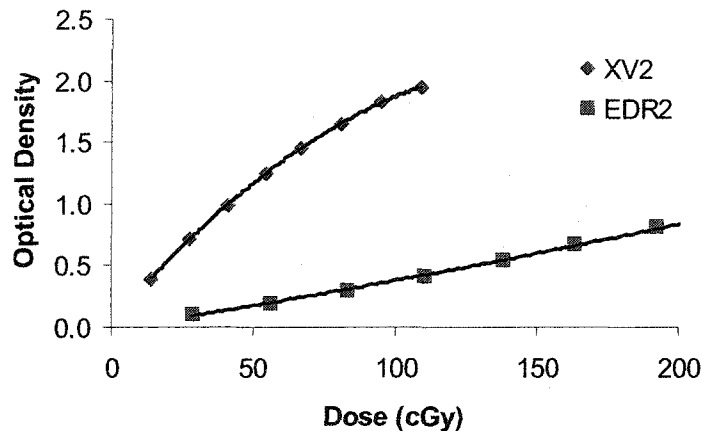


Figure 3.4 Sample sensitometric curves for XV2 and EDR2 film. Recreated from (Childress, Dong et al. 2002).

3.2 Comparison of Dose Distributions

Dose distributions can be compared in two general ways: visually and numerically. Visual inspection is a qualitative and subjective measure of how similar the dose distributions appear. This type of comparison can be used for an approximate evaluation. A number of computer programs have been developed to quantitatively compare dose distributions. Qualitative and quantitative dose distribution comparison techniques are discussed in Section 3.2.1 and Section 3.2.2, respectively.

3.2.1 Qualitatively Comparing Dose Distributions

One method of comparing dose distributions is by visually examining the overlay of the calculated and measured dose distributions. Another visual method is to use two dose difference maps: one for differences where measured doses are greater than calculated doses and the other where measured doses are less than calculated doses (Mah, Antolak et al. 1989).

3.2.2 Quantitatively Comparing Dose Distributions

3.2.2.1 Dose Distribution Comparison Guidelines

In 1993, Van Dyk et al. recommended some guidelines for photon beam percent dose differences and distance to agreements (DTA). The percent dose difference for dose-pixel (i,j) is defined as:

$$\% \text{ dose difference}(i, j) = \frac{(Dose_{meas}(i, j) - Dose_{calc}(i, j))}{Dose_{meas}(i, j)} * 100\% \quad (3.9).$$

The percent dose difference metric is calculated for all dose-pixels in the entire region of interest (ROI) of the measured dose distribution. The distance to agreement is defined as the distance from the calculated dose-pixel to the nearest point or contour of the same value in the measured dose distribution. Once the closest point or contour in the measured dose distribution is found, the distance in units of pixels is determined. The DTA is then calculated by multiplying this distance by the pixel size (in units of mm per pixel). The DTA calculation is illustrated in Figure 3.5.

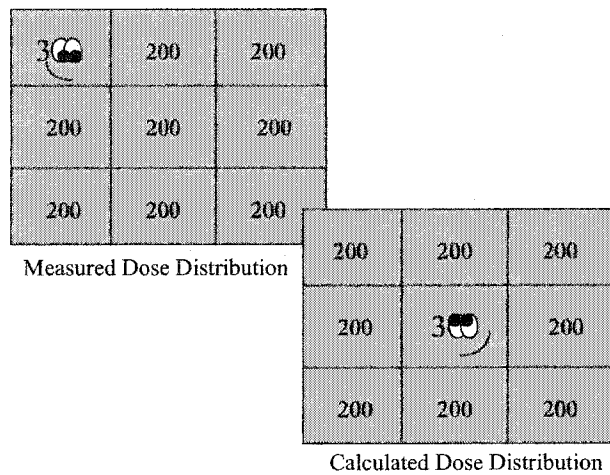


Figure 3.5 Illustration of how distance to agreement is determined. In this figure, the dose-pixel in the calculated dose distribution with a value of 300 searches for the nearest point or contour with a value of 300 in the measured dose distribution. In this case it is $\sqrt{2}$ pixels away and the DTA is $\sqrt{2}$ multiplied by the pixel size.

The DTA is more likely to fail in regions of low-dose gradient even when doses are very similar, and percent dose difference is more likely to fail in regions of high-dose gradient even though like doses may be in very close proximity (Harms, Low et al. 1998). For this reason, different guidelines were proposed for high-dose versus low-dose regions and for high-dose gradient versus low-dose gradient regions. High-dose gradients were defined to be where pixel doses changed $\geq 30\% \text{ cm}^{-1}$ and low-dose regions were less than 7% of the normalization dose. Van Dyk et al. set the dose difference and DTA requirements for open photon beams to be 3% with respect to the normalization dose between measured and calculated doses in high-dose/low-dose gradient regions; 4 mm in high-dose gradient regions; and 3% in low-dose/low-dose gradient regions (Van Dyk, Barnett et al. 1993). These criteria alone, which are useful in determining if two dose-pixels are alike, are not sufficient to determine whether or not two dose distributions are similar. Because a dose distribution contains many dose-pixels, typically on the order of 200x200, there must be an overall measure of agreement between two dose distributions based on the individual dose-pixel pass/fail

results. Van Dyk et al. further recommend that 67% (1 standard deviation) of the dose-pixels agree within the dose difference or DTA specifications (Van Dyk, Barnett et al. 1999).

As described above, in different regions of a treatment field, different agreements can be expected. Several regions of a treatment field, each with a different expected tolerance, have been identified in TG-53 (Fraass, Doppke et al. 1998). These include inner and outer regions, and a penumbra region (Figure 3.6).

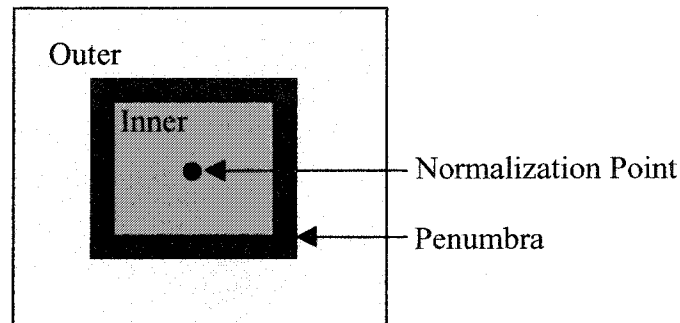


Figure 3.6 Beam's eye view of different regions of a treatment field for a conventional square treatment field (adapted from TG-53).

The inner beam is defined as the central high dose, low dose gradient portion of the beam; the penumbral region is the high dose gradient region ± 0.5 cm along each beam edge; and the outside region is the low dose, low dose gradient region outside the penumbra.

The expected agreement between doses in measured and calculated dose distributions for a square treatment field delivered to a homogeneous phantom by region outlined in TG-53 are the following percent dose difference and DTA values: normalization point 0.5% with respect to the normalization dose, inner region 1.5%, penumbral regions 2 mm, and outer region 2%. For MLC shaped

fields higher achievable thresholds are recommended: 1% for normalization point, 3% for the inner region, 3 mm for penumbral regions, and 5% for the outer region (Fraass, Doppke et al. 1998). Although no thresholds are recommended for IMRT fields, the MLC shaped field recommendations may be a good starting point for determining these values. Some difficulties that arise in threshold determination for IMRT fields are that IMRT fields can have numerous high dose regions and numerous high dose gradient regions dispersed throughout the treatment field for each beam. In addition, a normalization point should be a point that is representative of the PTV dose, and it should be in a low-dose gradient region (ICRU 1993). These requirements may not be met in an IMRT treatment field; therefore, a normalization point may be very difficult to identify.

3.2.2.2 Two Metric Software Tool

Harms et al. developed a software tool that calculated dose differences with respect to a normalization value, as well as, distance to agreements (Harms, Low et al. 1998). The two metrics are calculated independently for all regions and only one of the metrics must pass for a dose-pixel to be in agreement. Because two metrics are calculated, the technique will pass a dose-pixel if the percent difference between the doses is sufficiently low or if equivalent doses are in close proximity. The locations which failed to meet either criteria could be displayed in a binary image (pass or fail).

3.2.2.3 The Gamma Evaluation

Low et al. created the gamma evaluation that simultaneously incorporates the percent dose difference and the distance to agreement metrics to compare dose distributions (Low, Harms et al. 1998). By doing so, a quantitative quality index

was determined for each dose-pixel in the dose distribution images. This numerical quality index could then be presented in a greyscale image. The gamma evaluation software tool allowed the user to specify thresholds for each of the metrics (e.g. 3% for dose difference and 4 mm for DTA).

Because the gamma evaluation is an important precursor to the dose distribution comparison software developed in this work, it will be discussed in more detail than the other dose distribution comparison tools. In the gamma evaluation, the percent dose difference, $\delta(r_m, r_c)$, is defined as the dose, reported as a percent of some normalization dose, at a point in the calculated dose distribution minus the dose at a point in the measured dose distribution. Note that the normalized dose distribution used in the gamma evaluation is not the same as the absorbed dose difference which is also defined as the dose difference between the calculated and measured dose distributions but reported in cGy.

$$\delta(r_m, r_c) = D_c(r_c) - D_m(r_m) \quad (3.10).$$

Similarly, the distance between these two points, $r(r_m, r_c)$ is:

$$r(r_m, r_c) = |r_c - r_m| \quad (3.11).$$

The gamma index for the set of points examined combines dose difference and distances with their respective acceptance criteria as follows:

$$\Gamma(r_m, r_c) = \sqrt{\frac{r^2(r_m, r_c)}{\Delta d_M^2} + \frac{\delta^2(r_m, r_c)}{\Delta D_M^2}} \quad (3.12)$$

where Δd_M is the distance to agreement criteria and ΔD_M is the dose difference criteria. The smallest $\Gamma(r_m, r_c)$ value for each dose-pixel in the measured dose

distribution is then chosen to get the $\gamma(r_m)$ value. Mathematically this is described as:

$$\gamma(r_m) = \min \{ \Gamma(r_m, r_c) \} \forall \{ r_c \} \quad (3.13).$$

According to these equations, a $\Gamma(r_m, r_c)$ value for a point in the measured dose distribution is compared to every other point in the calculated dose distribution. In practice Low et al. placed some constraints on the distance to which dose-pixels would be compared. If $\gamma \leq 1$, the dose-pixel at r_m matches the calculated distribution within the user-specified thresholds, and if $\gamma > 1$, the dose-pixel does not match.

The gamma evaluation was used by Depuydt et al. in a clinical setting where it was found to be an easy way to verify IMRT fields. Once again the acceptance or rejection of data points was based on user-specified criteria for dose differences and DTA.

The gamma evaluation has some limitations. Firstly, at low doses the absorbed dose difference may be more important than percent difference so it should potentially be examined as well. Secondly, it may also be useful to know which criteria (e.g. DTA or percent dose difference) were not met for a given point. Thirdly, sampling may be a problem. In Low et al.'s paper the data was fit to a continuous function but the dose distributions are pixelated images; therefore discrete points must be compared. These shortcomings of the gamma evaluation identified the need to develop a model that uses independent metrics to evaluate the agreement between dose distributions, as described in Section 4.2.1.

3.2.3 Beam's Eye View Software

A beam's eye view (BEV) software tool was created in-house by MacKenzie and others (MacKenzie, Lachaine et al. 2002). The purpose of the software was to compare measured and calculated dose distributions for inverse-planned IMRT treatment fields. We used some of this software in this thesis. A brief description of the software follows. The calculated dose distribution is loaded into Matlab. The measured dose distribution is determined using the measured film image and its corresponding dose – pixel value table. The measured dose distribution is then resampled so that the dose-pixel dimensions are the same size as those in the calculated dose distribution. Rectangular regions of interest for the measured and calculated images are then user-selected. The images are then resized by padding them with the appropriate number of zeros so that the two images are the same size before matching or registering the images. The software then calculates a dose difference map and dose difference histogram, which can be used to visually inspect dose differences between measured and calculated distributions. Maximum and isocentre values for each dose distribution; standard deviation and mean error between dose-pixel values from the two dose distributions; and a ratio of the maximum dose-pixel value in the measured dose distribution to the maximum dose-pixel value in the calculated dose distribution are also calculated.

3.2.4 Image Registration

In order to compare two dose distributions, the two images must be properly aligned. It may be necessary to shift, rotate, and resize one of the images to accomplish this alignment or registration. In this work, image registration was done using both pinprick and cross-correlation techniques.

3.2.4.1 Use of Fiducial Markers and Pinpricks for Image Registration

Image registration can be achieved by superimposing two pairs of fiducial markers to determine the translation, rotation and scaling required to align the fiducial points. This technique uses inherent anatomic information identified by the user to register the images (Toga and Banerjee 1993). Pinpricks made into the film may be used as fiducial markers for orientation of an image and to provide some known spatial co-ordinates.

3.2.4.2 Image Registration using Cross Correlation

The relationship between pixel values of two images, where the images are of the same patient and have been acquired using the same imaging modality, is approximately linear. A normalized cross correlation coefficient, r , can be used to measure alignment between the two images. The normalized cross correlation coefficient is described mathematically as:

$$r(i, j) = \frac{\sum_{x,y} [(f(x, y) - \bar{f})(g(x - i, y - j) - \bar{g})]}{\{\sum_{x,y} [f(x, y) - \bar{f}]^2 \sum_{x,y} [g(x - i, y - j) - \bar{g}]^2\}^{0.5}} \quad (3.14)$$

where $f(x, y)$ is the pixel value for pixel position (x, y) in image f ; $g(x - i, y - j)$, is the pixel value for the pixel in position (x, y) in image g after the image has been shifted by (i, j) ; and \bar{f} and \bar{g} are the average pixel values for each image (Lewis 1995). The correlation coefficient can range between -1 for a perfectly linear negative correlation and 1 for a perfectly linear positive correlation. A value of zero indicates no linear relationship between the two images (Ramsey and Schafer 1997).

The cross correlation matrix is obtained by moving one image with respect to the other and calculating r for each position. The largest value of r in the cross correlation matrix will occur where there is the strongest linear relationship between the pixel values of the two images (Hajnal, Hill et al. 2001). The relative offset between the two images can then be found by subtracting the location of the maximum value of r in the cross correlation matrix from the size of the images. One of the images can then be shifted accordingly to register the two images.

The best alignment is found by moving one image with respect to the other and finding the largest correlation coefficient; this will occur where there is the strongest linear relationship between image intensities.

A limitation of the cross correlation technique is that it would hide a systematic offset in the treatment delivery. Note that the edge of the calculated dose distribution does not necessarily correspond to the edge of the measured dose distribution before registration. An example of systematic offset is the collimator jaws were shifted with respect to the machine isocenter but the dimensions remained correct (Figure 3.7), registration through cross correlation would remove the shift in order to get the largest correlation between the measured and calculated dose distributions. If this type of systematic offset in the treatment delivery went unnoticed, the correct dose would not be delivered to the PTV. Once again, this would jeopardise tumour control or cause organs at risk to receive an intolerable amount of dose. Large systematic offsets can be detected using a technique that uses fiducial markers or pinpricks, or by thoroughly examining the MLC positions to ensure they are correct before the treatment is approved for clinical use.

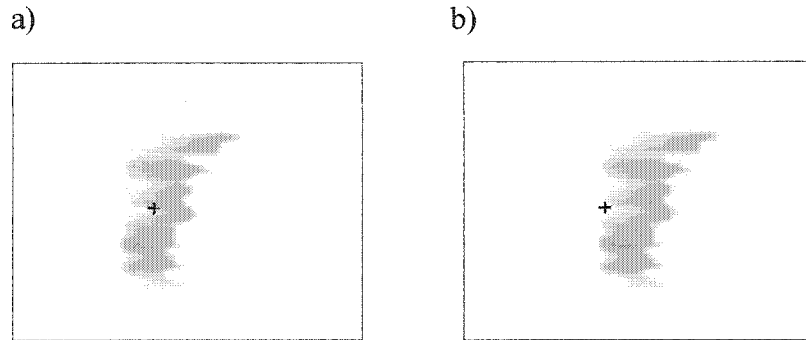


Figure 3.7 Example of systematic offset between two dose distributions. The field shown in (a) depicts the intended treatment field centred at isocenter represented by a "+". The field shown in (b) has been shifted 1.5 cm to the right with respect to isocenter.

3.3 References

- Almond, P. R., P. J. Biggs, B. M. Coursey, W. F. Hanson, M. S. Huq, R. Nath and D. W. Rogers (1999). "AAPM's TG-51 protocol for clinical reference dosimetry of high-energy photon and electron beams." *Med Phys* **26**(9): 1847-70.
- Barrett, H. H. and W. Swindell (1981). *Radiological Imaging - The Theory of Image Formation, Detection, and Processing*. New York, NY, Academic Press, Inc.
- Childress, N. L., L. Dong and Rosen, II (2002). "Rapid radiographic film calibration for IMRT verification using automated MLC fields." *Med Phys* **29**(10): 2384-90.
- Danciu, C., B. S. Proimos, J. C. Rosenwald and B. J. Mijnheer (2001). "Variation of sensitometric curves of radiographic films in high energy photon beams." *Med Phys* **28**(6): 966-74.
- Depuydt, T., A. Van Esch and D. P. Huyskens (2002). "A quantitative evaluation of IMRT dose distributions: refinement and clinical assessment of the gamma evaluation." *Radiother Oncol* **62**(3): 309-19.
- Eastman Kodak Co (2001). Health Imaging. **2002**. <http://www.kodak.com/>

- Fraass, B., K. Doppke, M. Hunt, G. Kutcher, G. Starkschall, R. Stern and J. Van Dyke (1998). "American Association of Physicists in Medicine Radiation Therapy Committee Task Group 53: quality assurance for clinical radiotherapy treatment planning." Med Phys **25**(10): 1773-829.
- Hajnal, J. V., D. L. G. Hill and D. J. Hawkes, Eds. (2001). Medical Image Registration, CRC Press.
- Harms, W. B., Sr., D. A. Low, J. W. Wong and J. A. Purdy (1998). "A software tool for the quantitative evaluation of 3D dose calculation algorithms." Med Phys **25**(10): 1830-6.
- Johns, H. E. and J. R. Cunningham (1983). The Physics of Radiology. Springfield, Il, Charles C Thomas.
- Ju, S. G., Y. C. Ahn, S. J. Huh and I. J. Yeo (2002). "Film dosimetry for intensity modulated radiation therapy: dosimetric evaluation." Med Phys **29**(3): 351-5.
- Khan, F. M. (1994). The Physics of Radiation Therapy. Baltimore, MD, Lippincott Williams & Wilkins.
- Lewis, J. P. (1995). Fast normalized cross-correlation. Industrial Light & Magic.
- Low, D. A., W. B. Harms, S. Mutic and J. A. Purdy (1998). "A technique for the quantitative evaluation of dose distributions." Med Phys **25**(5): 656-61.
- MacKenzie, M. A., M. Lachaine, B. Murray, B. G. Fallone, D. Robinson and G. C. Field (2002). "Dosimetric verification of inverse planned step and shoot multileaf collimator fields from a commercial treatment planning system." J. Appl. Clin. Med. Phys. **3**(2): 97-109.
- Mah, E., J. Antolak, J. W. Scrimger and J. J. Battista (1989). "Experimental evaluation of a 2D and 3D electron pencil beam algorithm." Phys Med Biol **34**(9): 1179-94.
- Ramsey, F. L. and D. W. Schafer (1997). The Statistical Sleuth: A course in methods of data analysis. Belmont, CA, Duxbury Press.
- Suchowerska, N., P. Hoban, M. Butson, A. Davison and P. Metcalfe (2001). "Directional dependence in film dosimetry: radiographic and radiochromic film." Phys Med Biol **46**(5): 1391-7.

Toga, A. W. and P. K. Banerjee (1993). "Registration revisited." Journal of Neuroscience Methods **48**: 1-13.

Van Dyk, J., Ed. (1999). Radiation Oncology Overview. The Modern Technology of Radiation Oncology: A Compendium for Medical Physicists and Radiation Oncologists. Madison, WI, Medical Physics Publishing.

Van Dyk, J., R. B. Barnett and J. J. Battista, Eds. (1999). Computerized Radiation Treatment Planning Systems. The Modern Technology of Radiation Oncology. Madison, WI, Medical Physics Publishing.

Van Dyk, J., R. B. Barnett, J. E. Cygler and P. C. Shragge (1993). "Commissioning and quality assurance of treatment planning computers." I J Rad Oncol Biol Phys **26**(2): 261-73.

Chapter 4 Materials and Methods

Chapter 4 discusses the specific film dosimetry methods and dose distribution comparison techniques used in this work.

4.1 Dosimetry

4.1.1 Selection of Film

Two films exhibiting properties good for megavoltage photon dosimetry are Kodak X-Omat V (XV) and Kodak EDR2 films. Both films are readily available at the Cross Cancer Institute. Films were compared by examining their sensitometric curves, and their spectral responses to perpendicular and parallel irradiation cases.

4.1.2 Generation of Sensitometric Curves

Traditionally, sensitometric curves are created using multiple films with a different dose delivered to each film. In this setup, dose is delivered to each film using, for example 10x10 cm², square fields. To simplify and reduce the time required to create the sensitometric curve, a step window method has been employed by some centres (Childress, Dong et al. 2002; Gagne, Warkentin et al. 2002; MacKenzie, Lachaine et al. 2002). In the step window technique, which was used in this work, multiple subfields on the same film receive different doses. All doses were delivered using 6 or 15 MV photon beams on a Varian 2300 EX linear accelerator equipped with a 120-leaf MLC (Varian Oncology Systems, Palo Alto, CA).

Calibration step windows were generated in Solid Water™ (Gammex RMI, Middleton, WI). Each film type was exposed perpendicularly to the central axis at a 10 cm depth (Figure 4.1) to 6 MV and 15 MV IMRT step and shoot patterns consisting of 12, 4 x 4 cm², subfields set in a 19.6 x 22.4 cm² collimated field (Figure 4.2). The dose delivered to each subfield was varied to approximately cover the recommended dose range of each film (Table 4.1). Recall, the latitude of XV film is 5-100 cGy and for EDR film it is 25-400 cGy.

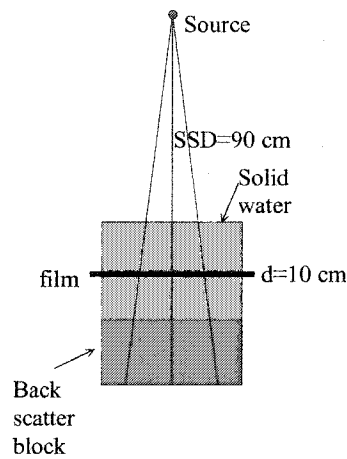


Figure 4.1 Experimental setup for generating sensitometric curve.

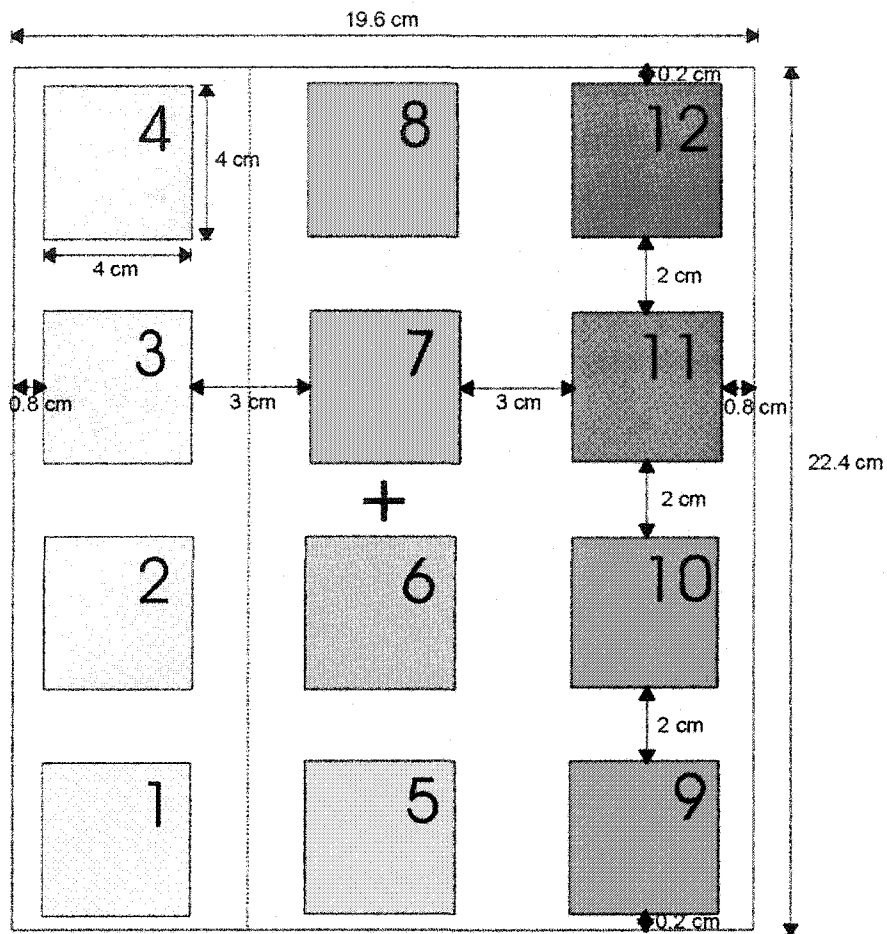


Figure 4.2 Film calibration step window.

| Subfield Number | Calibration Step Window (XV) | Calibration Step Window (EDR) |
|-----------------|------------------------------|-------------------------------|
| 1 | 10 | 40 |
| 2 | 20 | 80 |
| 3 | 30 | 120 |
| 4 | 40 | 160 |
| 5 | 50 | 200 |
| 6 | 60 | 240 |
| 7 | 70 | 280 |
| 8 | 80 | 320 |
| 9 | 90 | 360 |
| 10 | 100 | 400 |
| 11 | 110 | 440 |
| 12 | 120 | 480 |

Table 4.1 Number of monitor units delivered to each subfield for irradiation of calibration step window for XV and EDR films.

4.1.2.1 Ion Chamber Measurements

An Exradin A12 farmer type ion chamber was centred in each of the 12 subfields in order to get a dose at 10 cm depth in Solid WaterTM for each of the subfields. The chamber has a sensitive volume of 0.651 cm³ (Med-Tec 2002) and was paired with a Capintec Model 192 electrometer. The ion chamber, electrometer and cable were calibrated as a primary substandard at the NRCC. Ion chamber measurements were taken with a source to surface distance of 90 cm and then converted to absorbed dose in accordance with the TG-51 protocol.

When the ion chamber doses are applied to measurements made on a different day, drift in the linear accelerator was accounted for by multiplying the dose values by a ratio of output factors as described in Equation 3.6.

4.1.2.2 Film Irradiation for Sensitometric Curves

Films in ready-pack radiation envelopes were placed at 10 cm depth in solid water with a source to surface distance of 90 cm. The XV film was irradiated with 240 MU using the step window MLC file to give a maximum dose of about 90-100 cGy to the subfield with the highest dose. Similarly the EDR film was irradiated with four times the MU (960) to give a maximum dose of about 350-400 cGy to the subfield with the highest dose (Table 4.1).

4.1.2.3 Creation of Sensitometric Curves

A software tool was developed using Matlab (The Math Works, Natick, MA) to generate a sensitometric curve from step window films and respective ion chamber measurements. To determine the average pixel value at the centre of each subfield, the user first outlines a rectangle enclosing all of the subfields by clicking on the outermost corners. The software then automatically determines the centre of each subfield and selects a user-specified number of pixels to average over. These regions are then displayed to ensure proper alignment. Average subfield pixel values are then paired with doses previously measured using the ion chamber and corrected for linac output and number of monitor units delivered to the step window. An additional data pair of zero dose and background pixel value was also added to the sensitometric curve in order to set the lowest limit of dose and pixel value. Pixel values below this minimum value, which occur rarely due to film emulsion differences, are assigned zero dose. The data was then fit using a 3rd order polynomial, which gave the best consistent fit to the pixel value and dose data. A sensitometric output data set file was then created with doses calculated for integer pixel values from 0 to 255. This software was used to generate a sensitometric data set for each step window film created in

this work. The sensitometric data sets could then be used to convert pixelated images into absorbed dose distributions comprised of dose-pixels.

4.1.3 Generation of Calculated Dose Distribution

To generate the calculated dose distributions for patient treatment, Helax-TMS is used to determine beam parameters such as beam directions, beam weights, and MLC positions to provide a desirable dose distribution. For verification purposes, the patient treatment field is altered so that films can be irradiated with 0° gantry and collimator rotations, and the calculation is performed in a BEV plane at 10 cm depth in a flat water tank. The rest of the field parameters remain identical to those of the planned treatment field.

4.1.4 Generation of Measured Dose Distribution

To generate the measured dose distributions, film is irradiated using the calculated verification treatment field at 10 cm depth in solid water using the setup shown in Figure 4.1. Once this film has been processed and scanned, the 2-D pixelated image is converted to a 2-D dose distribution using the sensitometric data set generated using the calibration step window irradiated on the same day.

4.1.5 Film Processing

Films were developed using a Kodak X-Omat 270 RA processor (Eastman Kodak Co., Rochester, NY). Films were scanned using a VIDAR VXR film digitizer (VIDAR Systems Corp, Herndon, VA) with a 71 dpi resolution and 8-bit depth. The film digitizer was calibrated prior to scanning each set of film to “compensate for variations from pixel to pixel in both the white and black ends of the greyscale to produce an even, consistent scan” (VIDAR 1998). We assume

that this means that the light is turned off on the scanner to set the black end of the greyscale to 255 and the light is turned on with no film in the scanner to set the white end of the greyscale to 0.

A new sensitometric curve was generated for each set of irradiated films. By doing so, errors due to changes in linac output and beam quality, processing, and scanning could be limited. The accuracy of film dosimetry is sensitive to processing conditions including temperature, concentration of chemicals, time film spends in each chemical bath, and emulsion differences between films and within a film (Johns and Cunningham 1983; Khan 1994; Bushberg, Seibert et al. 2002). Since slight variations in film speed are expected between film batches (Bushberg, Seibert et al. 2002), XV and EDR2 films for a given analysis were taken from the same respective boxes. The automatic film processor regulates chemical concentrations and developer temperature. To ensure processor stability, however, the processor was left on for research use after being used clinically for the day and the 'ready' light for the internal temperature sensor was checked before films were developed. Additionally, two previously processed films and an unexposed film was processed prior to the films of interest, and the films for each analysis were irradiated, developed and scanned as a group to minimize any small differences in linac output, processing and scanning conditions.

4.1.6 Film Scanning

For the sake of simplicity, pixel values not optical density values are used in the film dosimetry techniques. Data from the film digitizer was converted to pixel values using the linear optical density translation table built into the Vidar software. Pixel values are approximately linearly related to optical density by the following equation (VIDAR 1998):

$$\text{pixel value} = \frac{256}{3.0} * OD \quad (4.1).$$

The assumption that pixel values are linearly related to optical density was investigated by comparing average scanned pixel values in the central region of each of the subfields to the optical density measurements taken with a densitometer at the centre of the subfields for five different films.

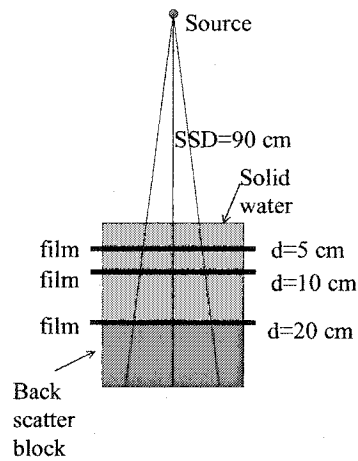
In addition, it has been suggested that VIDAR scanners are highly non-linear in the horizontal direction due to scatter from the scanning light (Childress and Rosen 2003). The optical density versus pixel value comparison was used to investigate this. If the scanner introduced error horizontally, the scanned pixel values would not be linearly related to optical density.

4.1.7 Examination of Film Spectral Response

Film response to radiation was examined to see if sensitometric curves generated from a calibration step window orientated perpendicular to the beam at 10 cm depth could be used to generate sensitometric curves at other orientations and depths. If films exhibited a large spectral response, each orientation and depth that dose needs to be determined at, would require a step window film to be irradiated in the same geometry. To investigate the spectral response of the film, calibration step windows were irradiated at 5 and 20 cm depths and in a parallel orientation relative to the beam and compared to the perpendicular irradiation at 10 cm. (Figure 4.3(a)). It is assumed that the film thickness is negligible and that the film does not significantly perturb the radiation beam. Subfield pixel values for the step window irradiated at 5 and 20 cm depth were converted to dose using the sensitometric calibration curves established at 10 cm depth. The dose from

these three irradiated films was then compared to point doses measured at 10 cm depth and corrected for differences in depth using percentage depth dose. Differences between the calculated and measured doses at 5 and 20 cm determined from the perpendicular film irradiation might indicate a spectral dependence of the film. If, however, the calculated and measured values are well matched, the method of using the sensitometric curve generated at 10 cm depth to calculate dose at any depth of film may be justified.

a)



b)

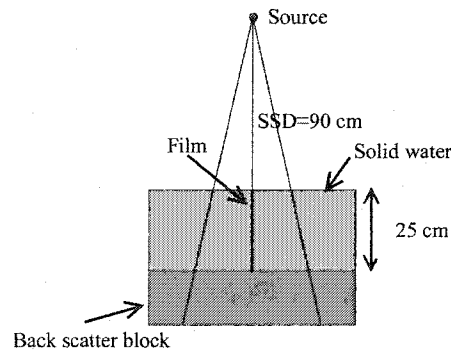


Figure 4.3 Experimental setup for perpendicular (a) and parallel (b) film irradiation

To examine the validity of using the perpendicular calibration step window for determining doses for films irradiated at different orientations, the films were sandwiched between sheets of solid water and then irradiated “edge on” by a 15 MV beam with a 10x10 cm² field (Figure 4.3(b)). The dose distribution delivered to the film was then determined by scanning the film and creating a map of pixel values for the film. The pixel values were converted to dose using the calibration curves established at 10 cm depth. A Matlab program was developed to find the dose profiles of the irradiated films in the horizontal and vertical directions. These dose profiles for XV and EDR film were then plotted against Helax-calculated dose profiles to see how well the experimental results agreed.

4.1.8 Determination of Error in Film Dosimetry Technique

Errors in ion chamber measurements and pixel values of the calibration step window films for the 12 subfields were determined by repeating measurements and irradiating multiple films, respectively. The ion chamber measurements were repeated during the same experiment and on different days while the pixel value measurements were taken for 5 different films that were irradiated, processed, and scanned as a batch.

Errors introduced in dose by fitting sensitometric measurement points were determined by generating sensitometric curves for 5 different calibration step window films. The error was determined by comparing measured subfield doses to those calculated using the equation of the best-fit 3rd order polynomial line. For example, the dose measured in subfield 1 was compared to the dose calculated when the pixel value for subfield 1 was input in the equation of the best-fit line.

4.2 Comparison of dose distributions

4.2.1 Quantitative Comparison of Dose Distributions using DDComp

The Dose Distribution Comparitor software (DDComp) developed as a part of this project uses three metrics to compare dose distributions: percent dose difference, absorbed dose difference, and distance to agreement (DTA) (Hudson, Fallone et al. 2003). The absorbed dose difference at dose-pixel (i,j) is defined by:

$$\text{Absorbed dose difference}(i, j) = Dose_{meas}(i, j) - Dose_{calc}(i, j) \quad (4.2).$$

The percent dose difference and DTA were calculated as described in Section 3.2.2.1. The DTA metric was only calculated in high-dose gradient regions. In this software, the metrics are evaluated independently and if a dose-pixel passes at least one of the metric criteria, it passes the combined metric and the dose-pixel is deemed to be the same in both the measured and calculated dose distributions. Passing dose-pixels are depicted by zeros; whereas, failing dose-pixels are shown as ones. To determine whether or not a dose-pixel passes the metric analysis, the binary results of the three metrics are multiplied. Consequently, if any of the metrics has a binary result of 0 (pass) for a given dose-pixel, the combined metric result is also 0 (pass) for that dose-pixel. In low-dose regions where DTA was not calculated, a result of 1 (fail) is assigned for the combined metric calculation only. As a result, the combined metric in these regions depends only on the absorbed dose difference and percent dose difference metrics.

The absorbed dose difference may be more important than percent dose difference especially at low and high doses. For example, 5% of 10 cGy is only 0.5 cGy which may not be a clinically relevant dose difference; whereas 5% of 4 Gy is 20 cGy which is probably an unacceptable dose difference. As stated earlier, a maximum difference of 5% between the prescribed and delivered dose is a reasonable clinical goal. In terms of absorbed dose, for a typical dose of 2 Gy per fraction, this translates to about a 10 cGy threshold. A reasonable spatial accuracy requirement for patient and organ positioning is 4 mm (Van Dyk 1999). These clinically relevant goals were considered when thresholds for these works were set.

If all of the pixels in a given region of the calculated dose distribution are higher or lower than the dose-pixels in the same region of the measured dose distribution, an equivalent pixel must be found outside that particular region. In other words, it will have a large DTA. For this reason, we expect DTA to be sensitive to the magnitude and sign of absorbed dose differences between the dose distributions, and to the spatial distributions of high and low dose regions in the dose distributions.

Dose-pixels were omitted from the DTA analysis if a matching value was not found in the measured dose distribution. For example, if the maximum dose in the calculated dose distribution does not exist in the measured dose distribution. Similarly, a dose-pixel was omitted from the entire analysis if the measured dose-pixel value was less than, for example, 2% of the maximum dose. The purpose of this user-selected low-dose rejection threshold is to avoid a possible division by zero in the percent dose difference calculation and to select the region of interest in which the dose distributions are compared.

DDComp requires that the calculated and measured dose distributions be registered, that they have dose-pixels that are the same size and that the dose matrices be the same size (e.g. the same number of rows and columns in the dose calculation matrix). User input to DDComp includes thresholds for the 3 metrics; input files of measured and calculated dose matrices; and a low-dose rejection threshold. The software tool outputs a number of numerical results and figures. Statistics are given for each of the three metrics including the number of dose-pixels analyzed, and the number and percentage of dose-pixels that failed. Visual outputs are images of the two input dose distributions; images showing the magnitude of the three metrics at each dose-pixel; histograms for each of the three metrics; a combined metric pass/fail histogram; an image showing the number of metrics passed (0-3); and a polar plot of the DTA metric. The polar plot is a plot of the direction and magnitude of the DTA metric and it can be used to identify a systematic offset of one dose distribution with respect to the other. In order to exaggerate the appearance of any systematic offset, only the dose-pixels in the top 25th percentile with respect to dose were used in the polar plot.

4.2.2 Image Resampling and Registration

The IMRT BEV verification software, previously developed in-house, was used to convert the scanned films to dose distributions; to resample the film's dose distribution to match the resolution of the calculated dose distribution; and to register the images using cross correlation. To investigate physical offsets between the dose distributions that would be masked by the cross-correlation technique as described in Section 3.2.4.2, an additional image registration technique using film pinpricks was developed. For this second type of image registration, point markers were drawn on a shielding tray (Figure 4.4). The tray with the position markers was then placed in the tray mount, to create the corners of a 24 x 28 cm² rectangle at 10 cm depth. To maintain correct orientation, additional position markers were drawn on two of the corners.

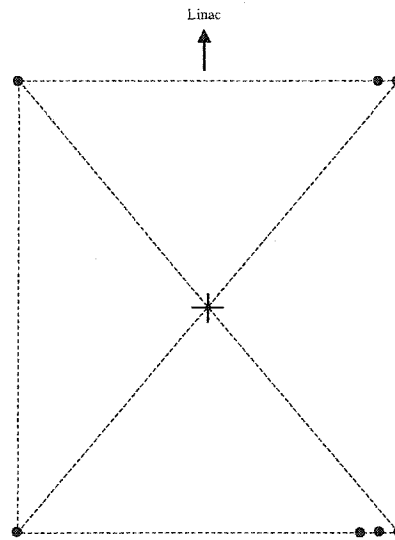


Figure 4.4 Schematic of pinprick positioning tray. Isocentre and connector lines are included to show relative geometry.

The location of the pinpricks was chosen such that they were well outside most IMRT treatment fields but would still fit on a standard piece of film. After irradiating and developing the film, the treatment isocentre was determined in the measured dose distribution by connecting the two sets of diagonal corner markers and finding the point of intersection (Figure 4.4). The correct orientation of the measured image was obtained by rotating the image until the line connecting the top two pinpricks became a horizontal line on the image display screen. To register the measured and calculated dose distributions, isocentres were physically overlaid.

A method for determining the accuracy of image registration and two methods for determining the correlation between two images were investigated. Various test cases, consisting of two images, were registered using the Matlab normalized cross correlation function. The maximum cross correlation value, the offset between the maximum cross correlation value and the centre of the cross correlation matrix, and the full width at half maximum (FWHM) of the cross

correlation matrix were then determined. Since the images were first registered during the IMRT BEV verification process, peak offsets of zero in the x and y directions are expected. If the offset is zero, the images are perfectly aligned (Mathworks 2003). In addition, the better the correlation between the two images, the closer the peak cross correlation value will be to 1 (Toga and Banerjee 1993) and the sharper the peak will be, therefore the smaller the FWHM is expected to be.

Use of the FWHM has a few inherent problems for application with the cross-correlation matrix. First of all, the FWHM is a 1-D measure while the cross-correlation matrix is 2-D and is not, in general, radially symmetric. In this work, the FWHM was taken to be the average of the FWHM for a slice through the peak cross correlation value in both the x and y directions. In addition, the size of the cross-correlation matrix and its shape affect the FWHM. It is thought that, because the cross correlation matrix does not necessarily follow a Gaussian distribution, the FWHM may not be a good representation of the correlation between two registered images.

To test the sensitivity of the FWHM and the cross correlation value to the goodness of fit, 6 test cases were registered using cross correlation and peak offset, peak cross correlation value and FWHM were calculated. The test cases compared two identical dose distributions, two dose distributions from two different treatment fields, two identical dose distributions but with one of them shifted with respect to the other, and a few calculated/measured dose distribution pairs.

For the clinical applications of this work, dose distributions were registered first with pinpricks to look for large systematic offsets between them,

and then with cross correlation for a more accurate registration. Peak offsets were then examined to ensure images were properly registered.

4.2.3 Test Cases to Validate DDComp

In order to examine the correct operation of the DDComp program, multiple test cases were run through the software and compared to manual calculations. A test case was performed for each combination of pass and failure for each of the 3 metrics (percent dose difference, absorbed dose difference, and distance to agreement) (Table 4.2).

| Test Case # | Abs. Dose Diff. | % Dose Diff. | DTA | Combined |
|-------------|-----------------|--------------|------|----------|
| 1 | Pass | Pass | Pass | Pass |
| 2 | Pass | Fail | Pass | Pass |
| 3 | Fail | Pass | Pass | Pass |
| 4 | Fail | Fail | Pass | Pass |
| 5 | Pass | Pass | Fail | Pass |
| 6 | Pass | Fail | Fail | Pass |
| 7 | Fail | Pass | Fail | Pass |
| 8 | Fail | Fail | Fail | Fail |

Table 4.2 Metric pass/fail for software test cases. "Pass" means that all of the dose-pixels met the metric criteria; "fail" means that some of the dose-pixels in the matrix did not meet the metric criteria.

Hypothetical 3x3 measured and calculated dose distributions, in units of cGy, are given in Table 4.3.

| Measured Dose | | | Calculated Dose | | |
|---------------|-----|-----|-----------------|-----|-----|
| (cGy) | | | (cGy) | | |
| 200 | 200 | 200 | 205 | 205 | 205 |
| 200 | 200 | 200 | 205 | 200 | 205 |
| 200 | 200 | 200 | 205 | 205 | 205 |

Table 4.3 Simple hypothetical measured and calculated dose distributions (cGy).

Manual calculations for the three metrics are given in Table 4.4 for the two dose distributions shown in Table 4.3. The DTA calculations in the following table are given in units of dose-pixels rather than in millimetres.

| Abs. Dose Diff. | % Dose Diff. | DTA |
|-------------------------------------------|-------------------------------------------------|-------------------------------------------------|
| (cGy) | | (dose-pixels) |
| $\begin{bmatrix} 5 & 5 & 5 \end{bmatrix}$ | $\begin{bmatrix} 2.5 & 2.5 & 2.5 \end{bmatrix}$ | $\begin{bmatrix} 1.41 & 1 & 1.41 \end{bmatrix}$ |
| $\begin{bmatrix} 5 & 0 & 5 \end{bmatrix}$ | $\begin{bmatrix} 2.5 & 0 & 2.5 \end{bmatrix}$ | $\begin{bmatrix} 1 & 0 & 1 \end{bmatrix}$ |
| $\begin{bmatrix} 5 & 5 & 5 \end{bmatrix}$ | $\begin{bmatrix} 2.5 & 2.5 & 2.5 \end{bmatrix}$ | $\begin{bmatrix} 1.41 & 1 & 1.41 \end{bmatrix}$ |

Table 4.4 Absorbed dose difference, percent dose difference and DTA matrices calculated for the above measured and calculated dose distributions.

Desired metric pass/fail combinations were achieved by altering the metric pass criteria according to Table 4.5.

| Test Case # | Abs. Dose Diff. (cGy) | % Dose Diff. | DTA (dose-pixels) |
|-------------|--------------------------|--------------|----------------------|
| 1 | 5 | 2.5 | 1.41 |
| 2 | 5 | 2 | 1.41 |
| 3 | 4 | 2.5 | 1.41 |
| 4 | 4 | 2 | 1.41 |
| 5 | 5 | 2.5 | 1 |
| 6 | 5 | 2 | 1 |
| 7 | 4 | 2.5 | 1 |
| 8 | 4 | 2 | 1 |

Table 4.5 Test case criteria to achieve metric pass/fail combinations shown in Table 4.2.

The distance to agreement polar plot was tested by taking two simple and identical matrices, shifting one of them by a known amount, and then examining the direction and magnitude of offset in the plot. To test the polar plot with larger matrices, a calculated dose distribution was created by taking a clinical measured dose distribution and shifting it by 10 dose-pixels in one or two of the cardinal directions. One such polar plot created using two matrices, 1 shifted with respect to the other, is shown in Section 5.2.3.

4.2.4 Dependence of DDComp on Various Parameters

The following five parameters were investigated for their effect on the comparison of dose distributions: the method of selecting the region of interest, error/noise in the dose distributions, dose distribution normalization, changing the reference dose distribution from the measured to the calculated dose distribution, and the values of the metric thresholds. Unless otherwise specified, thresholds for

these investigations were set to 5 cGy for absorbed dose difference, 3% for percent dose difference and 4 mm for DTA.

4.2.4.1 Selection of Region of Interest

A region of interest is selected where the dose distributions are to be compared. The region of interest (ROI) can be selected in two ways. The first is manually by having the user click around the region of the dose distribution image that included the treatment field plus the penumbral regions. The second is to have the user input a percent of the maximum dose below which values are considered to be background and not to be included in the comparison. For example, if the maximum dose in the measured dose distribution is 100 cGy and the user inputs 2 % as the background dose, then metrics are not calculated for pixels with doses below 2 cGy. Although the first method allows the user to define the ROI based on his or her expertise, we thought the use of a background threshold value was a better option for two reasons. Firstly, the manual ROI selection technique requires user interaction. This is not only time-consuming but it also introduces user bias. For example, if the user knows there will be a discrepancy between the two dose distributions in a certain region, he or she may wish to leave it out of the analysis. Secondly, the manual ROI selection method has the potential of leaving out penumbral regions where there may be disagreement between the measured and calculated doses.

4.2.4.2 Dose Distribution Uncertainties

The effect of uncertainties in the measured and/or calculated dose distribution to the dose comparison results was investigated by applying “noise” to the dose-pixels in a dose distribution (Equation 4.3) and seeing how this affected the results of DDComp. The noise is set by generating a pseudo-random number in Matlab from a Gaussian distribution with a mean of 0 and a variance of

1, and by multiplying this number by the desired variance, σ , to specify the amount of noise added. The doses and random numbers are given in units of cGy.

$$Dose(i, j) = Dose(i, j) + (random\ number) * \sigma \quad (4.3).$$

Uncertainties in the measured dose can arise from a number of factors including film emulsion non-uniformities, processing errors, and scanning errors. In this investigation, the measured dose distribution with the added noise is compared to the same measured dose distribution without the added noise. Hence, all dose-pixels that fail any of the comparison metrics fail due to the introduction of noise.

4.2.4.3 Dose Distribution Normalization

The effect of normalizing the calculated dose distribution to the measured dose distribution was investigated. The calculated dose distribution was normalized to either: 1) the maximum dose-pixel value in the measured dose distribution or 2) the mean dose-pixel value in the measured dose distribution ROI. To normalize the calculated dose distribution to the maximum dose-pixel value, all of the dose-pixel values in the calculated dose distribution were multiplied by a ratio of maximum dose-pixel value in the measured dose distribution to the maximum pixel value in the calculated dose distribution as described by Equation 4.4.

$$Dose(i, j)_{calc} \text{ normalized to max} = Dose(i, j)_{calc} * \frac{Max_{meas}}{Max_{calc}} \quad (4.4).$$

Likewise, to normalize the calculated dose distribution by mean dose-pixel value, all of its dose-pixels were multiplied by the mean dose-pixel value in the

measured dose distribution and divided by the mean dose-pixel value in the calculated dose distribution as described by Equation 4.5.

$$Dose(i, j)_{calc} \text{ normalized to mean} = Dose(i, j)_{calc} * \frac{Mean_{meas}}{Mean_{calc}} \quad (4.5).$$

4.2.4.4 Definition of the Reference Dose Distribution

In order to do a comparison between two dose distributions, one is chosen to be the reference dose distribution and the other the comparison dose distribution. In this work, the measured dose distribution is considered to be the reference dose distribution and the calculated dose distribution is considered to be the comparison dose distribution. If the definitions of the reference and comparison dose distributions are reversed, different results may be obtained. To determine how the results are affected, the measured and calculated dose distributions for IMRT treatment beams were defined both ways, and the metric results were compared.

4.2.4.5 Impact of Changing Metric Thresholds for the Metrics

The metric thresholds could have a big impact on the pass/fail statistics in the comparison of dose distributions. The sensitivity to the thresholds was investigated for each metric by varying the threshold slightly for a given metric while leaving the thresholds of the other two metrics at their default values. In addition, the impact of the individual metrics was determined by setting the thresholds for the other two metrics to zero. By doing so, all dose-pixels that passed did so by satisfying one metric's criteria.

4.3 Clinical Application

The film dosimetry technique was first applied to some conventional square fields to look at its clinical applicability in simple situations. 5x5 and 10x10 cm² square fields were created using the collimator jaws. XV film was then placed at 10 cm depth in solid water with an SSD of 90 cm. Four films were irradiated for the conventional square field analysis: a 5x5 cm² and 10x10 cm² irradiated with 100 MUs for both 6 MV and 15 MV photons. A calibration step window for each beam energy was delivered to another film during the same experiment that the square fields were irradiated. The resulting sensitometric curves were then used to convert the pixel values to a dose distribution. Helax-TMS was used to calculate dose distributions on a square water phantom irradiated with a 5x5 cm² field and a 10x10 cm² field. DDComp was then used to compare the measured and calculated dose distributions in terms of absorbed dose difference, percent dose difference, and distance to agreement.

To investigate more complex clinical situations, XV verification films were irradiated for each of the treatment beams comprising several IMRT treatments. Calculated and measured dose distributions were then compared using DDComp. Five IMRT patient treatments, 8 beams each, were analyzed to establish metric statistics representative of previous clinically approved IMRT plans. A single IMRT beam was also verified on 3 different days to look at the reproducibility of the process.

Metric thresholds for percent dose difference and distance to agreement were set according to those suggested by Van Dyk et al. as discussed in Section 4.2.1. Specifically, percent dose difference threshold was set to 3% and distance to agreement threshold was set to 4 mm. The absorbed dose difference threshold was chosen to be 5 cGy. All 3 metrics were calculated in high-dose

gradient regions but only the percent dose difference and absorbed dose difference metrics were calculated elsewhere.

4.4 References

- Bushberg, J. T., J. A. Seibert, E. M. Leidholdt and J. M. Boone (2002). The Essential Physics of Medical Imaging. Philadelphia, PA, Lippincott Williams & Wilkins.
- Childress, N. L., L. Dong and Rosen, II (2002). "Rapid radiographic film calibration for IMRT verification using automated MLC fields." Med Phys **29**(10): 2384-90.
- Childress, N. L. and I. Rosen (2003). DoseLab 3.04 User Manual. <http://dosedlab.sourceforge.net/manual.html>
- Gagne, I., B. Warkentin, H. Thompson, M. A. MacKenzie and G. C. Field (2002). "A procedure to improve the reliability of IMRT film verification." Med Phys **29**(8): 1943.
- Hudson, A. D., B. G. Fallone and G. C. Field (2003). "A Software Tool to Quantitatively Compare Dose Distributions." Med Phys **30**(7): 1952.
- Johns, H. E. and J. R. Cunningham (1983). The Physics of Radiology. Springfield, Il, Charles C Thomas.
- Khan, F. M. (1994). The Physics of Radiation Therapy. Baltimore, MD, Lippincott Williams & Wilkins.
- MacKenzie, M. A., M. Lachaine, B. Murray, B. G. Fallone, D. Robinson and G. C. Field (2002). "Dosimetric verification of inverse planned step and shoot multileaf collimator fields from a commercial treatment planning system." J. Appl. Clin. Med. Phys. **3**(2): 97-109.
- Mathworks (2003). Image Processing Toolbox User's Guide Version 4. **2003**. www.mathworks.com
- Med-Tec (2002). Exradin Farmer Type Chamber. **2002**. <http://www.medtec.com/>
- Toga, A. W. and P. K. Banerjee (1993). "Registration revisited." Journal of Neuroscience Methods **48**: 1-13.

Van Dyk, J., Ed. (1999). Radiation Oncology Overview. The Modern Technology of Radiation Oncology: A Compendium for Medical Physicists and Radiation Oncologists. Madison, WI, Medical Physics Publishing.

VIDAR (1998). VIDAR VXR Film Digitizer User's Guide for 32-bit TWIAN for Windows. Herndon, VA, VIDAR Systems Corporation.

Chapter 5 Results and Discussions

5.1 Dosimetry

5.1.1 Generation of Sensitometric Curves

5.1.1.1 Sensitometric Curves for XV and EDR Films

Sensitometric curves were created using both XV and EDR films irradiated using the step window method, together with ion chamber measured doses, and fit with a 3rd order polynomial. The pixel value corresponding to a dose of zero is the background pixel value for the film. The background value is taken as the average pixel value of a developed non-irradiated film from the same batch as the step window film. For the XV film, the background pixel value was about 11.0 and for EDR film it was about 12.4. It is possible to get pixel values slightly less than the background that could lead to a predicted negative dose using the sensitometric curves due to, for example, inhomogeneities in the film emulsion or differences in film processing conditions. For this reason, the dose is set to zero for all pixel values less than the background pixel value.

The doses measured using the ion chamber at the centre of each subfield ranged from about 14-100 cGy for the XV film irradiated with 15 MV photons and 12.5-87 cGy for the XV film irradiated with 6 MV photons. Doses delivered to the EDR films were 4 times larger because its latitude is approximately 4 times higher. The day-to-day linac dose output described in Section 3.1.1.2 was found to vary from about 98.5-101.5 cGy/100 MU for the 6 MV beam and 98-102 cGy/100 MU for the 15 MV beam.

The equation of the best-fit line was used to create a table of pixel values versus dose for pixel values ranging from 0 to the maximum scanned pixel value, typically in the 150 to 180 range. Sample sensitometric curves for XV and EDR films created with 6 MV and 15 MV photons are shown in Figure 5.1 through Figure 5.4. Errors in dose and pixel values are too small to be seen.

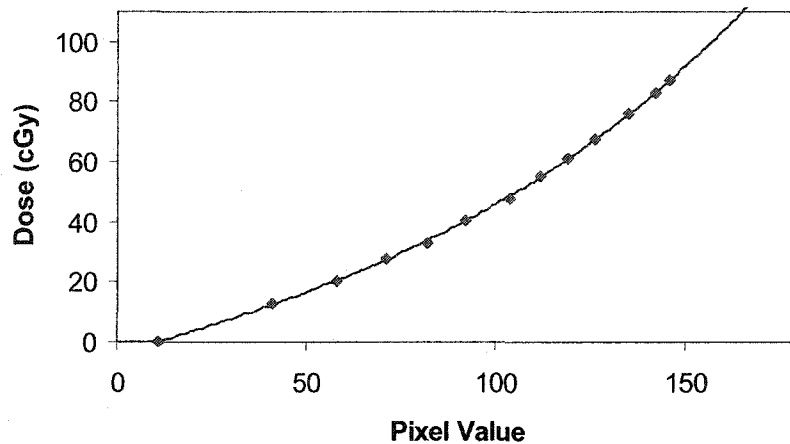


Figure 5.1 Sample sensitometric curve for XV film irradiated with a 6 MV photon beam. The best-fit line through the data is described by: $dose = -4.1 + 0.379 * pix + 0.000122 * pix^2 + 0.000011 * pix^3$, $R^2 = 0.9998$.

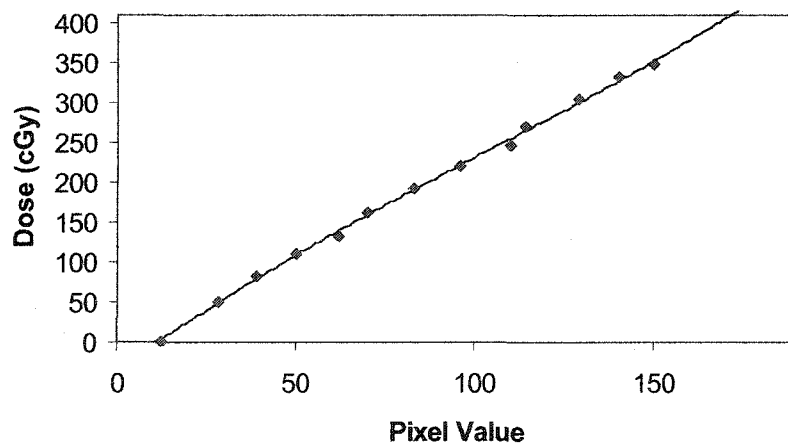


Figure 5.2 Sample sensitometric curve for EDR film irradiated with a 6 MV photon beam. The best-fit line through the data is described by: $dose = -37.7 + 3.3 * pix - 0.00936 * pix^2 + 0.000031 * pix^3$, $R^2 = 0.9983$.

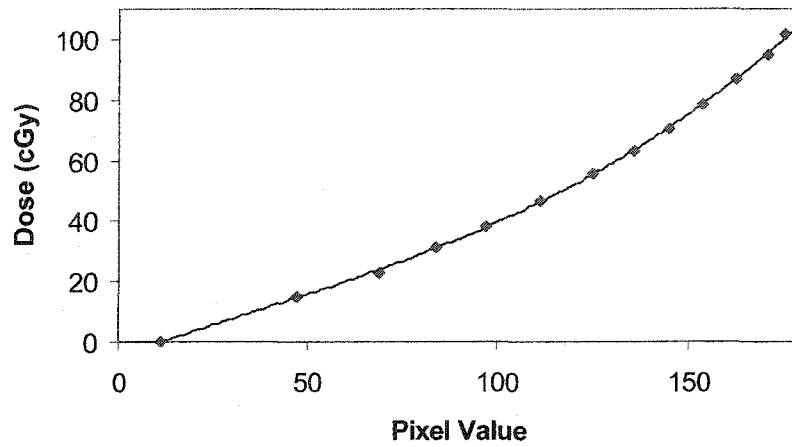


Figure 5.3 Sample sensitometric curve for XV film irradiated with a 15 MV photon beam. The best-fit line through the data is described by: $dose = -4.74 + 0.4316 * pix - .000998 * pix^2 + .000011 * pix^3$, $R^2=0.9999$.

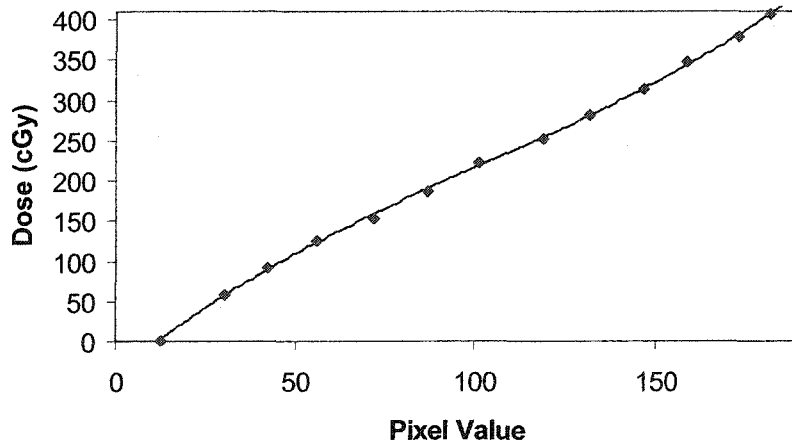


Figure 5.4 Sample sensitometric curve for EDR film irradiated with a 15 MV photon beam. The best-fit line through the data is described by: $dose = -40.8 + 3.69 * pix - .0167 * pix^2 + .000054 * pix^3$, $R^2=0.9995$.

| Film | Energy | Curve Fit | R ² Value |
|------|--------|------------------------------------------------------------------------------------|----------------------|
| XV | 6 | dose = -4.1 + 0.379*pix + 0.000122*pix ² + 0.000011*pix ³ | 0.9998 |
| EDR | 6 | dose = -37.7 + 3.3*pix - .00936*pix ² + .000031*pix ³ | 0.9983 |
| XV | 15 | dose = -4.74 + 0.4316*pix - .000998*pix ² + .000011*pix ³ | 0.9999 |
| EDR | 15 | dose = -40.8 + 3.69*pix - .0167*pix ² + .000054*pix ³ | 0.9995 |

Table 5.1 Summary of curve fits for XV and EDR films irradiated with 6 and 15 MV photons.

The accuracy of the sensitometric tables generated for pixel values from 0 to the maximum scanned pixel value depends on the goodness of fit of the polynomial curve through the data points. From Table 5.1, we see that R² values are slightly better for the XV film than for the EDR film, and slightly better for the 15 MV than for the 6 MV photon sensitometric curves. However, in all cases the curve fits are very good.

The data points for the EDR sensitometric curves do not fall smoothly along the line of best fit especially for 6 MV. The same fit problem can also be seen with the XV sensitometric curve, although the pattern is much less pronounced. The average discrepancy between the 12 discrete dose measurements and the doses predicted by the curve fit are 0.7% for XV film irradiated using a 6 MV beam; 2.2% for EDR film irradiated using a 6 MV beam; 0.9% for XV film irradiated using a 15 MV beam; and 1.5% for EDR film irradiated using a 15 MV beam

Because the disagreement between discrete points and the sensitometric fit curve is caused by the differential response between ion chamber and film depending on the subfield position, it is very difficult to correct for. Instead the discrepancy between the data points and the line of best fit is an indication of

error in the technique. It is suggested that if the 3rd order polynomial fit does not appear to fit the sensitometric curve data points well, a different type of film should be used or the step window approach to generate the curve should be avoided.

5.1.1.2 Film Scanning - Linearity of Pixel Value with Optical Density

The relationship between optical density and pixel value was investigated along with potential scanner non-linearity, by comparing pixel values determined using the automated film scanner to optical densities measured using a manual densitometer. The analysis was performed on each of the 12 subfields for 5 films each of XV and EDR. Because the data shown in Figure 5.5 has an almost perfectly linear relationship, the film scanning does not appear to introduce any significant error. The graphs of the pixel value versus optical density have slopes of 62.5 and 61.0. This does not support VIDAR's claim that optical density multiplied by 256/3.0 equal pixel value for optical densities up to about 2.2 (VIDAR's equation predicts a slope of 85.3 but our results show slopes of around 60). However, the relationship between pixel value and optical density is very linear.

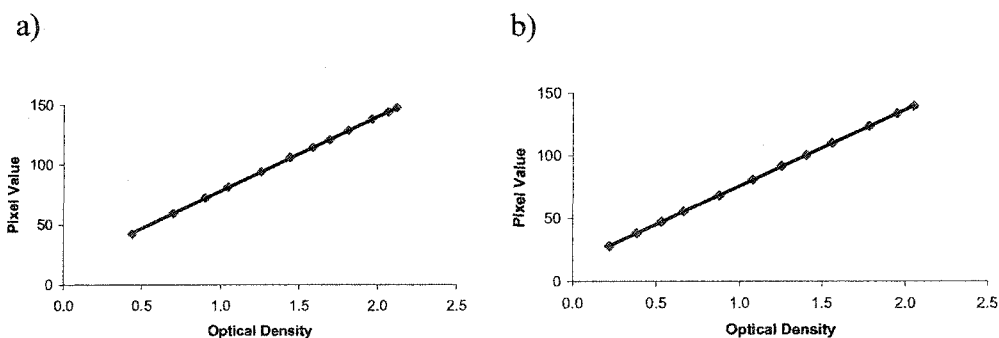


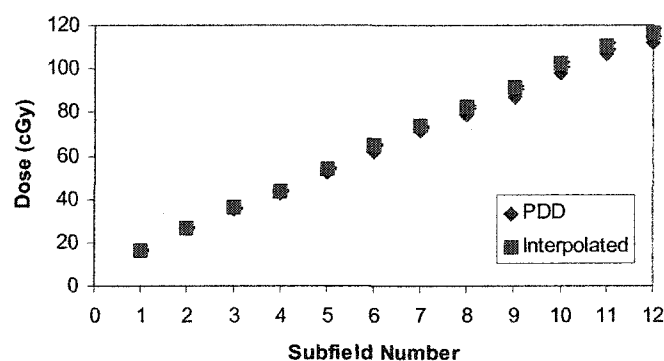
Figure 5.5 Pixel value versus optical density for XV (a) and EDR films (b) irradiated with 6 MV photons in the step window pattern. The linear fit to the XV data has an equation of $y = 62.48x + 15.526$ and an R^2 value of 0.9999; and the EDR data has a linear fit of $y = 61.013x + 14.827$ and an R^2 value of 1.

5.1.2 Examination of Film Spectral Response

5.1.2.1 Results of Perpendicular Film Irradiation

Doses determined at 5 and 20 cm depths using the two methods described in Section 4.1.7 are shown for XV and EDR films in Figures 5.6 and 5.7. Doses labeled PDD were determined by multiplying step window ion chamber doses at 10 cm depth by a ratio of PDDs. Interpolated doses were determined by converting pixel values at the centre of the subfields taken at depth to dose using a sensitometric curve generated for 10 cm depth.

a)



b)

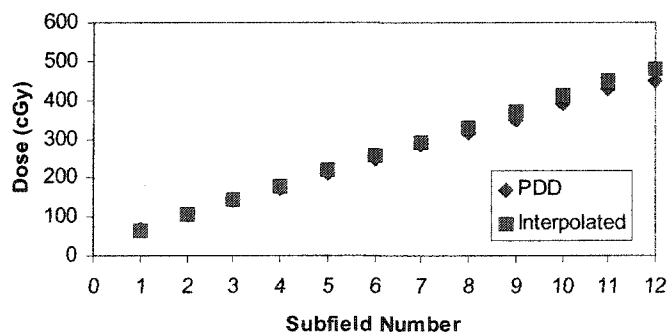
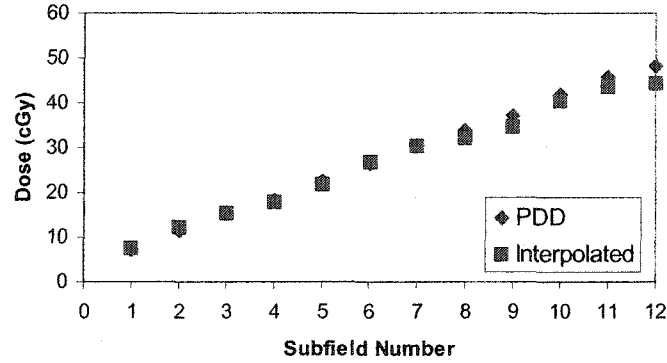


Figure 5.6 Doses at 5 cm depth in solid water for XV (a) and EDR (b) films irradiated with a 6 MV beam.

a)



b)

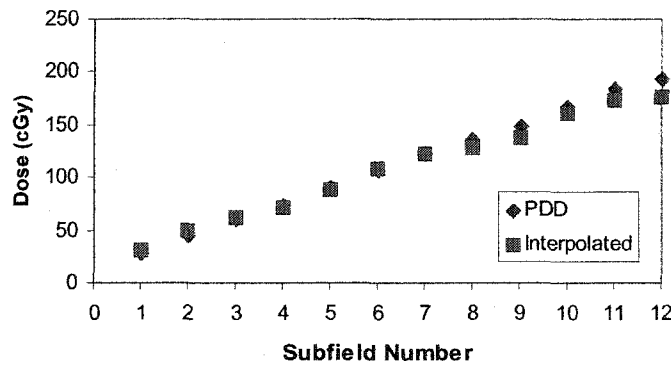


Figure 5.7 Doses at 20 cm depth in solid water for XV (a) and EDR (b) films irradiated with a 6 MV beam.

From Figure 5.6 and Figure 5.7 we see that doses determined by converting pixel values obtained at the depth of interest to dose using the calibration film obtained at 10 cm depth, do not agree very well with those calculated from doses measured at 10 cm depth using percent depth doses. Thus, the depth that the step window calibration film is taken appears to be important. This is true for XV and EDR film and is especially true for higher doses. The discrepancy between doses determined by the two different methods may have resulted because the PDD tables used at the Cross Cancer Institute are average

PDDs from multiple linacs; therefore, doses at 5 and 10 cm calculated using these average PDDs may not be exact. Despite this possible explanation for the disagreement, it is recommended that a calibration step window be created for each depth of interest.

5.1.2.2 Results of Parallel Film Irradiation

Vertical and horizontal dose profiles for XV and EDR films are shown with corresponding calculated profiles in Figures 5.8 and 5.9. The vertical profiles are taken at isocentre and the horizontal profiles are taken at 10 cm depth.

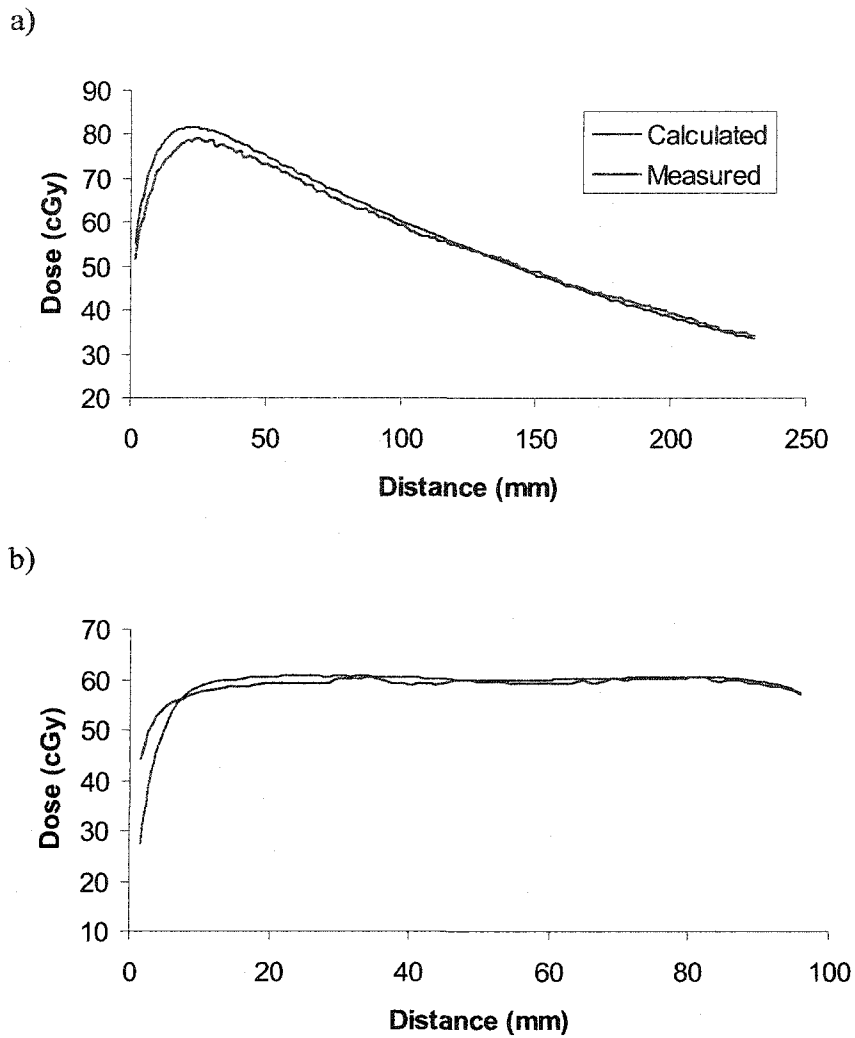


Figure 5.8 XV film measured and Helax TMS calculated vertical (a) and horizontal (b) dose distributions. The vertical profile was taken through the centre of the phantom and the horizontal dose distribution was taken at 10 cm depth.

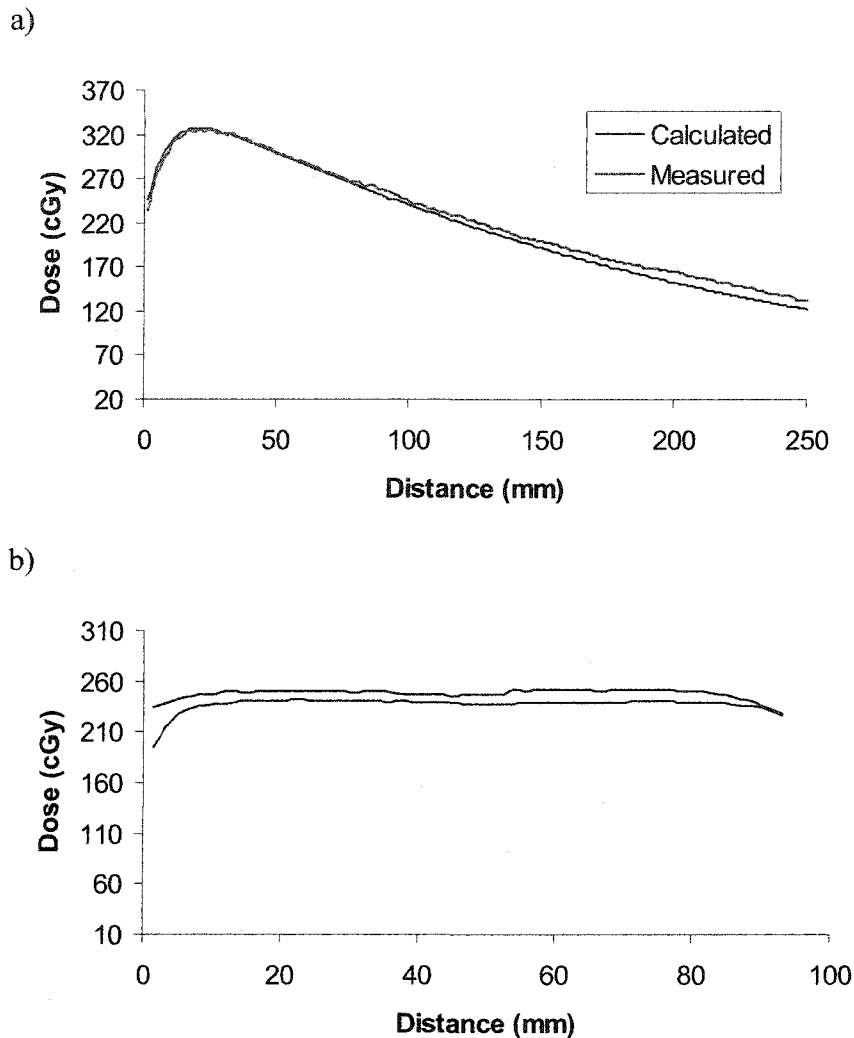


Figure 5.9 EDR film measured and Helax TMS calculated vertical (a) and horizontal (b) dose distributions. The vertical profile was taken through the centre of the phantom and the horizontal dose distribution was taken at 10 cm depth.

It has been shown that both XV and EDR film have similar vertical and horizontal dose profiles (Figure 5.8 and Figure 5.9) for doses in the respective films' latitudes. Measured doses for both films agreed within about 2% or less to the doses at the same position calculated using Helax-TMS. However, the slopes of the vertical profile curves for the measured and calculated doses are slightly

different which may be evidence of film spectral dependence. The poorest fit is seen for XV film in the build-up region in the horizontal dose distribution where discrepancy between measured and calculated doses at the same position is up to about 5%. To avoid any film spectral dependence, calibration step windows created perpendicularly to the beam, should not be used to determine dose distributions for films irradiated at other orientations.

5.1.3 Error in Film Dosimetry Technique

Ion chamber measurements were taken at the centre of the subfields on a few occasions. The average dose and the percent standard deviation are given for each subfield for 6MV and 15 MV measurements in Table 5.2. The average percent standard deviation in dose measured for the 6 MV beams at the centre of the subfields is 1.1%. The average percent standard deviation in dose measured for the 15 MV beams at the centre of the subfields is slightly lower (0.8%). This may indicate that there is more day-to-day variation in beam quality for the 6 MV beam.

| 6 MV | | | 15 MV | | |
|-------------|--------------------|----------------------|-------------|--------------------|----------------------|
| Subfield MU | Average Dose (cGy) | % Standard Deviation | Subfield MU | Average Dose (cGy) | % Standard Deviation |
| 10 | 12.5 | 1.0 | 10 | 14.4 | 1.7 |
| 20 | 19.9 | 1.0 | 20 | 22.8 | 0.8 |
| 30 | 27.1 | 0.7 | 30 | 31.1 | 0.6 |
| 40 | 32.8 | 1.0 | 40 | 38.2 | 0.6 |
| 50 | 40.0 | 1.0 | 50 | 46.2 | 1.0 |
| 60 | 47.4 | 0.8 | 60 | 54.9 | 1.1 |
| 70 | 54.8 | 1.4 | 70 | 62.8 | 0.3 |
| 80 | 60.6 | 1.0 | 80 | 69.9 | 1.0 |
| 90 | 66.7 | 1.3 | 90 | 78.0 | 0.6 |
| 100 | 75.1 | 1.3 | 100 | 86.4 | 0.4 |
| 110 | 82.2 | 1.2 | 110 | 94.2 | 0.8 |
| 120 | 86.1 | 1.1 | 120 | 100.8 | 0.8 |

Table 5.2 Average and % standard deviation for doses measured using an ion chamber at the centre of each subfield for 6 and 15 MV photons.

To examine the consistency and stability of the sensitometric curve generation, the irradiation, film processing, film scanning and the software pixel determination, 5 step window calibration films were created for each type of film using 6 MV photons. The average pixel value at the centre of each subfield was then determined. The mean pixel values and the percent standard deviation from the mean for the 5 scans are shown in Table 5.3. The average percent standard deviation in pixel values was 0.8% for the XV film and 0.6% for EDR film.

| XV film | | | EDR film | | |
|----------------|---------------------------|----------------------------|----------------|---------------------------|----------------------------|
| Subfield MU | Average Pixel Value | % Standard Deviation | Subfield MU | Average Pixel Value | % Standard Deviation |
| 10 | 42.0 | 0.0 | 40 | 28.0 | 0.0 |
| 20 | 59.0 | 1.7 | 80 | 38.0 | 0.0 |
| 30 | 72.0 | 1.2 | 120 | 47.4 | 1.2 |
| 40 | 81.2 | 1.0 | 160 | 55.4 | 1.0 |
| 50 | 93.8 | 1.6 | 200 | 68.0 | 0.0 |
| 60 | 105.8 | 0.9 | 240 | 80.2 | 0.6 |
| 70 | 114.4 | 0.4 | 280 | 91.6 | 0.6 |
| 80 | 120.8 | 0.5 | 320 | 100.0 | 0.7 |
| 90 | 128.2 | 0.4 | 360 | 109.8 | 0.8 |
| 100 | 138.0 | 0.3 | 400 | 123.4 | 0.7 |
| 110 | 144.0 | 0.5 | 440 | 133.4 | 0.7 |
| 120 | 147.4 | 0.5 | 480 | 139.2 | 0.6 |

Table 5.3 Average pixel value for 5 XV and 5 EDR films at the centre of each subfield and the error in the average pixel. Step window films were irradiated with 6 MV photons.

To see how the error in pixel value affects dose, a sensitometric curve, and then a dose – pixel value table, was created for each of the five step window films. The standard deviation of dose corresponding to all pixel values in the film's linear dose range was then determined for both XV and EDR film (Table 5.4). The average percent standard deviation in dose corresponding to pixel values in XV and EDR linear range were 1.6% and 0.8%, respectively.

| Film | Linear Dose Range (cGy) | Corresponding Pixel Value Range | Average % Std. Dev. in Dose |
|------|-------------------------------|---------------------------------------|-----------------------------------|
| XV | 5 - 100 | 12 - 161 | 1.6 |
| EDR | 25 - 400 | 13 - 158 | 0.8 |

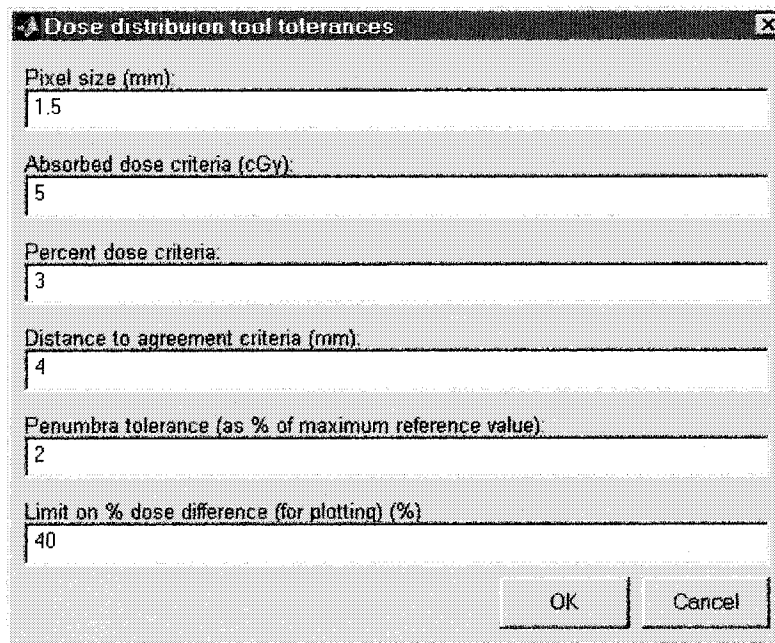
Table 5.4 Standard deviation in dose in the linear dose range due to differences in pixel value measurements and sensitometric fits between 5 films.

5.2 Comparison of dose distributions

5.2.1 Quantitative Comparison of Dose Distribution Using DDComp

5.2.1.1 DDComp User-Interface

The DDComp user-interface allows the user to specify certain parameters as shown in Figure 5.10. These parameters are pixel size; thresholds for the absorbed dose difference, percent dose difference, and DTA; background threshold and plotting limit for the distance to agreement.



| Parameter | Value |
|------------------------------------------------------|-------|
| Pixel size (mm) | 1.5 |
| Absorbed dose criteria (cGy) | 5 |
| Percent dose criteria | 3 |
| Distance to agreement criteria (mm) | 4 |
| Penumbra tolerance (as % of maximum reference value) | 2 |
| Limit on % dose difference (for plotting) (%) | 40 |

Figure 5.10 Screen shot of user-interface to input thresholds in DDComp.

5.2.1.2 Example of Output Generated by DDComp

The treatment plan dose distribution and the treatment verification film dose distribution were compared for one field from an IMRT treatment of a head and neck patient. Figure 5.11 and Figure 5.12 are the measured and calculated dose distributions that were compared in this example. The two dose distributions have been registered and modified so that their pixel sizes are the same. These distributions have the same number of pixels, and are displayed on the same dose scale so obvious differences can be detected by the user. The maximum dose in the calculated dose distribution is 51.1 cGy and the maximum dose in the measured dose distribution is 48.8 cGy. The average doses in the measured and calculated dose distributions are 7.1 and 7.8 cGy, respectively.

The absorbed dose differences between dose-pixels are displayed in Figure 5.13. Because the dose distribution image is largely red in colour, we see that the measured doses in the centre of the treatment field are greater (i.e. hotter) than the calculated doses; therefore, it is possible that normal tissues within the treatment volume are receiving more dose than planned. In the penumbral region, the measured dose is lower than the calculated dose in some spots and higher in others. This may indicate that the Helax modeling of the penumbra is not as accurate as it could be. In the case where the measured dose is greater than the calculated dose (red), the film could be over-responding to low energy photons. A histogram of absorbed dose differences is given in Figure 5.14. Here absorbed dose differences are sorted into bins of clinical relevance as specified by the user. In this case, bins of ± 5 cGy, -5 to -10 cGy, -10 to -15 cGy etc, and 5 to 10 cGy, 10 to 15 cGy etc were chosen. This display shows that the overwhelming majority (97.2%) of the calculated dose distribution dose-pixels lie within 5 cGy of the measured dose distribution.

Figure 5.15 is an image of percent dose differences between the measured and calculated dose distributions. We see large percent dose differences around the edge of the region of interest. These could be a combination of disagreement between measured and calculated penumbral effects and an increase in percent dose differences because of small differences in low absorbed doses. The histogram of percent dose difference (Figure 5.16) shows that the majority of the dose-pixels are greater than $\pm 5\%$ different between the measured and calculated dose distributions. The percent of calculated dose-pixels that are within 3% of the corresponding measured dose point is 15.5%.

Figure 5.17 shows the distance from a dose-pixel in the calculated dose distribution to the nearest contour of the same value in the measured dose distribution. Both the distance to agreement map and the histogram (Figure 5.18) show that although most points in the comparison dose distribution are within 4 mm of the same dose in the measured dose distribution, some are up to 70 mm away. Note that the DTA was calculated for fewer pixels than the other metrics because not all of the pixels in the ROI were in high-dose gradient regions.

A map of the total number of metrics failed for each dose-pixel is given in Figure 5.19. Dose-pixels in the measured dose distribution that were less than 2% of the maximum dose in the measured dose distribution were not included in the metric analysis and appear white. We see that only a few dose-pixels failed all 3 of the metrics. Most of the dose-pixels are shown to have failed 1 of the metric tests but a large number failed none or two of the tests. It is possible that a dose-pixel failing 2 of the tests did not pass at least one test if that dose-pixel was in a low-dose gradient region since DTA was calculated only for high-dose gradients. Another possibility is that if a dose in the calculated dose distribution is greater than the maximum measured dose, the DTA cannot be found; therefore, the DTA is not determined for these dose-pixels. In the IMRT example presented

here, the DTA was not determined for dose-pixels in the calculated dose distribution that were greater than 48.8 cGy. A histogram of overall results of the metric analysis is given in Figure 5.20. Dose-pixels that pass at least one of the metrics tests appear in the “Pass” bin while those that failed all applicable metrics failed the analysis. In this example 99.9% of the dose-pixels passed at least 1 of the tests (0.1% of the dose-pixels failed all tests).

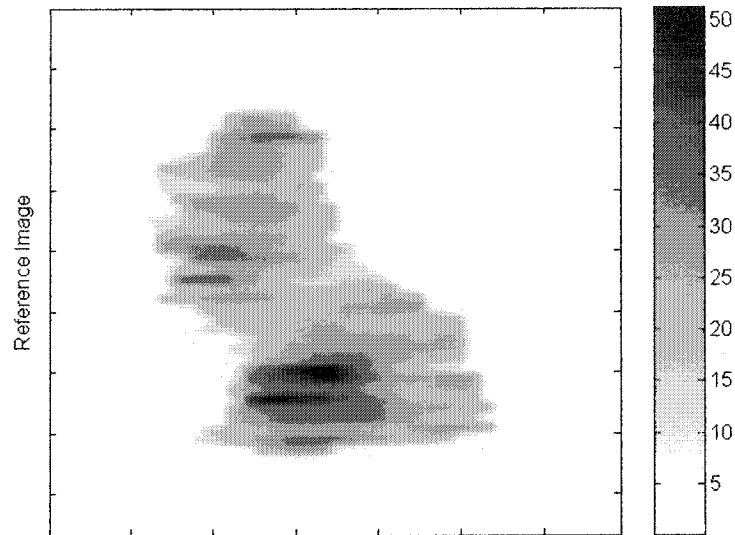


Figure 5.11 Measured (reference) dose distribution.

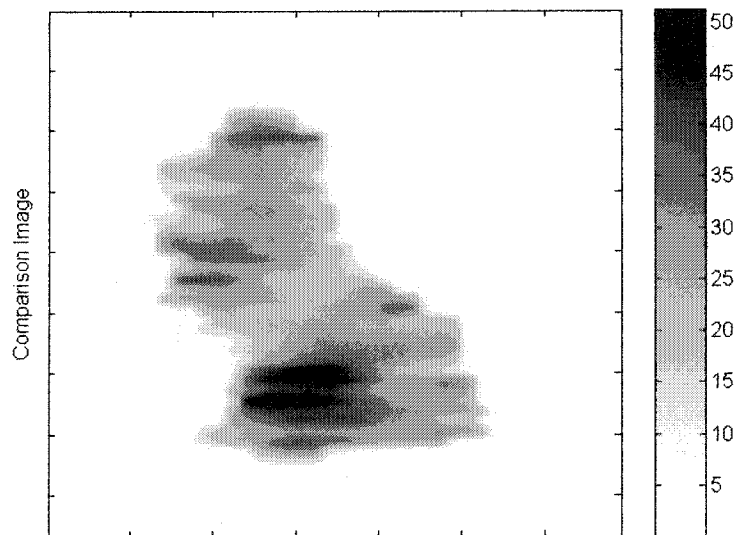


Figure 5.12 Calculated (comparison) dose distribution.

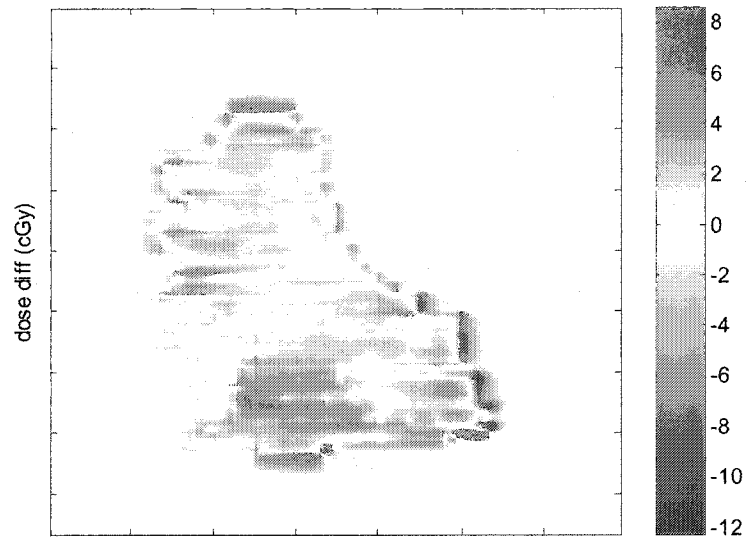


Figure 5.13 Absorbed dose difference (cGy). Dose-pixels shown in red are greater in the measured dose distribution while those in blue are greater in the calculated dose distribution.

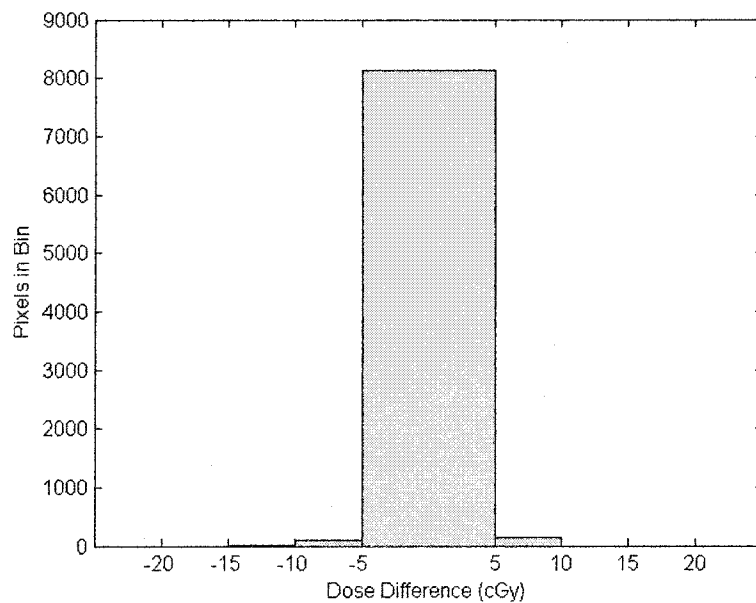


Figure 5.14 Histogram of dose difference (cGy). 8133 of 8372 dose-pixels (97.2%) are within 5 cGy of the measured result.

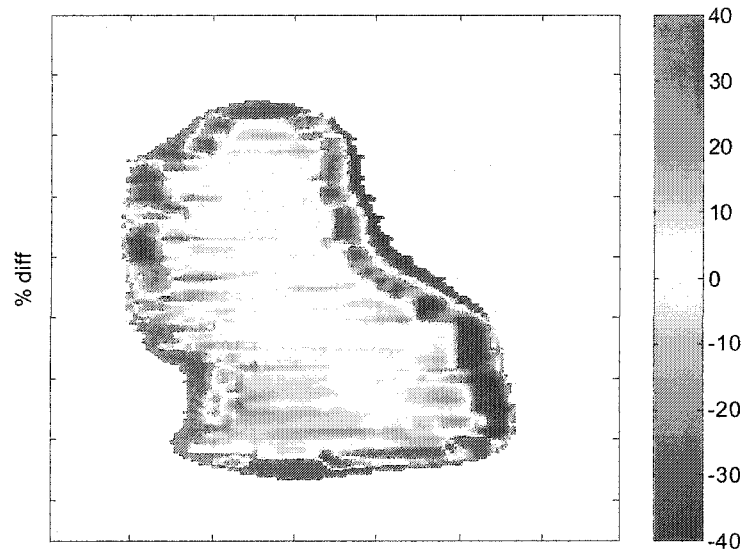


Figure 5.15 Percent dose difference.

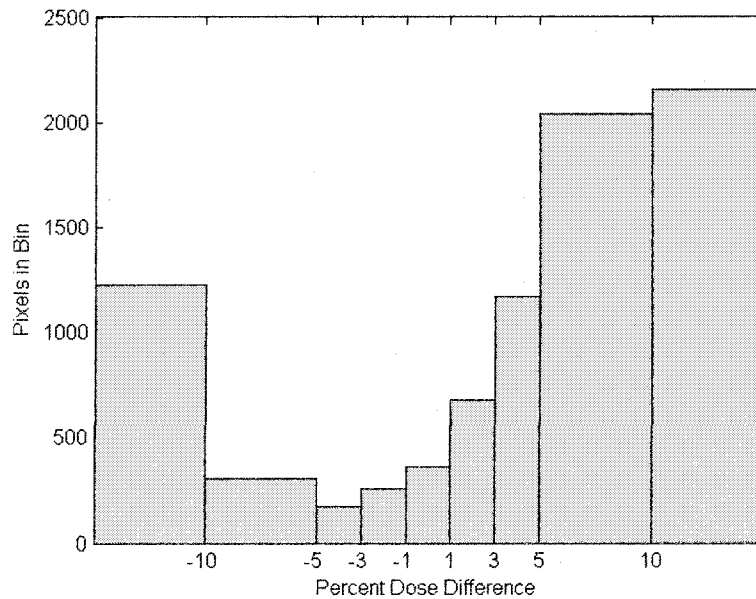


Figure 5.16 Histogram of percent dose difference. 1297 of 8372 dose-pixels (15.5%) are within 3% of the measured result.

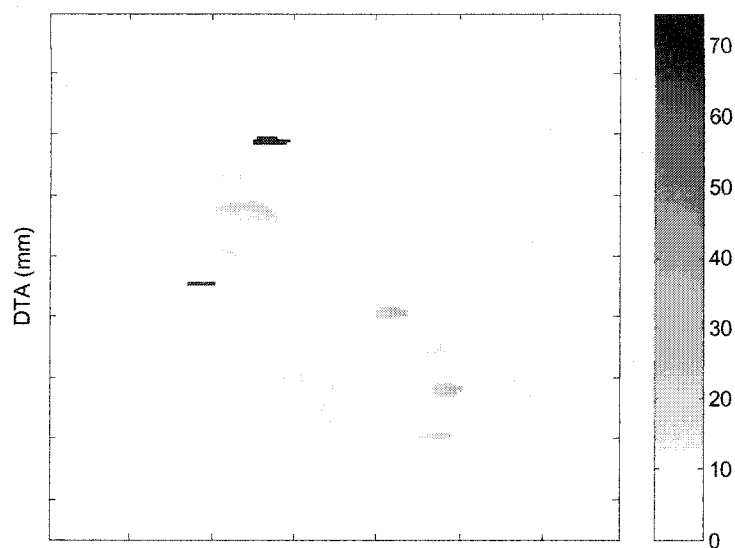


Figure 5.17 Distance to agreement (mm).

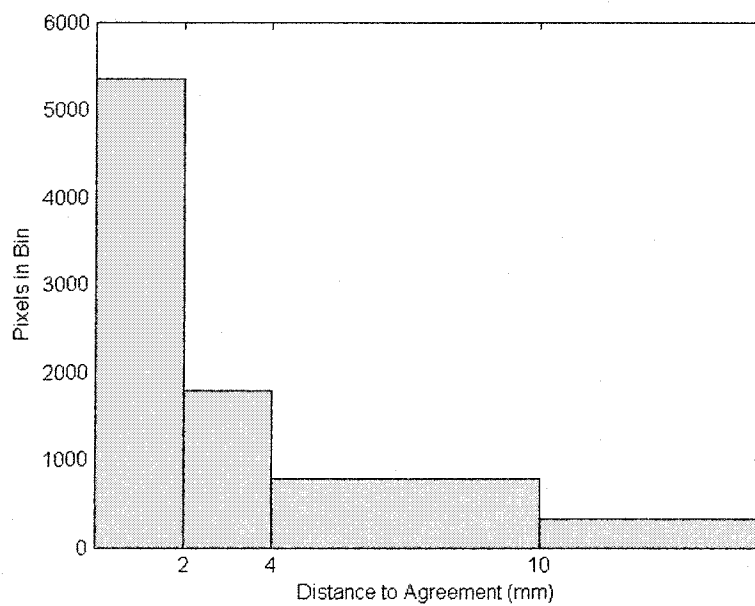


Figure 5.18 Histogram of distance to agreement. 7140 of 8263 dose-pixels (86.4%) are within 4 mm of the measured result.

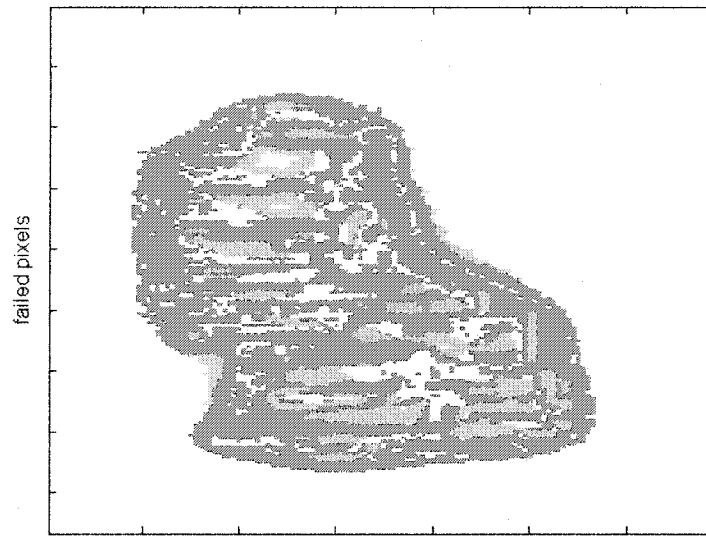


Figure 5.19 Combined metric results. Red represents failing all 3 tests, yellow 2 tests, blue 1 test, and white represents failing no tests.

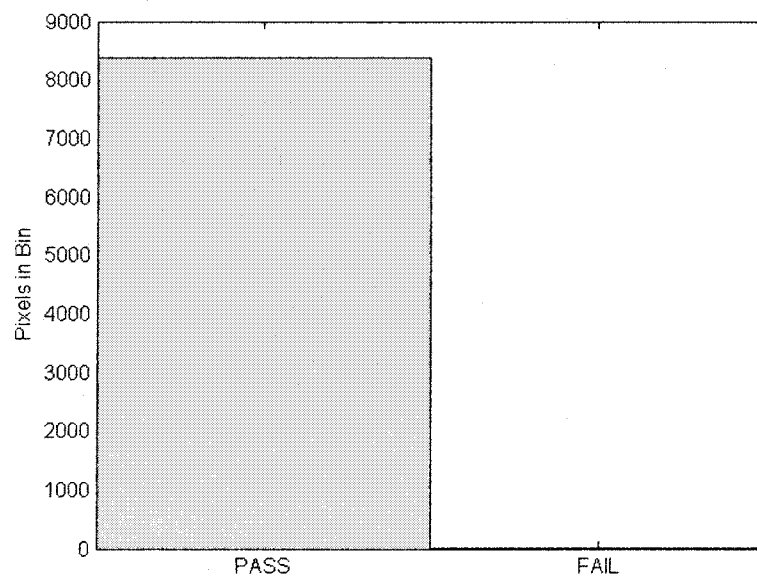


Figure 5.20 Dose-pixels passing at least one test. 8367 of 8372 dose-pixels (99.9%) passed at least one test.

The magnitude and direction of the distance to agreement are displayed using the distance to agreement polar plot (Figure 5.21). Because the points on the figure appear to be relatively symmetric about the origin, there is no evidence of systematic offset between the two dose distributions being compared. The DTA polar plot is useful as a visual tool to ensure that proper image registration has been achieved between the two dose distributions. The polar plot should be used in conjunction with another measure of image registration, such as the peak cross correlation offset, because the DTA results are dependent on the absorbed dose differences between dose distributions. For example, if one dose distribution has higher doses overall than the other, the DTA polar plot may be skewed even if the dose distributions are registered correctly.

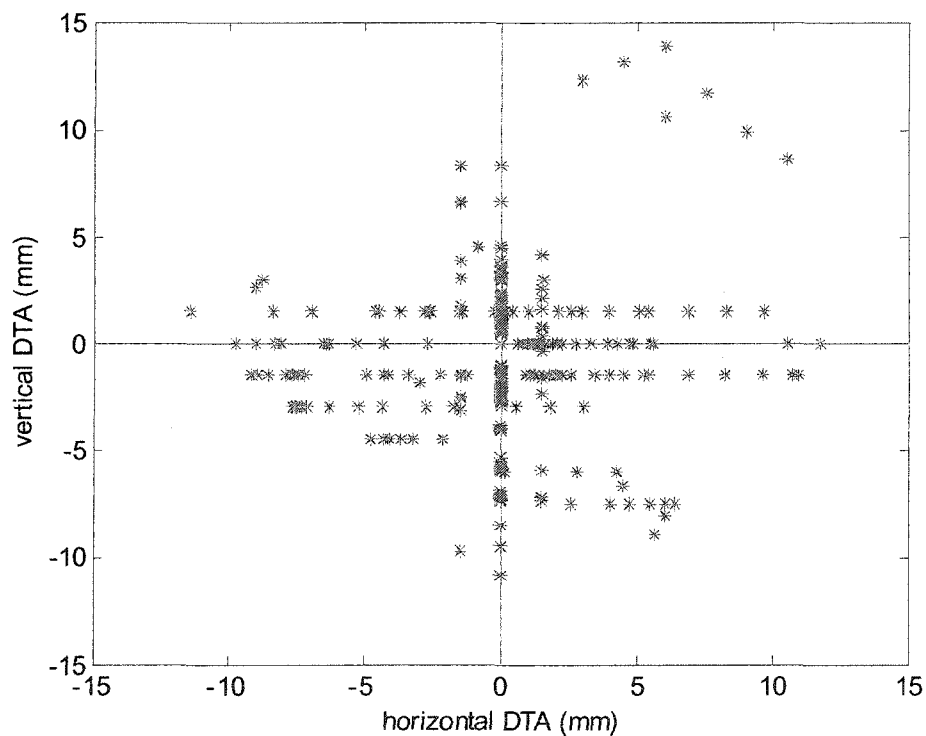


Figure 5.21 Distance to agreement polar plot. No systematic offset seen.

5.2.2 Image Registration

Measures of agreement between two images were evaluated by re-registering several test cases using the cross correlation technique and determining the peak offset, peak cross correlation value, and the FWHM (Table 5.5). The identical images test case is two identical registered images; the different images test case is images from two different treatment fields; the identical shifted images test case is two identical images, one of which has been shifted 10 pixels in the y direction with respect to the other image; and the similar images test cases are sets of measured and calculated images for three treatment fields.

| Test Case | Peak Offset [x,y] (pixels) | Peak Cross Correlation Value | FWHM (pixel width) |
|---------------------------------------|----------------------------------|------------------------------------|--------------------------|
| Identical images | [0,0] | 1.00 | 50.5 |
| Different images | [-2,1] | 0.831 | 58 |
| Identical images shifted 10 pixels | [0,-10] | 1.00 | 50.5 |
| Similar images (1) | [0,0] | 0.995 | 51 |
| Similar images (2) | [0,0] | 0.995 | 28 |
| Similar images (3) | [0,0] | 0.996 | 42 |

Table 5.5 Goodness of fit parameters for 6 simple test cases.

The FWHM parameter agrees with the peak cross correlation value for the first 4 test cases. That is, for a pair of images that are more highly correlated, and therefore with a peak cross correlation value closer to 1.00, the FWHM is smaller. However, the FWHM results are not consistent with the peak cross correlation value for the 3 different test cases for similar images. FWHM values are not well correlated to the peak cross correlation value for these test cases. Variations of

the FWHM, such as the FWHM normalized to the size of the cross-correlation matrix, were also calculated; but no technique was consistent with the cross-correlation parameter. It is our opinion that the best measure of how well two images or dose distributions are correlated is the peak cross-correlation value. Hence, the FWHM was seen as unnecessary, and was not used in the remainder of this image registration technique evaluation.

| Beam Number | Cross Correlation | | Pinprick Registration | |
|-------------|-------------------|--------------|-----------------------|--------------|
| | Peak Offset | Corr. Coeff. | Peak Offset | Corr. Coeff. |
| 1 | [0,0] | 0.996 | [2,1] | 0.995 |
| 2 | [0,0] | 0.996 | [2,2] | 0.996 |
| 3 | [0,0] | 0.995 | [1,0] | 0.995 |
| 4 | [0,0] | 0.991 | [1,0] | 0.990 |
| 5 | [0,0] | 0.991 | [1,1] | 0.991 |
| 6 | [0,0] | 0.994 | [2,2] | 0.995 |
| 7 | [0,0] | 0.992 | [-1,1] | 0.990 |
| 8 | [0,0] | 0.994 | [1,1] | 0.991 |

Table 5.6 Peak offset and correlation coefficients for 8 beams from an IMRT patient treatment. Each measured and calculated dose distribution pair was registered in two different ways: using normalized cross-correlation and using the pinprick registration technique.

The results for 8 beams from an IMRT patient treatment shown in Table 5.6 demonstrate that the normalized cross-correlation technique is more accurate than the pinprick registration. The peak offsets for the cross correlation technique are all zero pixels in the x and y directions while offsets for the pinprick technique range from 0 to 2 pixels for the x and y directions. In addition, most of the correlation coefficients are higher for the cross correlation technique. The differences in the results for the two registration techniques are likely the human error inherent to the pinprick registration. Spatial errors are introduced

when the pinpricks are made in the film using the shadows given off by the markings on the tray. Another error is introduced during the user-selection of the pinpricks in the Matlab registration software.

5.2.3 Results of Test Cases to Validate DDComp

Calculations of the three metrics for the two hypothetical dose distributions shown in Table 4.3 were performed using DDComp. The results of the DDComp calculations (Table 5.7) are identical to those done manually (Table 4.4).

| Abs. Dose Diff. (cGy) | % Dose Diff. | DTA (dose-pixels) |
|---------------------------------------------------------------------|-------------------------------------------------------------------------------------|---------------------------------------------------------------------------------|
| $\begin{bmatrix} 5 & 5 & 5 \\ 5 & 0 & 5 \\ 5 & 5 & 5 \end{bmatrix}$ | $\begin{bmatrix} 2.5 & 2.5 & 2.5 \\ 2.5 & 0 & 2.5 \\ 2.5 & 2.5 & 2.5 \end{bmatrix}$ | $\begin{bmatrix} 1.41 & 1 & 1.41 \\ 1 & 0 & 1 \\ 1.41 & 1 & 1.41 \end{bmatrix}$ |

Table 5.7 Absorbed dose difference, percent dose difference and DTA matrices calculated using DDComp for the measured and calculated dose distributions shown in Table 4.3.

The binary results of the test cases are shown in Table 5.8. Recall that passing dose-pixels are depicted by zeros and failing dose-pixels are depicted by ones. The results for the test cases matched the expected pass/fail results outlined in Table 4.2. In cases where metric thresholds were exceeded, a 1 is found. For example, in test case #3, the absorbed dose difference threshold was set to 4 and the absorbed dose difference for all of the dose-pixels except the centre one was 5. Because the absorbed dose difference exceeded the threshold for these dose-pixels, these dose-pixels failed this metric and are represented by a 1 in the absorbed dose difference binary pass/fail matrix.

| Test Case # | Abs. Dose Diff. | % Dose Diff. | DTA | Combined |
|-------------|---------------------------------------------------------------------|---------------------------------------------------------------------|---------------------------------------------------------------------|---------------------------------------------------------------------|
| 1 | $\begin{bmatrix} 0 & 0 & 0 \\ 0 & 0 & 0 \\ 0 & 0 & 0 \end{bmatrix}$ | $\begin{bmatrix} 0 & 0 & 0 \\ 0 & 0 & 0 \\ 0 & 0 & 0 \end{bmatrix}$ | $\begin{bmatrix} 0 & 0 & 0 \\ 0 & 0 & 0 \\ 0 & 0 & 0 \end{bmatrix}$ | $\begin{bmatrix} 0 & 0 & 0 \\ 0 & 0 & 0 \\ 0 & 0 & 0 \end{bmatrix}$ |
| 2 | $\begin{bmatrix} 0 & 0 & 0 \\ 0 & 0 & 0 \\ 0 & 0 & 0 \end{bmatrix}$ | $\begin{bmatrix} 1 & 1 & 1 \\ 1 & 0 & 1 \\ 1 & 1 & 1 \end{bmatrix}$ | $\begin{bmatrix} 0 & 0 & 0 \\ 0 & 0 & 0 \\ 0 & 0 & 0 \end{bmatrix}$ | $\begin{bmatrix} 0 & 0 & 0 \\ 0 & 0 & 0 \\ 0 & 0 & 0 \end{bmatrix}$ |
| 3 | $\begin{bmatrix} 1 & 1 & 1 \\ 1 & 0 & 1 \\ 1 & 1 & 1 \end{bmatrix}$ | $\begin{bmatrix} 0 & 0 & 0 \\ 0 & 0 & 0 \\ 0 & 0 & 0 \end{bmatrix}$ | $\begin{bmatrix} 0 & 0 & 0 \\ 0 & 0 & 0 \\ 0 & 0 & 0 \end{bmatrix}$ | $\begin{bmatrix} 0 & 0 & 0 \\ 0 & 0 & 0 \\ 0 & 0 & 0 \end{bmatrix}$ |
| 4 | $\begin{bmatrix} 1 & 1 & 1 \\ 1 & 0 & 1 \\ 1 & 1 & 1 \end{bmatrix}$ | $\begin{bmatrix} 1 & 1 & 1 \\ 1 & 0 & 1 \\ 1 & 1 & 1 \end{bmatrix}$ | $\begin{bmatrix} 0 & 0 & 0 \\ 0 & 0 & 0 \\ 0 & 0 & 0 \end{bmatrix}$ | $\begin{bmatrix} 0 & 0 & 0 \\ 0 & 0 & 0 \\ 0 & 0 & 0 \end{bmatrix}$ |
| 5 | $\begin{bmatrix} 0 & 0 & 0 \\ 0 & 0 & 0 \\ 0 & 0 & 0 \end{bmatrix}$ | $\begin{bmatrix} 0 & 0 & 0 \\ 0 & 0 & 0 \\ 0 & 0 & 0 \end{bmatrix}$ | $\begin{bmatrix} 1 & 0 & 1 \\ 0 & 0 & 0 \\ 1 & 0 & 1 \end{bmatrix}$ | $\begin{bmatrix} 0 & 0 & 0 \\ 0 & 0 & 0 \\ 0 & 0 & 0 \end{bmatrix}$ |
| 6 | $\begin{bmatrix} 0 & 0 & 0 \\ 0 & 0 & 0 \\ 0 & 0 & 0 \end{bmatrix}$ | $\begin{bmatrix} 1 & 1 & 1 \\ 1 & 0 & 1 \\ 1 & 1 & 1 \end{bmatrix}$ | $\begin{bmatrix} 1 & 0 & 1 \\ 0 & 0 & 0 \\ 1 & 0 & 1 \end{bmatrix}$ | $\begin{bmatrix} 0 & 0 & 0 \\ 0 & 0 & 0 \\ 0 & 0 & 0 \end{bmatrix}$ |
| 7 | $\begin{bmatrix} 1 & 1 & 1 \\ 1 & 0 & 1 \\ 1 & 1 & 1 \end{bmatrix}$ | $\begin{bmatrix} 0 & 0 & 0 \\ 0 & 0 & 0 \\ 0 & 0 & 0 \end{bmatrix}$ | $\begin{bmatrix} 1 & 0 & 1 \\ 0 & 0 & 0 \\ 1 & 0 & 1 \end{bmatrix}$ | $\begin{bmatrix} 0 & 0 & 0 \\ 0 & 0 & 0 \\ 0 & 0 & 0 \end{bmatrix}$ |
| 8 | $\begin{bmatrix} 1 & 1 & 1 \\ 1 & 0 & 1 \\ 1 & 1 & 1 \end{bmatrix}$ | $\begin{bmatrix} 1 & 1 & 1 \\ 1 & 0 & 1 \\ 1 & 1 & 1 \end{bmatrix}$ | $\begin{bmatrix} 1 & 0 & 1 \\ 0 & 0 & 0 \\ 1 & 0 & 1 \end{bmatrix}$ | $\begin{bmatrix} 1 & 0 & 1 \\ 0 & 0 & 0 \\ 1 & 0 & 1 \end{bmatrix}$ |

Table 5.8 Binary pass/fail matrices for each metric as well as the combined metric. 0 indicates pass; 1 indicates fail.

In the above test cases, the DTA was determined for dose-pixels in a low dose gradient region where absorbed dose difference and percent dose difference play the major role. During the testing phase of the software, the DTA was determined for all regions. In the clinical version of DDCComp used to obtain all of the subsequent results, the distance to agreement was calculated only for high dose gradient regions defined as $\geq 30\% \text{ cm}^{-1}$ (Van Dyk, Barnett et al. 1993).

An example of a polar plot created by comparing a measured dose distribution to the same dose distribution shifted down by 10 pixels and right by 10 pixels is shown in Figure 5.22. From this example we see that the polar plot can be used as a qualitative tool to determine whether or not there is a large systematic offset between two dose distributions, but the magnitude of the offset is difficult to determine.

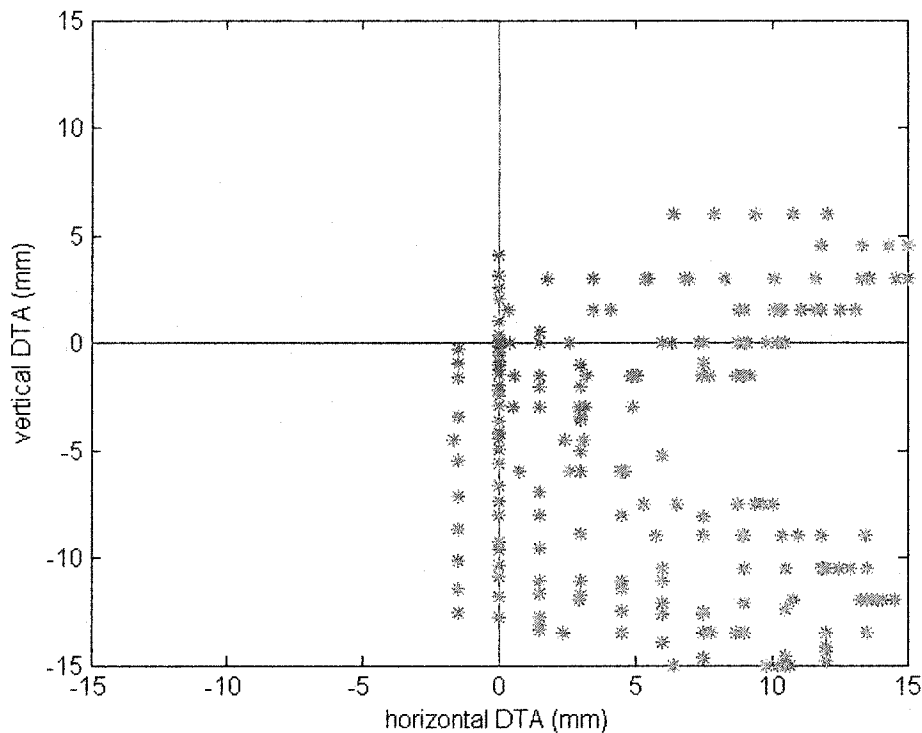


Figure 5.22 Polar plot created by comparing two dose distributions where the calculated dose distribution was identical to the measured dose distribution but it was shifted by 10 pixels (15 mm) in the right and down directions.

5.2.4 Dependence of DDComp on Various Parameters

5.2.4.1 Dose Distribution Uncertainties

The results of adding uncertainties in the form of Gaussian noise to the dose distribution as described in Section 4.2.4.2 are summarized in Table 5.9. Recall that the added noise had a mean of 0. The variance of the noise was set to 0.001, 0.01 and 0.1 in this analysis. Adding noise to the dose distribution greatly affects the percent difference results. A particularly large percent difference was found at low dose levels. This type of noise also effected the distance to agreement results but to a much lesser degree. Even with the addition of noise

with relatively small variance, the percent dose difference results were very sensitive. The increase in failures can be attributed to large changes in percent dose difference in low-dose regions with small changes in the absorbed doses due to the addition of noise. Absorbed dose difference results and combined metric results are not shown because absorbed doses changed much less than the 5 cGy threshold and therefore were not affected by the addition of noise/uncertainties in this investigation.

| Metric | Percentage of dose-pixels failed | | |
|-------------------------|----------------------------------|------|------|
| | Variance of Noise | | |
| | 0.001 | 0.01 | 0.1 |
| Percent dose difference | 4.5 | 17.8 | 37.3 |
| Distance to agreement | 0.1 | 0.1 | 1.1 |

Table 5.9 Metric % failure results for dose distributions compared with the same distribution plus noise. Thresholds for percent dose difference and DTA were set to 3%, and 4 mm, respectively.

5.2.4.2 Dose Distribution Normalization

Methods of normalizing dose distributions by the maximum of mean dose-pixel values were described in Section 4.2.4.3. The effect of normalization on the dose distribution software tool was significant for all metrics, especially the distance to agreement (Table 5.10). As stated previously, metric thresholds were set to 5 cGy for absorbed dose difference, 3% for distance to agreement, and 4 mm for the DTA. We strongly feel that the dose distributions should not be normalized to one another before they are analyzed. By forcing either the maximum or mean dose-pixel values in the two dose distributions to be the same, real differences in the dose distributions could be masked. It is possible, then, for the incorrect number of monitor units to be delivered to a treatment field without

the verification picking up on this error. Consequently, an overdoseage or an underdosage could be unknowingly delivered to the PTV. In addition, normalizing to the maximum means that the two dose distributions are being adjusted based on a single dose-pixel out of many and the exact dose at this dose-pixel may not be accurate. In other words, a $1.5 \times 1.5 \text{ mm}^2$ section of the dose distribution has a large uncertainty associated with it, and this uncertainty would be propagated through the entire dose distribution if it is normalized by a single dose-pixel.

| Metric | Percent of dose-pixels failed | | |
|--------------------------|-------------------------------|------------------------------------|---------------------------------|
| | Unnormalized | Normalized to the maximum ROI dose | Normalized to the mean ROI dose |
| Absorbed dose difference | 5.0 | 3.9 | 3.6 |
| Percent dose difference | 93.5 | 75.5 | 74.3 |
| Distance to agreement | 14.1 | 3.8 | 31.3 |
| Combined metric | 2.6 | 0.14 | 0.2 |

Table 5.10 Percent failure statistics for the dose distribution software for an unnormalized comparison dose distribution; a comparison dose distribution normalized to the maximum dose-pixel value in the reference dose distribution; and a comparison dose distribution normalized to the mean dose-pixel value in the reference dose distribution.

In general, the metric percent failures are lower for the normalized dose distribution comparisons than for the unnormalized dose distribution comparison which demonstrates that normalizing the calculated dose distribution potentially hides differences between the measured and calculated dose distributions.

The distance to agreement metric is most significantly affected by the normalization to the mean dose. One possible explanation for this is that the

normalization causes the calculated dose to have an overall dose decrease in the high dose gradient regions. If the calculated dose distribution is generally lower in dose than the measured, a matching dose may only be found near the edge of the treatment field, i.e. potentially further away.

5.2.4.3 Definition of the Reference Dose Distribution

It is clear that the direction of comparison, as described in Section 4.2.4.4, does affect the dose distribution software statistics (Table 5.11). The case where the reference dose distribution is the measured dose distribution, and the comparison dose distribution is the calculated dose distribution is shown in the middle column. These definitions of the reference dose distribution and comparison dose distribution are the default used in DDComp. In the third column, the definitions of the reference and comparison dose distributions are reversed. Here the reference dose distribution is defined as the calculated dose distribution and the comparison dose distribution is defined as the measured dose distribution. The metric with the largest sensitivity to the definition of the reference and comparison dose distributions is the distance to agreement metric. This is another example of how DTA is sensitive to the magnitude and sign of absorbed dose differences. The direction of comparison, however, should not be an issue as long as the definition of the reference dose distribution stays constant for all verification procedures.

| Metric | Percentage of dose-pixels failed | |
|--------------------------|----------------------------------------------------------|------------------------------------------------------------|
| | Reference dose distribution is the measured distribution | Reference dose distribution is the calculated distribution |
| Absorbed dose difference | 5.0 | 3.9 |
| Percent dose difference | 93.5 | 94.8 |
| Distance to agreement | 14.1 | 31.7 |
| Combined metric | 2.6 | 1.0 |

Table 5.11 Percent failure statistics for a calculated/measured dose distribution pair when the reference dose distribution was defined to be the first the measured dose distribution and second the calculated dose distribution.

5.2.4.4 Impact of Changing Metric Thresholds for the Metrics

The results presented in Table 5.12 were obtained by varying the threshold of one of the metrics while leaving metric thresholds for the other 2 metrics at their default values. The percentages of dose-pixels failing are quite sensitive to the metric thresholds. In particular, small changes in the absorbed dose difference and distance to agreement thresholds resulted in a relatively large change in percent failure for each respective metric, as well as the number of dose-pixels that did not pass any of the metrics. On the other hand, changes in the percent dose difference threshold had less of an impact on the percentage of dose-pixels failing the percent dose difference metric and no change was seen in the percentage of dose-pixels failing the combined metric.

| Metric | Threshold | Percentage of dose-pixels failed | |
|--------------------------|-----------|----------------------------------|-----------------|
| | | Metric failure | Combined metric |
| Absorbed dose difference | 4 cGy | 13.9 | 7.3 |
| | 5 cGy | 5.0 | 2.6 |
| | 6 cGy | 1.1 | 0.3 |
| Percent dose difference | 2% | 95.5 | 2.6 |
| | 3% | 93.5 | 2.6 |
| | 5% | 89.4 | 2.6 |
| Distance to agreement | 3 mm | 25.1 | 3.2 |
| | 4 mm | 14.1 | 2.6 |
| | 5 mm | 10.6 | 2.4 |

Table 5.12 Percent failure statistics for a absorbed dose difference, percent dose difference and distance to agreement when the threshold values are changed.

The importance of each metric in enabling a dose-pixel to pass was determined by setting the thresholds for the other two metrics to zero (i.e. to fail when the doses in the measured and calculated dose distributions are not exactly the same) (Table 5.13). The results show that absorbed dose difference and distance to agreement play a larger role than percent dose difference in passing dose-pixels for this particular IMRT field analysis. We see that the absorbed dose difference is responsible for passing 95.0% of the dose-pixels for the IMRT beam investigated; the percent dose difference was responsible for passing 6.5% of the dose-pixels and the DTA was responsible for passing 82.2% of the dose-pixels.

| Metric Examined | % of dose-pixels passed by a metric |
|--------------------------|-------------------------------------|
| Absorbed dose difference | 95.0 |
| Percent dose difference | 6.5 |
| Distance to agreement | 82.2 |

Table 5.13 Percent of dose-pixels in an IMRT field that are passed by each of the metrics.

The discrepancy between the numbers of dose-pixels passed by each individual metric may be a reflection of the metric thresholds. Since only 6.5% of the dose-pixels agreed within 3%, it is possible that this threshold level is too low, or perhaps the other thresholds are too high and are allowing a bad treatment plan to pass the analysis. It is possible that different metric thresholds should be determined for different maximum dose ranges. For example, lower absorbed dose difference and percent dose difference thresholds may be necessary for a low-dose treatment field compared to a high-dose treatment field. If possible, these thresholds could be set by looking at the NTCP and TCP curves.

5.3 Clinical Application

5.3.1 Conventional 10x10 and 5x5 fields

The results for the conventional 10x10 and 5x5 cm² treatment fields irradiated using 15 and 6 MV photon beams are shown in Table 5.14. Doses measured using film agree within 2% to those calculated by Helax-TMS for both field sizes and both energies examined.

| Energy (MV) | Field size (cm ²) | Max calculated dose (cGy) | Max measured dose (cGy) | Discrepancy (%) |
|-------------|-------------------------------|---------------------------|-------------------------|-----------------|
| 15 | 10 x 10 | 215.3 | 214.2 | 0.5 |
| 15 | 5 x 5 | 199.8 | 196.5 | 1.7 |
| 6 | 10 x 10 | 221.8 | 218.1 | 1.7 |
| 6 | 5 x 5 | 199.1 | 195.9 | 1.6 |

Table 5.14 Calculated and measured doses for conventional square fields irradiated with 6 and 15 MV photons. Doses were calculated using Helax TMS and measured doses using XV film.

The film dosimetry technique gave satisfactory results with respect to the maximum doses for the conventional square fields. The dose distributions were then run through DDComp to find out representative values for percent metric failures for conventional 10x10 cm² and 5x5 cm² fields irradiated using 6 and 15 MV photons (Table 5.15). Due to the simplicity of the fields, the agreement between the measured and calculated dose distributions is expected to be good.

| Energy (MV) | Field size (cm ²) | Percentage of dose-pixels failed | | | |
|-------------|-------------------------------|----------------------------------|-------------------------|-----------------------|-----------------|
| | | Absorbed dose difference | Percent dose difference | Distance to agreement | Combined metric |
| 15 | 10 x 10 | 6.7 | 69.8 | 36.7 | 0.0 |
| 15 | 5 x 5 | 5.6 | 86.1 | 40.7 | 0.0 |
| 6 | 10 x 10 | 7.6 | 74.3 | 45.6 | 0.3 |
| 6 | 5 x 5 | 9.3 | 83.0 | 54.3 | 2.0 |

Table 5.15 Percent failure of metrics for conventional square fields analysed using DDComp.

The percentage of dose-pixels failing the absorbed dose difference metric for the conventional square fields was between 5.6 and 9.3%; the percentage of

dose-pixels failing the percent dose difference was between 69.8 and 86.1; and the percentage of dose-pixels failing the DTA was between 36.7 and 54.3%. The percentage of dose-pixels not passing any metric was between 0.3% and 2.0% for the conventional square fields irradiated using the 6 MV beam indicating very good agreement between the measured and calculated dose distributions. The agreement between the dose distributions was even better for the conventional square fields irradiated using a 15 MV beam. For the 15 MV beam, the percentage of dose-pixels failed for the combined metric was 0.0% for both the 10x10 cm² and 5x5 cm² fields.

5.3.2 IMRT Treatment Verification for 5 Patients

Five clinical IMRT treatment plans (a total of 40 treatment fields) were randomly chosen and run through DDComp to determine typical pass/fail values for IMRT treatment fields using metric criteria of 4 mm, 3% and 5 cGy. The percent of dose-pixels failing each of the metrics are given in Table 5.16. Results are averaged for 8 beams for each patient and then the average percentage failure of the metrics for the 5 plans are also given. Maximum doses in the treatment fields ranged from about 42 cGy to 97 cGy; therefore, the 5 cGy absorbed dose difference threshold ranged from about 5% to 12% of the maximum dose in the respective field.

| Patient number | Percentage of dose-pixels failed | | | |
|----------------|----------------------------------|-------------------------|-----------------------|------------------|
| | Absorbed dose difference | Percent dose difference | Distance to agreement | Combined metric |
| 1 | 16.2 ± 6.0 | 75.3 ± 1.3 | 95.0 ± 1.2 | 12.1 ± 5.1 |
| 2 | 9.0 ± 3.9 | 72.8 ± 1.9 | 94.4 ± 2.4 | 5.6 ± 3.1 |
| 3 | 8.3 ± 3.2 | 73.3 ± 3.1 | 95.3 ± 1.4 | 5.0 ± 2.6 |
| 4 | 9.3 ± 2.3 | 75.2 ± 3.6 | 94.7 ± 0.9 | 5.3 ± 1.4 |
| 5 | 10.6 ± 2.4 | 77.5 ± 2.1 | 96.5 ± 1.0 | 6.4 ± 1.7 |
| Average | 10.7 ± 3.2 | 74.8 ± 1.9 | 95.2 ± 0.8 | 6.9 ± 3.0 |

Table 5.16 Percent failure of metrics for 5 clinical IMRT treatment verifications done with film and analysed using the dose distribution software tool.

The average percent of dose-pixels failing each metric for the 5 clinical IMRT treatment plans are: 10.7% for the absorbed dose difference; 74.8% for the percent dose difference; 95.2% for the DTA; and, 6.9% did not pass at least one metric. The high percentage failure for the DTA is likely due to the large sensitivity of the DTA to relatively large absorbed dose differences as described in Section 4.2.1.

5.3.3 Reproducibility

To investigate the reproducibility of these techniques including film irradiation, processing and scanning, and the comparison of dose distributions, the analysis of one of the IMRT treatment beams was repeated on 3 different days. Percent failures for each of the metrics for this reproducibility analysis are given in Table 5.17.

| Day | Percentage of dose-pixels failed | | | |
|----------------|----------------------------------|-------------------------|-----------------------|------------------|
| | Absorbed dose difference | Percent dose difference | Distance to Agreement | Combined metric |
| 1 | 1.6 | 76.4 | 10.4 | 0.0 |
| 2 | 2.9 | 84.5 | 13.6 | 0.1 |
| 3 | 1.9 | 84.1 | 13.4 | 0.1 |
| Average | 2.1 ± 0.7 | 81.7 ± 4.6 | 12.5 ± 1.8 | 0.1 ± 0.0 |

Table 5.17 Percent failure of metrics for a single IMRT clinical treatment beam verified using film on three separate days.

Average percent failures and their standard deviation, for the metrics in the repeated beam verification were (2.1±0.7)% for the absorbed dose difference; (81.7±4.6)% for the percent dose difference; (12.5±1.8)% for the DTA; and, (0.1±0.0)% for the combined metric. The error in the metrics varied from 0% for the overall analysis to 33% (0.7÷2.1*100%) for the absorbed dose difference. The significantly lower percentage of pixels failing the DTA metric for the single IMRT beam compared to those in Section 5.3.2 is likely the result of much smaller absorbed dose differences.

The results show some day to day fluctuation. This may be caused by differences in linac beam quality, processing errors, or scanning errors.

5.4 References

- Van Dyk, J., R. B. Barnett, J. E. Cygler and P. C. Shragge (1993).
 "Commissioning and quality assurance of treatment planning computers."
I J Rad Oncol Biol Phys **26**(2): 261-73.

Chapter 6 Conclusions

The purpose of this work was to create a clinically useful way to perform treatment verifications. It is imperative that measured and calculated dose distributions are in agreement for radiation therapy treatments to be safe and effective. This thesis examined three components of a dose delivery verification technique. These are film dosimetry, the comparison of measured and calculated dose distributions, and the clinical applications of these techniques.

6.1 Dosimetry

2-D dose distributions were obtained using film in this work. A calibration step window technique was used to generate a sensitometric curve that was then used to convert the pixel values from an irradiated film into absorbed dose. Some disagreement, on the order of 1-2%, was found between discrete data points and the curve of best fit for the sensitometric curves generated using the step window calibration films. This disagreement is more significant for EDR than for XV film. Consequently, XV was thought to be a better film for use with the calibration step window. Therefore, XV was used for the clinical dosimetry applications in this work. In cases where delivered doses exceed 100 cGy, however, EDR would be a more appropriate film than XV because of its higher latitude.

To ensure that the film scanner was not introducing any significant errors, the relationship between optical density and pixel value was investigated. The pixel values measured at the centre of each subfield using the film scanner were found to be linearly related to the optical density measured using a manual densitometer, as expected. The R^2 values for the plots of pixel value versus optical density were 0.9999 for XV film and 1 for EDR film.

Film spectral dependence was investigated by analyzing films irradiated perpendicular to the beam central axis at three different depths, and by irradiating a film parallel to the beam central axis. The results demonstrated that the sensitometric curve generated for film irradiated in the perpendicular orientation at 10 cm depth and applied at depths of 5 and 20 cm had differences on the order of 4%. In the case of the parallel film irradiation, the calculated and measured doses had differences on the order of 2%. However, the vertical profile curves for the measured and calculated doses had slightly different slopes. The discrepancies between the measured and calculated dose distributions in the perpendicular and parallel film irradiation investigations, may indicate that a single sensitometric curve is not valid for calculated dose distributions for films irradiated at other gantry angles and at other depths because of film spectral dependence. It is recommended that step window calibration film be created for each depth/orientation combination that dose distributions are required.

Dose measurements made using an ion chamber at the centre of each subfield varied by 0.3-1.7% between measurement days. These errors were limited by correcting doses for day-to-day linac output variation on days when dose was not measured directly. Reproducibility errors in the measured pixel values for the film dosimetry techniques developed in these works are on the order of 0 to 2%. These errors, in turn, were found to lead to dose errors of about 1.6% for XV film and 0.8% for EDR film.

6.2 Comparison of Dose Distributions

Software was developed to compare calculated and measured dose distributions. This software, DDComp, was used to calculate absorbed dose difference, percent dose difference, and distance to agreement metrics, as well as

a combined pass/fail metric. An example was shown of the output images, histograms, and statistics from DDComp.

DDComp requires that dose distributions be registered prior to the analysis. Peak offset, peak cross-correlation value and FWHM were examined using several test cases to assess their usefulness in determining whether the image registration was good, and the degree to which two images are correlated. It was found that the quality of registration could be measured using the peak offset. The peak cross correlation value can be used as a measure of agreement between two images, but for a more in-depth examination of the agreement between two dose distributions, the dose distribution comparison software tool should be used.

It is suggested that both the pinprick registration technique and the cross correlation technique be performed if there are any doubts as to whether or not there are any systematic offsets introduced by the treatment delivery. The pinprick registration technique can be used to detect physical offsets on the order of several millimetres. If none of these relatively large offsets are found, the cross-correlation technique can then be used to provide a more accurate registration of the dose distributions (within 1 pixel or 1.5 mm in our work).

This dose distribution software promises to be useful for comparing IMRT dose distributions. The results of the test cases to validate DDComp were consistent with expected results. It was found that the dose distribution software tool results are dependent on several parameters. Our results show that noise/uncertainty in the measured or calculated dose distribution can have a large effect on the percent dose difference metric. For example, adding random noise in units of cGy with a mean of 0 and a variance of 0.1 caused 37.3% of the dose-pixels to fail the absorbed dose difference metric. Normalizing the dose

distributions to either the maximum or mean ROI dose has a significant effect on all of the metrics, especially DTA. For example, 14.1% of the dose-pixels failed the unnormalized comparison for the DTA metric while 31.3% of the dose-pixels failed the comparison when the calculated dose distribution was normalized by the mean dose in the measured dose distribution. Normalization is not recommended because it can mask dose differences. Reversing the definition of the reference dose distribution from the measured to the calculated dose distribution also has significant impact on the metric results; and, in particular, the DTA. The percentage of dose-pixels that failed the DTA metric changed from 14.1% to 31.7% when the reference dose distribution was changed from the measured distribution to the calculated distribution. Metric sensitivity to the definition of the reference dose distribution indicates that it is important to be consistent (in this work it is always defined as the measured dose distribution). The metric results are especially sensitive to the metric thresholds. An example of this sensitivity is the percentage of dose-pixels that failed the absorbed dose difference metric went from 13.9% to 1.1% when the threshold was changed from 4 cGy to 6 cGy.

6.3 Clinical Application

When the film dosimetry and dose distribution comparison techniques were used to compare calculated and measured dose distributions for conventional 10 x 10 and 5 x 5 cm² fields, the maximum doses were found to agree within 2%. The following are DDComp metric results for the comparison of four conventional square field measured and calculated dose distribution pairs. The percentage of pixels that failed the combined metric was 0.0% for the 5x5 cm² and 10x10 cm² fields irradiated using a 15 MV beam; 0.3% for the 10x10 cm² field irradiated using a 6 MV beam, and 2% for the 5x5 cm² field irradiated using a 6 MV beam.

Typical results for the agreement between measured and calculated dose distributions for IMRT fields were identified by verifying 40 IMRT fields using the techniques presented in this thesis. On average, $(10.7 \pm 3.1)\%$ of the dose-pixels in the measured dose distribution were not within 5 cGy of the calculated dose distribution, and $(74.8 \pm 1.9)\%$ of the dose-pixels in the measured dose distributions were not within 3% of the dose at the same location in the calculated dose distribution. In addition, $(95.2 \pm 0.8)\%$ of the dose-pixels in the high-dose gradient regions were not within 4 mm of the same dose in the calculated dose distribution, and $(6.9 \pm 3.0)\%$ of the dose-pixels did not pass any of the metric criteria. An average of about 93% of the dose-pixels in the IMRT test cases passed the combined metric analysis; therefore, we feel that Van Dyk's recommended 67% agreement level (Section 3.2.4.1) is too lenient for clinical use. Perhaps a value of 85% or 90% would be more appropriate.

The verification techniques were found to be fairly reproducible. When a verification of an IMRT treatment field was repeated on three different days, the effect on the metrics of absorbed dose difference and distance to agreement were quite small in terms of percent failure. Additionally, the differences in the percentage of dose-pixels failing the combined metric results were negligible. The percentage of dose-pixels failing for the absorbed dose difference was found to be $(2.1 \pm 0.7)\%$, $(81.7 \pm 4.6)\%$ for the percent dose difference, $(12.5 \pm 1.8)\%$ for the DTA, and $(0.1 \pm 0.0)\%$ for the combined metric. The reproducibility could be investigated further by verifying other treatment fields on multiple days.

6.4 Future Work

It would be useful to implement this work clinically. For centres using EPID dosimetry, the use of DDCComp could strengthen existing IMRT verification techniques. For example, if we add DDCComp to the BEV IMRT verification tool

at the Cross Cancer Institute, a more quantitative verification tool would result. With both tools combined, dose distributions can be compared in many ways including a dose difference histogram, maximum and isocentre values, mean standard deviation between the distributions and metric images, histograms, and statistics. Centres not using EPID dosimetry may benefit from the implementation of both the film dosimetry and dose distribution comparison techniques presented in this thesis.

Advances in radiobiological modeling are required to determine clinically meaningful thresholds for each of the metrics. Model predictions can then be integrated into this work by outlining the PTV and PRV regions on the dose distributions and applying different thresholds to each based on the radiobiological data.

Metric results for many more IMRT clinical fields would be useful to establish acceptable levels of failure for each of the metrics and what percentage of dose-pixels should pass the overall analysis for the treatment plan to be accepted.

6.5 Final Conclusions

The hypothesis of this work, namely that film dosimetry together with a quantitative method of comparing calculated and measured dose distributions can be used to verify treatment fields, was supported by the results. These techniques can be used to ensure planned dose distributions are delivered accurately and precisely to achieve maximum therapeutic benefit to the patient.

Bibliography

- Almond, P. R., P. J. Biggs, B. M. Coursey, W. F. Hanson, M. S. Huq, R. Nath and D. W. Rogers (1999). "AAPM's TG-51 protocol for clinical reference dosimetry of high-energy photon and electron beams." Med Phys **26**(9): 1847-70. (20, 21)
- Barrett, H. H. and W. Swindell (1981). Radiological Imaging - The Theory of Image Formation, Detection, and Processing. New York, NY, Academic Press, Inc. (26)
- Boyer, A. L., L. Xing and P. Xia (1999). Beam Shaping and Intensity Modulation. The Modern Technology of Radiation Oncology: A Compendium for Medical Physicists and Radiation Oncologists. J. Van Dyk. Madison, WI, Medical Physics Publishing. (13, 14, 15)
- Bushberg, J. T., J. A. Seibert, E. M. Leidholdt and J. M. Boone (2002). The Essential Physics of Medical Imaging. Philadelphia, PA, Lippincott Williams & Wilkins. (48)
- Canadian Cancer Society (2003). Cancer glossary. <http://www.cancer.ca>. (6)
- Canadian Cancer Society (2003). Risk Reduction. <http://www.cancer.ca>. (7)
- CancerBACUP (2002). Booklet series. <http://www.cancerbacup.org.uk/>. (7)
- Childress, N. L., L. Dong and Rosen, II (2002). "Rapid radiographic film calibration for IMRT verification using automated MLC fields." Med Phys **29**(10): 2384-90. (29, 42)
- Childress, N. L. and I. Rosen (2003). DoseLab 3.04 User Manual. <http://doselab.sourceforge.net/manual.html>. (49)
- Danciu, C., B. S. Proimos, J. C. Rosenwald and B. J. Mijnheer (2001). "Variation of sensitometric curves of radiographic films in high energy photon beams." Med Phys **28**(6): 966-74. (28)
- Eastman Kodak Co (2001). Health Imaging. **2002**. <http://www.kodak.com/>. (29, 47)
- Ezzell, G. A., J. M. Galvin, D. Low, J. R. Palta, I. Rosen, M. B. Sharpe, P. Xia, Y. Xiao, L. Xing and C. X. Yu (2003). "Guidance document on delivery, treatment planning, and clinical implementation of IMRT: Report of the

- IMRT subcommittee of the AAPM radiation therapy committee." Med Phys **30**(8): 2089-2115. (15, 16)
- Fraass, B., K. Doppke, M. Hunt, G. Kutcher, G. Starkschall, R. Stern and J. Van Dyke (1998). "American Association of Physicists in Medicine Radiation Therapy Committee Task Group 53: quality assurance for clinical radiotherapy treatment planning." Med Phys **25**(10): 1773-829. (32, 33)
- Gagne, I., B. Warkentin, H. Thompson, M. A. MacKenzie and G. C. Field (2002). "A procedure to improve the reliability of IMRT film verification." Med Phys **29**(8): 1943. (1, 42)
- Glasgow, G. P. (1999). Brachytherapy. The Modern Technology of Radiation Oncology: A Compendium for Medical Physicists and Radiation Oncologists. J. Van Dyk. Madison, WI, Medical Physics Publishing. (7)
- Hajnal, J. V., D. L. G. Hill and D. J. Hawkes, Eds. (2001). Medical Image Registration, CRC Press. (38)
- Hall, E. J. (2000). Radiobiology for the Radiologist. Philadelphia, PA, Lippincott Williams & Wilkins. (10)
- Harms, W. B., Sr., D. A. Low, J. W. Wong and J. A. Purdy (1998). "A software tool for the quantitative evaluation of 3D dose calculation algorithms." Med Phys **25**(10): 1830-6. (31, 33)
- Horn, J. W. and E. J. Sondik (1989). "Person-years of life lost due to cancer in the United States, 1970 and 1984." Am J Public Health **79**(11): 1490-3. (6)
- Hudson, A. D., B. G. Fallone and G. C. Field (2003). "A Software Tool to Quantitatively Compare Dose Distributions." Med Phys **30**(7): 1952. (52)
- ICRU, International Commission on Radiation Units and Measurements (1976). ICRU Report 24: Determination of Absorbed Dose in a Patient Irradiated by Beams of X or Gamma Rays in Radiotherapy Procedures. Washington, DC. (11)
- ICRU, International Commission on Radiation Units and Measurements (1993). ICRU Report 50: Prescribing, Recording, and Reporting Photon Beam Therapy. Washington, DC. (12, 33)
- ICRU, International Commission on Radiation Units and Measurements (1999). ICRU Report 62: Prescribing, Recording and Reporting Photon Beam Therapy (Supplement to ICRU Report 50). Washington, DC. (12, 13)

- Johns, H. E. and J. R. Cunningham (1983). The Physics of Radiology. Springfield, IL, Charles C Thomas. (10, 24, 27, 48)
- Ju, S. G., Y. C. Ahn, S. J. Huh and I. J. Yeo (2002). "Film dosimetry for intensity modulated radiation therapy: dosimetric evaluation." Med Phys **29**(3): 351-5. (28)
- Khan, F. M. (1994). The Physics of Radiation Therapy. Baltimore, MD, Lippincott Williams & Wilkins. (13, 20, 28, 48)
- Khan, F. M. (2003). Intensity-Modulated Radiation Therapy. The Physics of Radiation Therapy. Philadelphia, PA, Lippincott Williams & Wilkins. (15)
- Lewis, J. P. (1995). Fast normalized cross-correlation. Industrial Light & Magic. (37)
- Low, D. A., W. B. Harms, S. Mutic and J. A. Purdy (1998). "A technique for the quantitative evaluation of dose distributions." Med Phys **25**(5): 656-61. (33)
- MacKenzie, M. A., M. Lachaine, B. Murray, B. G. Fallone, D. Robinson and G. C. Field (2002). "Dosimetric verification of inverse planned step and shoot multileaf collimator fields from a commercial treatment planning system." J. Appl. Clin. Med. Phys. **3**(2): 97-109. (36, 42)
- Mah, E., J. Antolak, J. W. Scrimger and J. J. Battista (1989). "Experimental evaluation of a 2D and 3D electron pencil beam algorithm." Phys Med Biol **34**(9): 1179-94. (30)
- Mathworks (2003). Image Processing Toolbox User's Guide Version 4. **2003**. www.mathworks.com. (56)
- Med-Tec (2002). Exradin Farmer Type Chamber. **2002**. <http://www.medtec.com/>. (45)
- National Cancer Institute of Canada (2004). Canadian Cancer Statistics 2004. Toronto, ON. <http://www.ncic.cancer.ca>. (6, 7)
- Ramsey, F. L. and D. W. Schafer (1997). The Statistical Sleuth: A course in methods of data analysis. Belmont, CA, Duxbury Press. (37)
- Statistics Canada (1997). Health Statistics. <http://www.statcan.ca/>. (6)

- Steel, G. G. (2003). The radiobiology of tumours. Basic Clinical Radiobiology, 3rd Edition. G. G. Steel. New York, NY, Arnold. (8)
- Suchowerska, N., P. Hoban, M. Butson, A. Davison and P. Metcalfe (2001). "Directional dependence in film dosimetry: radiographic and radiochromic film." Phys Med Biol **46**(5): 1391-7. (28)
- Toga, A. W. and P. K. Banerjee (1993). "Registration revisited." Journal of Neuroscience Methods **48**: 1-13. (37, 56)
- Van Dyk, J., Ed. (1999). Radiation Oncology Overview. The Modern Technology of Radiation Oncology: A Compendium for Medical Physicists and Radiation Oncologists. Madison, WI, Medical Physics Publishing. (8, 9, 10, 20, 32, 53)
- Van Dyk, J., R. B. Barnett and J. J. Battista, Eds. (1999). Computerized Radiation Treatment Planning Systems. The Modern Technology of Radiation Oncology. Madison, WI, Medical Physics Publishing. (14)
- Van Dyk, J., R. B. Barnett, J. E. Cygler and P. C. Shragge (1993). "Commissioning and quality assurance of treatment planning computers." I J Rad Oncol Biol Phys **26**(2): 261-73. (30, 31, 93)
- VIDAR (1998). VIDAR VXR Film Digitizer User's Guide for 32-bit TWIAN for Windows. Herndon, VA, VIDAR Systems Corporation. (47, 48)
- Webb, S. (1997). The Physics of Conformal Radiotherapy: Advances in Technology. Philadelphia, PA, Institute of Physics Publishing. (15, 16)